Dissertation
submitted to the
Combined Faculties of the Natural Sciences and Mathematics
of the Ruperto-Carola-University of Heidelberg, Germany
for the degree of
Doctor of Natural Sciences

Put forward by

Alessandro Angioi

born in Cagliari, Italy
Oral examination: July 25, 2018

Multi-Particle Effects in Strong-Field Quantum Electrodynamics

Referees: PD Dr. Antonino Di Piazza
Prof. Dr. Joerg Jaeckel

Zusammenfassung

In dieser Arbeit untersuchen wir nichtlineare Compton-Streuung, einer der grundlegendsten Prozesse der Quantenelektrodynamik in einem starken elektromagnetischen Hintergrundfeld. Man kann sich die nichtlineare Compton-Streuung als einen Prozess vorstellen, bei dem ein freies Elektron mit einem Laserfeld streut und dabei Strahlung erzeugt. Mit der bevorstehenden Eröffnung einiger Petawatt-Laseranlagen wird die nichtlineare Compton-Streuung routinemäßig getestet werden, insbesondere um die Dynamik von Plasmen zu verstehen, die mit starken Feldern interagieren.

Trotz seiner vielversprechenden Anwendungen wurde dieser Prozess bisher immer für einzelne Teilchen mit einem genau definierten Anfangsimpuls untersucht. Wir werden zeigen, welche Effekte entstehen, wenn sich anfänglich ein oder mehrere Elektronen in einem Wellenpaketzustand befinden; Insbesondere interessiert uns, welche Modifikationen durch Quanteneffekte hervorgerufen werden und welche stattdessen eine klassische Erklärung haben. Darüber hinaus werden wir uns im Fall mehrerer Teilchen auf die Kohärenz der emittierten Strahlung konzentrieren und berechnen, wie Quanteneffekte die Frequenzen begrenzen, bei denen die Strahlung kohärent sein kann, selbst in einem Bereich, der typischerweise mit der klassischen Elektrodynamik assoziiert wird.

Abstract

In this work we study Nonlinear Compton Scattering, one of the most fundamental processes of Quantum Electrodynamics in a strong electromagnetic field background. One can imagine Nonlinear Compton Scattering as a process where a free electron scatters with a laser field, and while doing so it generates radiation. With the imminent inauguration of some Petawatt laser facilities, Nonlinear Compton Scattering will be routinely tested, especially in order to understand the dynamics of plasmas interacting with strong fields.

Despite its promising applications, this process has always been studied for single particles with a well-defined initial momentum. We will show which effects arise when initially one or multiple electrons are in a wave packet state; in particular, we will be interested in which modifications are brought about by quantum effects, and which instead have a classical explanation. Moreover, in the multi-particle case, we will focus on the coherence of the emitted radiation, and calculate how quantum effects limit the frequencies at which the radiation can be coherent even at a regime typically associated with Classical Electrodynamics.

In connection with the work on this thesis, the following article was published in a refereed journal:

- A. Angioi, F. Mackenroth, and A. Di Piazza,
  Nonlinear single Compton scattering of an electron wave packet,
  Physical Review A **93**, 052102 (2017).

Moreover, also in connection with the work on this thesis, the following preprint was submitted:

- A. Angioi and A. Di Piazza,
  Quantum Limitation to the Coherent Emission of Accelerated Charges,
  Submitted on 01.12.2017 (arXiv:1712.01123).

Contents

List of Figures

Chapter 1

Introduction

To this day, the theory that best describes fundamental particles and their interactions is the Standard Model; this theory is embedded in the theoretical framework of Quantum Field Theory (QFT), where elementary particles are thought of as excitations of underlying entities called quantum fields [Peskin and Schroeder, 1995; Weinberg, 1995]. Although the Standard Model cannot account for some phenomena which are of great importance in our quest for the full description of physical processes in the universe (for instance, one fundamental force, gravity, is still not fully understood at a quantum level), it shapes our knowledge of particle physics. According to the Standard Model, matter interacts via the exchange of bosons, which have the role of force carriers. Among the bosons of the Standard Model, the photon, i. e., the boson associated with the electromagnetic field, has some quite peculiar features; a striking difference between it and the other force carriers of the Standard Model is that the photon possesses neither charge of any kind nor mass: this allows it to propagate in vacuum for infinitely large distances without decaying, and so it can make it possible for arbitrarily distant objects to exert a force on each other.

Arguably, in order to explain the vast majority of the world that surrounds us, the electromagnetic interaction has a privileged role. In fact, the electromagnetic interaction alone is responsible for the structure of the atoms (if we take for granted that nuclei are stable), which for many practical purposes can still be thought of as the fundamental building blocks of matter: this is the case in Chemistry and most fields related to it. Moreover, although there are many major technological achievements of mankind that harnessed the energy stored in nuclei or in gravitational fields in order to achieve our goals, the degree of control we have over electromagnetic fields is unparalleled, and constitutes the basis for most of human technology.

In order to further improve our understanding of such an important interaction it is worthwhile, then, to restrict our attention to the QFT that deals only with

electrically charged particles and their interactions via the electromagnetic field: Quantum Electrodynamics (QED). Since QED was the first Quantum Field Theory that successfully served the purpose of modeling a fundamental interaction, it has been the blueprint for most of the Quantum Field Theories developed subsequently; in fact, it was from the study of QED that powerful tools such as Feynman diagrams [Feynman, 1949] were developed, and where the appearance of divergent quantities (i. e., the problem of infinities) stimulated a systematic study of renormalization [Feynman, 1948; Schwinger, 1948, 1949; Tomonaga and Oppenheimer, 1948; Dyson, 1949; Gell-Mann and Low, 1954]. QED has been tested over and over in a vast number of experiments, both at low energies [Odom et al., 2006; Gabrielse et al., 2006; Miller et al., 2007] (see also [Karshenboim, 2005], and references therein) and high energies [Levine et al., 1997]. Just to give an idea of the accuracy that precision tests of QED at low energies are able to achieve, the fine structure constant α, the parameter that determines the strength of electromagnetic interactions, has been measured [Gabrielse et al., 2006] with a relative error of around one part in a billion. Interestingly enough, very few physicists remember the value of α, although almost everyone remembers its inverse, approximately 137.

Another notable experiment was recently performed in Heidelberg [Sturm et al., 2014], where by combining QED calculations with state-of-the-art experimental techniques it was possible to measure the mass of the electron with a remarkably tiny relative error of $3 \cdot 10^{-11}$. This level of precision is quite surprising, for a theory that unfortunately, as many other Quantum Field Theories, cannot be solved exactly. This is not a problem in many scenarios because, since $\alpha \ll 1$, it can be possible to study the electromagnetic interaction between particles perturbatively in α. This means that in experiments involving charged particles one could calculate the interaction between them as a sum of many contributions, which can be interpreted as due to the exchange of an increasing number of photons between the charged particles themselves. It can be shown that the more photon emissions/absorptions these contributions contain, the more they are suppressed by an increasingly high power of α, so it is possible at some point to truncate this series and obtain results which are accurate enough for the purpose of the experiment.

However, it is not always practical, or even possible, to treat the electromagnetic interaction perturbatively. This happens when the interaction is strong enough to alter the quantum states of particles in such a way that it cannot be regarded as a small perturbation anymore. For instance, the quantum state of an electron bound to an atomic nucleus is not similar at all to the quantum states of a free electron, so that in general one cannot regard atoms as systems where free electrons exchange a small number of photons with an oppositely charged particle, the nucleus. Even a laser field, if strong enough, could modify the quantum state of particles in a similar fashion. In fact, the discovery of two techniques called Chirped Pulse Amplification (CPA) [Strickland and Mourou, 1985] and Optical Parametric Chirped Pulse Amplification (OPCPA) [Piskarskas et al., 1986] led to a dramatic increase in

the highest peak intensities of optical laser pulses. This increase in intensity comes at the cost that both CPA and OPCPA cannot produce arbitrarily long pulses, but only ultrashort ones where the electric field oscillates only a few times. Still, the most powerful lasers built so far, like Vulcan [Vulcan, website], Astra-Gemini [Astra-Gemini, website], HERCULES [HERCULES, website], BELLA [BELLA, website], and planned ones, such as ELI [ELI, website], HiPER [HiPER, website], APOLLON [APOLLON, website], and XCELS [XCELS, website], are based on either CPA or OPCPA. Record intensities of about $10^{22}\,\mathrm{W/cm^2}$ have been already reported [Yanovsky et al., 2008], and intensities of the order of $10^{24}\,\mathrm{W/cm^2}$ are envisaged in future laser facilities [ELI, website; XCELS, website]. While traveling through an electromagnetic field of this intensity, it is unlikely that an electron will exchange only a few photons with the laser field itself [Ritus, 1985], and perturbative calculations become quickly unpractical or meaningless. This regime is often called the Strong-Field sector of QED, and its study is promising [Ehlotzky et al., 2009; Di Piazza et al., 2012] for both theoretical reasons (experiments at this extreme regime will advance our understanding of the electromagnetic interactions, and could serve as a probe in the search of new physics beyond the Standard Model [Kurilin, 1999; Gies et al., 2006; Gies, 2009; Mendonça, 2007; Döbrich and Gies, 2010; Heinzl, Ilderton and Marklund, 2010; Villalba-Chávez et al., 2016]) and technological reasons (by exploiting some processes of Strong-Field QED it could be possible, for instance, to build gamma-ray sources of unprecedented intensity and brilliance [Ridgers et al., 2013; Sarri et al., 2014; Yu et al., 2016; Gonoskov et al., 2017; Bashinov et al., 2017; Gong et al., 2017, 2018; Liu et al., 2018]).

More quantitatively, the features of the interaction between a laser field, having an amplitude $\mathcal{E}$ and angular frequency ω, and an electron (mass m and charge $e < 0$) can be characterized by the value of the Lorentz- and gauge-invariant parameter

$$\xi = \frac{|e|\mathcal{E}}{\omega mc}, \tag{1.1}$$

where c is the speed of light. The parameter ξ has both a classical and a quantum interpretation. Classically, we can interpret it as $|e|\mathcal{E}c/\omega$, the work performed by the laser field in one reduced laser wavelength (c/ω), in units of the electron's rest energy mc^2; thus, for ξ larger than unity we can expect the electron, even if initially at rest, to quickly reach relativistic energies while interacting with the laser field. We can expect then relativity to play a role in the study of the motion of the electron; this implies that the dynamics of the electron will have a nonlinear dependence on the laser field's amplitude, and qualitatively new effects can be studied and measured. Moreover, by multiplying and dividing by $\hbar$, the reduced Planck's constant, we can also give a quantum interpretation to ξ as the work performed by the laser field in one reduced Compton wavelength ($\lambda_C = \hbar/mc$) of the electron, $|e|\mathcal{E}\hbar/mc$, in units of the energy of the laser photons, $\hbar\omega$; in this context, ξ larger than one would hint at the fact that processes involving the exchange

of multiple laser photons start becoming more important than ones involving a single photon [Berestetskii et al., 1982; Ritus, 1985; Di Piazza et al., 2012]. At optical frequencies, fields with a peak intensity of the order of $10^{18}\,\mathrm{W/cm^2}$, which are routinely available in laboratories, reach already the regime $\xi \sim 1$.

While the parameter ξ tells us when relativistic or multiphoton effects start becoming important, it would also be useful to have a similar parameter that indicates when it is mandatory to use a quantum theory rather than a classical one. In order to find this parameter, let us highlight the main differences between Classical and Quantum Electrodynamics. The most striking one at first is that while classical particles move along trajectories, in QED particles are excitations of quantum fields, and it is not always possible to associate them with a single trajectory in a meaningful way. Moreover, Classical Electrodynamics predicts that accelerated charges emit radiation in a continuous fashion [Jackson, 1999], and this radiation is usually calculated, via the Liénard-Wiechert potentials, as a functional of the particles' trajectory. This procedure is intrinsically plagued by a fundamental problem: it completely neglects the back-reaction that the fields exert on the charges, thus, since particles can emit radiation without any consequence on their trajectories, energy conservation is violated. In QED, instead, this is not a problem, because the electromagnetic radiation is quantized in photons, and whenever a particle emits a photon it will also recoil, so the total energy and momentum will be conserved. In particular, whereas the energy spectrum of the radiation emitted classically can, in principle, extend to arbitrarily high energies, in QED, because of energy-momentum conservation, there is an upper bound on the energy of the photons that a particle can emit (i. e., at most a particle could transform all of its kinetic energy into photons, but not more than that).

It can be shown [Baier et al., 1998] that for electrons having a well-definite value of the momentum and relativistic energies ε the effects due to the quantization of their motion are negligible with respect to the effects associated with recoil; the onset of the latter kind of effects is controlled by a Lorentz- and gauge-invariant parameter called χ. We will discuss this parameter in greater detail in Chapter 2; at this point, suffice it to say that it is related to the ratio between the electric field that an electron feels in its rest frame and the quantity $\mathcal{E}_{cr} = m^2c^3/\hbar|e| \approx 1.3 \times 10^{16}\ \mathrm{V/cm}$, the so-called "critical field" (or "Schwinger field") of QED [Sauter, 1931; Schwinger, 1951; Ritus, 1985; Di Piazza et al., 2012]. A constant and uniform electric field of strength $\mathcal{E}_{cr}$ could give to an electron-positron pair an energy comparable to its rest energy $2mc^2$ over a distance of the order of $\lambda\!\!\!^{-}_C$; pictorially, this energy could bring into existence a virtual electron-positron pair, making the vacuum unstable under decay into pairs [Schwinger, 1951]. The strongest laser fields that are attainable in the laboratory as of today, and even the ones envisaged in the near future, are orders of magnitude weaker than the critical field. However, even if the peak electric field $\mathcal{E}$ of a laser is much weaker than $\mathcal{E}_{cr}$ (at optical frequencies, a field so intense would have an intensity $\mathcal{I}_{cr} \sim 10^{29}\,\mathrm{W/cm^2}$), an electron which is

ultrarelativistic in the laboratory, counterpropagating with respect to the laser field, would feel in its rest frame the field $\mathcal{E}$ multiplied by the electron's relativistic γ factor [Einstein, 1905; Jackson, 1999]. Electron beams with energies beyond several GeVs have been already produced, both via conventional accelerators [Patrignani, C. et al. (Particle Data Group), 2017] and laser-based ones [Leemans et al., 2014]; this amounts to $\gamma > 10^4$, so even with electric fields four orders of magnitude weaker than $\mathcal{E}_{cr}$ it is still possible to test QED in the Strong-Field regime. In fact, nonlinear effects of QED have been already probed in the presence of a relatively weak laser (peak intensity smaller than 10^{18} W/cm^2) by colliding it with a very energetic (50 GeV) electron beam [Bamber et al., 1999].

The nonlinear regime of QED, characterized by non-negligible ξ, χ, or both, is quite challenging to study; indeed, as we have previously mentioned, perturbative corrections to the free states of the electron field and of the electromagnetic field could be practically (or even theoretically) inapplicable. Still, overcoming the difficulties inherent in nonlinear QED is an effort worth making: the rewards are extremely interesting processes. For instance, the virtual electron-positron pairs that populate the QED vacuum allow it to behave like a polarizable medium, making it possible for many phenomena associated with electrodynamics in a nonlinear or anisotropic medium to take place in it [Heisenberg and Euler, 1936; Klein and Nigam, 1964; Baier and Breitenlohner, 1967; Adler et al., 1970; Bialynicka-Birula and Bialynicki-Birula, 1970; Baier et al., 1987, 1996; Rozanov, 1998; Fedotov and Narozhny, 2007; Di Piazza et al., 2007, 2008; Dinu et al., 2014; Karbstein and Shaisultanov, 2015; Karbstein and Sundqvist, 2016; Bragin et al., 2017; Gies et al., 2018]. In fact, in the QED vacuum it is possible for two photons to scatter via an electron-positron loop and exchange momentum; this is in striking contrast with one of the fundamental properties of the classical electromagnetic field, which is that, because of the linearity of Maxwell's equations with respect to both sources and fields, different modes of the field are uncoupled. Experimental searches for the signature of light-by-light scattering are being conducted [Della Valle et al., 2016], and evidence for this process has already been found in heavy-ion collisions [ATLAS, 2017]. Since light-by-light scattering is a fourth-order process, its cross section is suppressed and its direct detection very challenging. With increasingly strong fields, it is possible to enhance the light-by-light scattering probability, making it more accessible to experimental inquiries. For example, one could polarize the vacuum in a geometrically nontrivial way with strong lasers, and build in this way a realization of Young's experiment where a photon interacts with "a matterless double slit" entirely made of light [King et al., 2010]. This would make it possible to measure light-by-light scattering via its characteristic diffraction pattern on a screen; it is a very elegant way to exploit quantum interference in order to probe Strong-Field QED, and perhaps there are other methods that make use of quantum interference to test nonlinear effects in QED which are as fascinating as this, still waiting to be discovered.

The calculations of nonlinear QED can be significantly simplified if the laser field can be thought of as a classical field [Skoromnik and Feranchuk, 2014] with a plane-wave space-time stucture, i. e., its wave fronts are parallel planes. In this case, it is possible to work in the so-called "Furry picture" [Furry, 1951], and take into account the plane-wave laser field exactly. After doing this, one can study the remaining part of the electromagnetic field, i. e., nonlaser photons, with a perturbative series. This approximation can be applied to electrons interacting with an intense laser pulse, even if the laser is focused down to the Rayleigh's diffraction limit, as long as the electron collides head-on with the laser field, close to its focus, and if the transverse excursion of the electron is much smaller than the laser waist size (this last condition is satisfied if ξmc^2 is much smaller than the electron's energy in the laboratory frame [Landau and Lifshitz, 1975; Berestetskii et al., 1982]). It is worth noticing that there has been a great deal of interest [Bagrov et al., 1993; Baier et al., 1998; Wistisen, 2014; Di Piazza, 2014, 2015, 2017; Heinzl and Ilderton, 2017*a*,*b*] in finding techniques suitable to the study of QED processes happening in fields of more complex space-time structures that approximate better the fields obtainable in the laboratory (i. e., focused beams).

In the Furry picture, the two lowest-order processes in a laser field that have been studied the most are Nonlinear Breit-Wheeler Pair Production and Nonlinear Single Compton Scattering (NSCS). This thesis is devoted to the study of NSCS, where an electron traveling inside a laser field exchanges multiple photons with the laser field itself, while also emitting a single, non-laser photon. NSCS has been thoroughly studied in the literature; first in the presence of a monochromatic plane wave, where it is possible to obtain most results analytically [Goldman, 1964; Brown and Kibble, 1964; Nikishov and Ritus, 1964; Fried and Eberly, 1964; Ritus, 1985; Ivanov et al., 2004; Harvey et al., 2009; Corson et al., 2011; Wistisen, 2014], and then, when due to CPA and OPCPA ultrashort pulses became of interest, the NSCS rates were derived also in such background [Boca and Florescu, 2009; Heinzl, Seipt and Kämpfer, 2010; Boca and Florescu, 2011; Mackenroth and Di Piazza, 2011; Seipt and Kämpfer, 2011; Boca and Florescu, 2011; Dinu et al., 2012; Boca et al., 2012; Dinu, 2013; Krajewska et al., 2014; Titov et al., 2014; Angioi et al., 2016].

The results that are presented in this thesis are motivated by the fact that, with the notable exception of [Corson et al., 2011], in the study of Nonlinear Single Compton Scattering the initial state of the electron has always been chosen as a momentum eigenstate. Because of the uncertainty principle, this means that the electron has always been considered as delocalized everywhere in space, thus ignoring some possible finite-size effects. We relaxed this assumption, and considered NSCS of electron wave packets. In principle, since the initial state is then a superposition of different states, one could expect quantum interference in the spectrum of the emitted radiation; as we will show, this does not happen in a plane-wave if one considers only one electron in the initial state [Angioi

et al., 2016]. Instead, when multiple particles are present in the initial state there is indeed quantum interference in the emitted radiation [Angioi and Di Piazza, 2017], and in the regime of $\chi \ll 1$ it can be compared with the interference that classically is also expected when electrons follow accelerated trajectories that are close to each other [Jackson, 1999; Klepikov, 1985]. In particular, we focused on the coherence of the emitted radiation, i. e., we compared the total radiation emitted by the system of charges taken as a whole with the radiation they would emit individually; if the total emitted radiation at a certain frequency scales linearly with the number of particles we will call it "fully incoherent radiation", whereas if the emitted radiation scales as the square of the number of particles we will call it "fully coherent radiation". We have found that the quantum and classical emission spectra in general tend to agree up to a certain frequency, dependent on the shape of the initial quantum state of the electrons; above that frequency, we identified two effects (one of fully quantum origin, whereas the other one has a classical counterpart) which suppress the total radiation emitted and cause the emission to be incoherent.

It is worth noticing that currently adopted schemes for the study of plasmas (for a great review on the topic, see [Gonoskov et al., 2015]) treat the electromagnetic field modes in different ways, depending on their frequencies. If the frequency of a mode is lower than a certain threshold, it is treated classically and its evolution is given by the solution of Maxwell's equations on a grid, with sources given by the charges and currents in the plasma. In this frequency range, there is classical interference in the radiation emitted by different charges; depending on the system one is studying, and, more specifically, depending on the quantum state the studied particles are in, classical mechanics could greatly overestimate the coherence of the emitted radiation. On the other hand, when the frequency of a mode is large enough, the emitted radiation is treated stochastically and each particle, independently of the others, can emit photons at random times with a rate given by QED, in the approximation that the rate is the same as if the particle were traveling through a certain constant field (this approximation is not valid at lower frequencies [Di Piazza et al., 2017]). This procedure implies that the particles emit radiation in a completely incoherent way. Our results can be used to estimate when the assumptions of full coherence/incoherence in the emitted radiation are not fulfilled.

The dependence of the emitted radiation on the shape of the incoming wave packet when multiple particles are present could be exploited in order to experimentally test Nonlinear Single Compton Scattering at the level of quantum amplitudes. In order to do this, in upcoming facilities, aside of the study of the interaction between strong lasers and plasmas, one could perform complementary experiments with pulses of electrons in a well-defined quantum state [Baum, 2013], and analyze the radiation they emit and compare it to the classical prediction (which would take into account coherent emission and interaction between particles, but they would be

limited by the applicability range of classical mechanics), single-particle quantum predictions (which fundamentally cannot take into account coherent emission and interactions between different particles) and our QED calculations (which neglect the interaction between particles, but are not classical and still take into account coherent emission).

This thesis is organized as follows: in Chapter 2 we will review some basic concepts of Classical and QED, with a focus on processes happening in a plane-wave electromagnetic field background. Then, in Chapter 3, we will review the other pillar upon which this thesis is built: numerical methods for the quadrature of highly oscillatory integrals and Monte Carlo integration with importance sampling. Both Chapter 2 and Chapter 3 do not contain any new result, and serve only as a reference in order to make this thesis self-contained. In Chapter 4, we calculate the spectrum emitted by an electron initially in a wave packet state. Chapter 5 builds on this by showing the new features that can be expected when considering states with many particles (and, in particular, we have chosen two study the paradigmatic case where only two particles are present). Finally, in Chapter 6 we will draw some conclusions about our work and give an outlook for future research.

1.1 Units and Notation

In the rest of this thesis, we will use natural units, i. e., $\hbar = c = 1$; moreover, electromagnetic quantities will be expressed in Gaussian units (see Chapter 2), and the metric tensor is $g^{\mu\nu} = g_{\mu\nu} = \mathrm{diag}(1, -1, -1, -1)$, and summation over repeated indices is always assumed unless stated otherwise.

The electron charge e is negative and $e^2 = \alpha \approx 1/137$

The conjugate of a complex number z will be given by z^*.

A position in spacetime will be indicated, with a slight abuse of notation, by the four-vector $x^\mu = (t, x, y, z)$ (where t is the time and the other coordinates are spacelike). Other slight abuses of notation are present for the symbols e, i, α, β, and γ; however, they are used in contexts where the meaning of such symbols is immediately clear.

In order to make formulas more readable, point free notation for functions will be used when deemed necessary.

For other four-vectors a^μ it is understood that $a^\mu = (a^0, \boldsymbol{a})$ and $a_\mu = (a^0, \boldsymbol{a})$. The product between two four-vectors a^μ and b^μ will often be expressed as $(ab) = a_\mu b^\mu$.

The slashed symbol on a four vector, $\not{a}$, indicates its contraction with a Dirac gamma matrix γ^μ (see Chapter 2), i. e. $\not{a} = a_\mu \gamma^\mu$.

Chapter 2

Charged Particles in Strong Fields

In this chapter we will review the theoretical background needed in order to derive the results presented in Chapter 4 and Chapter 5; these topics are well-known, and many textbooks are devoted to their study [Landau and Lifshitz, 1975; Berestetskii et al., 1982; Jackson, 1999; Peskin and Schroeder, 1995]. Another good reference for QED in the presence of a strong background is [Mackenroth, 2014].

In Section 2.1, we review some elements of Classical Electrodynamics, especially the most relevant features of the motion of charges in plane-wave electromagnetic fields, and the classical predictions relative to the electromagnetic radiation they emit while moving. The Quantum treatment of the same problem, within the framework of Strong-Field QED, is reviewed in Section 2.2.

2.1 Classical Electrodynamics

Classical Electrodynamics is a theory that describes the interaction between charged particles and electromagnetic fields in the regime where quantum effects can be neglected, so that both the electric field $\boldsymbol{E}$ and the magnetic field $\boldsymbol{B}$ are vector-valued functions over the spacetime and particles (or particle densities) evolve according to classical equations. The differential equations that govern the electromagnetic field are called Maxwell's Equations; in natural units, they can be written as

$$\nabla \cdot \boldsymbol{E} = 4\pi\rho \tag{2.1}$$

$$\nabla \cdot \boldsymbol{B} = 0 \tag{2.2}$$

$$\nabla \times \boldsymbol{E} = -\frac{\partial \boldsymbol{B}}{\partial t} \tag{2.3}$$

$$\nabla \times \boldsymbol{B} = \frac{\partial \boldsymbol{E}}{\partial t} + 4\pi\boldsymbol{j}, \tag{2.4}$$

where ρ is the charge density and $\boldsymbol{j}$ is the current density. In vacuum, where $\rho = 0$ and $\boldsymbol{j} = 0$, they assume a remarkably symmetric form. Each of the Maxwell's equations expresses a fundamental property of the electromagnetic field, respectively the Gauss' theorem for the electric field, the non-existence of magnetic monopoles, Faraday's law of induction, and Ampère's law.

Maxwell's equations are typically solved by introducing two functions of space and time: the electrostatic potential Φ, which is a scalar function, and the vector potential $\boldsymbol{A}$. These two functions are such that

$$\boldsymbol{E} = -\boldsymbol{\nabla}\Phi - \frac{\partial \boldsymbol{A}}{\partial t} \tag{2.5}$$

$$\boldsymbol{B} = \boldsymbol{\nabla} \times \boldsymbol{A}. \tag{2.6}$$

Notice that Eq. (2.5) and Eq. (2.6) do not uniquely define Φ and $\boldsymbol{A}$; in fact, if Φ and $\boldsymbol{A}$ satisfy Eqs. (2.5) and (2.6) so does any potential Φ' and $\boldsymbol{A'}$ given by the transformation

$$\Phi' = \Phi(x) - \frac{\partial \Lambda}{\partial t} \tag{2.7}$$

$$\boldsymbol{A'} = \boldsymbol{A} + \boldsymbol{\nabla}\Lambda, \tag{2.8}$$

where Λ is a generic twice-differentiable function of space and time. This implies that a given configuration of the electromagnetic field can be represented not only by one pair of potentials $(\Phi, \boldsymbol{A})$, but by a whole class of them. This symmetry is called a gauge symmetry.

Maxwell's Equations and the way they transform when performing a change of reference frame were of fundamental importance in the development of special relativity [Einstein, 1905]; in fact, they transform well under Lorentz Transformations, and they can be written in an explicitly covariant fashion as

$$\partial_\alpha F^{\alpha\beta} = 4\pi j^\beta, \tag{2.9}$$

$$\iota^{\alpha\beta\gamma}\partial_\alpha F_{\beta\gamma} = 0, \tag{2.10}$$

where $j^\mu = (\rho, \boldsymbol{j})$ is the four-current, $\iota^{\alpha\beta\gamma}$ is the Levi-Civita tensor, and $F^{\mu\nu}$ is the electromagnetic field tensor; Eq. (2.10) is automatically satisfied if $F^{\mu\nu}$ is antisymmetric and, by introducing the four-potential $A^\mu(x) = (\Phi(x), \boldsymbol{A}(x))$, we can see that with $F_{\mu\nu} = \partial_\mu A_\nu - \partial_\nu A_\mu$ Eqs. (2.9) and (2.10) are equivalent to Eqs. (2.1) to (2.4).

Another equation of fundamental importance in Classical Electrodynamics is the equation that describes the force an electromagnetic field exerts on a charged particle, the so-called Lorentz force [Jackson, 1999; Berestetskii et al., 1982]. Relativistically, Lorentz force is a four-force (i. e., it is equal to the derivative of the

four-momentum of a particle with respect to the particle's proper time); for an electron, is given by [Landau and Lifshitz, 1975]:

$$\frac{\mathrm{d}p^{\mu}(s)}{\mathrm{d}s} = \frac{e}{m} F^{\mu\nu}(s) p_{\nu}(s), \tag{2.11}$$

where s is the proper time of the electron.

2.1.1 Electron in a Plane Wave: Trajectory and Emitted Radiation

All the processes studied in this thesis take place in vacuum solutions of Maxwell's equations with plane-wave symmetry, i. e., solutions that depend only on one phase $\eta = x_{\mu} k^{\mu}$, where $k^{\mu} = \omega(1, \boldsymbol{n})$ is a constant four-vector, $\boldsymbol{n}$ is a unit vector and ω is a frequency [Landau and Lifshitz, 1975]. For definiteness, let us choose a reference frame where $\boldsymbol{k}$ lies along the positive z axis; then $\eta = \omega(t - z) = \omega\phi$, where we introduced the light-cone coordinate $\phi = t - z$. The coordinate ϕ, together with $T = (t + z)/2$, x, and y, form a so-called light-cone basis, and as we will see it is a natural coordinate system to use for plane waves.

Let us focus on linearly polarized plane waves, i. e., electromagnetic fields given by the four-potential

$$\mathcal{A}^{\mu}_{L}(\phi) = \mathcal{A}^{\mu}\, \psi_{L}(\phi); \tag{2.12}$$

in this parametrization of $\mathcal{A}^{\mu}_{L}(\phi)$, the shape function $\psi_{L}(\phi)$, with modulus always smaller than one, encodes the spatiotemporal variation of the vector potential, and $\mathcal{A}^{\mu} = (0, -m\xi/e, 0, 0)$ is a constant amplitude which gives us a purely spatial polarization vector ϵ^{μ} directed along the x axis. With these particular choices we have fixed the gauge; in particular, the Lorentz gauge condition

$$\partial_{\mu} \mathcal{A}^{\mu}_{L}(\phi) = 0 \tag{2.13}$$

is satisfied, and this implies that $\boldsymbol{k} \cdot \boldsymbol{A} = \boldsymbol{k} \cdot \boldsymbol{\epsilon} = 0$.

The dynamics of an electron moving in the field given by the vector potential of Eq. (2.12) can be calculated via Eq. (2.11). In some special cases, such as in plane wave backgrounds, it is possible to solve exactly equations related to Eq. (2.11) that take into account the action of the electron's field on the electron itself [Di Piazza, 2008]. The force resulting from the electron's self interaction is called radiation reaction, and although it is a topic of great interest (see [Di Piazza et al., 2012] and references therein), we will not touch it in this thesis, and we will assume that the electron is not affected by its own field in classical calculations. This assumption is well-justified, as Landau and Lifshitz have shown in [Landau and Lifshitz, 1975], when the frequency ω and the typical value F of the components of the external electromagnetic field satisfy

$$\alpha\omega \ll m, \qquad F \ll \frac{F_{cr}}{\alpha}, \tag{2.14}$$

where $F_{cr} = m^2/|e|$ is the critical field of QED that we mentioned in Chapter 1.

If we neglect the field generated by the electron itself in the total electromagnetic tensor $F^{\mu\nu}$ (i. e., $F^{\mu\nu} = \partial^\mu \mathcal{A}_L^\nu - \partial^\nu \mathcal{A}_L^\mu$ is given only by the laser field) it is possible to solve Eq. (2.11) exactly. In particular, let us consider an electron counterpropagating with respect to the plane wave (i. e., with initial momentum $\boldsymbol{p} = (0, 0, -p)$ and $p > 0$); it is clear in this case that the electric force will act only on the x-component of p^μ (see the definition of $\boldsymbol{\mathcal{A}}$). Moreover, the magnetic force will never have any nonzero y-component since the magnetic field is always parallel to the y axis. As a result of how the electromagnetic forces act, the motion of an electron counterpropagating with respect to a laser field is confined to a plane parallel to the xz plane.

In the non-counterpropagating case, this is not true anymore, but in any case we can solve Eq. (2.11) to find the trajectory of the electron $\boldsymbol{r}(t)$ and its velocity at every time $\boldsymbol{\beta}(t)$. A moving electron is a source for the electromagnetic field, and via the Liénard-Wiechert potentials [Jackson, 1999; Landau and Lifshitz, 1975] it is possible to write the energy (differential in frequency ω' and solid angle Ω') it radiates away as

$$\frac{\mathrm{d}E}{\mathrm{d}\omega' \mathrm{d}\Omega'} = \frac{e^2 \omega'^2}{4\pi^2} \left| \int_{-\infty}^{+\infty} \mathrm{d}t\, \boldsymbol{n} \times (\boldsymbol{n} \times \boldsymbol{\beta}(t))\, e^{i\omega'(t - \boldsymbol{n}\cdot\boldsymbol{r}(t))} \right|^2 . \tag{2.15}$$

It is possible to write Eq. (2.15) in a covariant way by introducing the electron's "trajectory" in momentum $p^\mu(t)$ and the emitted photon's wave four-vector k'^μ; in particular, in the case of a plane wave, since the four-momentum of the electron and its position depend only on the plane wave's phase and $(p(\eta)k)$ is a constant of motion we can write [Mackenroth, 2014]

$$\frac{\mathrm{d}E}{\mathrm{d}\omega' \mathrm{d}\Omega'} = \frac{e^2 \omega'^2}{4\pi^2} \left| \int_{-\infty}^{+\infty} \mathrm{d}\eta\, \frac{p^\mu(\eta)}{(kp_0)}\, e^{i(kr(\eta))} \right|^2 , \tag{2.16}$$

where we indicated with p_0^μ the four-momentum of the electron asymptotically in the past. We report here that the four-momentum of an electron as a function of the plane wave phase can be calculated from Eq. (2.11) and it is equal to [Berestetskii et al., 1982]:

$$p^\mu(\phi) = p_0^\mu - e\mathcal{A}_L^\mu(\phi) + e\frac{(p'_j \mathcal{A}_L(\phi))}{(kp_0)} k^\mu - \frac{e^2}{2}\frac{\mathcal{A}_L^2(\phi)}{(kp_0)} k^\mu . \tag{2.17}$$

The trajectory of the electron can be obtained by integrating Eq. (2.17); depending on the shape of $\psi_L(\phi)$, this integral can be evaluated analytically.

2.2 Quantum Electrodynamics

As mentioned in Chapter 1, if an electron of momentum p^μ feels in its rest frame an electric field $\mathcal{E}_{rf}$ with strength comparable to $\mathcal{E}_{cr} = m^2/|e|$, the effects due to

Strong-Field QED become non negligible. It is possible to formulate this condition in an explicitly covariant way via the Lorenz- and gauge-invariant parameter

$$\chi = \frac{|e|\sqrt{|(F_{\mu\nu}p^{\nu})^2|}}{m^3}, \tag{2.18}$$

which reduces to $\mathcal{E}_{rf}/\mathcal{E}_{cr}$ in the rest frame of the electron. Thus, when $\chi \sim 1$ it is not possible to consider quantum effects as a small perturbation to classical mechanics, and this can be quite problematic if also $\xi > 1$, because multiphoton effects become increasingly important.

In order to derive how the electromagnetic field couples to particles such as electrons, i. e., fermions, let us consider the Dirac Lagrangian for an electron:

$$\mathcal{L}_D = \bar{\psi}\left(i\not{\partial} - m\right)\psi, \tag{2.19}$$

where $\psi(x)$ is the spinor field operator, $\bar{\psi}$ is its conjugate, and $\not{\partial} = \gamma^{\mu}\partial_{\mu}$ (the components of γ^{μ} are Dirac's matrices) [Peskin and Schroeder, 1995]. If we apply the Euler-Lagrange equations to $\mathcal{L}_D$, we can obtain the Dirac equation for ψ (and its conjugate for $\bar{\psi}$). Since physical quantities such as probabilities and currents are invariant under the local transformation

$$\psi(x) \longrightarrow e^{iq\Lambda(x)}\psi(x) \tag{2.20}$$

$$\bar{\psi}(x) \longrightarrow \bar{\psi}(x)e^{-iq\Lambda(x)} \tag{2.21}$$

(this is called a U(1) gauge transformation), one could ask himself whether also $\mathcal{L}_D$ is invariant or, at least, whether it changes by a total derivative with respect to time. Indeed, it is possible to show that, due to the transformation properties of the term

$$\bar{\psi}(x)\partial_{\mu}\psi(x) \to \bar{\psi}(x)e^{-iq\Lambda(x)}\partial_{\mu}e^{iq\Lambda(x)}\psi(x) = \bar{\psi}(x)(\partial_{\mu} + iq(\partial_{\mu}\Lambda(x)))\psi(x), \tag{2.22}$$

the Dirac Lagrangian $\mathcal{L}_D$ is not invariant under a gauge transformation: it transforms as

$$\mathcal{L}_D \longrightarrow \mathcal{L}_D + iq(\partial_{\mu}\Lambda)\bar{\psi}\psi. \tag{2.23}$$

In order to make $\mathcal{L}_D$ gauge-invariant, we could introduce new terms to it that will add to the total Lagrangian, once transformed, a term $-iq(\partial_{\mu}\Lambda)\bar{\psi}\psi$; in this way, the sum of $\mathcal{L}_D$ and of the new terms will indeed be gauge-invariant.

Let us introduce a vector field, $A_{\mu}(x)$, and minimally couple it to $\mathcal{L}_D$; this means that we need to replace the derivative ∂_{μ} appearing in Eq. (2.19) with $D_{\mu} = \partial_{\mu} + iqA_{\mu}(x)$ (in an equivalent way, we could regard this operation as an addition to the Lagrangian of an interaction term proportional to $A_{\mu}\bar{\psi}\gamma^{\mu}\psi$). Suppose also that the field $A_{\mu}(x)$ transforms into $A'_{\mu}(x)$ under a gauge transformation. Then, after a few elementary steps, one obtains

$$\bar{\psi}(x)\not{D}\psi(x) \to \bar{\psi}(x)\partial_{\mu}\psi(x) + iq\bar{\psi}(x)\gamma^{\mu}\left[(\partial_{\mu}\Lambda(x)) + A'_{\mu}(x)\right]\psi(x), \tag{2.24}$$

and so if we want a gauge-invariant Lagrangian the field A_μ must transform as $A_\mu \to A'_\mu = A_\mu + (\partial_\mu \Lambda)$, that is, as the four-vector potential of the electromagnetic field. In fact, it is easy to see that with the above-sketched procedure, we have derived the Lagrangian of the electromagnetic field coupled to fermions.

The starting point of QED is, in fact, the Lagrangian we just derived. For clarity, let us write it down explicitly:

$$\mathcal{L}_{QED} = \bar{\psi}\left(i\not{D} - m\right)\psi - \frac{1}{16\pi}F_{\mu\nu}F^{\mu\nu}, \tag{2.25}$$

where

$$D_\mu(x) = \partial_\mu + ieA_\mu(x) \tag{2.26}$$

is the so-called covariant derivative; it is the term $ieA_\mu(x)$ in it that couples the electromagnetic field to the Dirac field.

2.2.1 Furry Picture and Volkov States

As mentioned in Chapter 1, if the coupling term in $\mathcal{L}_{QED}$ cannot be considered as a small perturbation to the free fields anymore, the usual perturbative approach to QED is doomed to failure; this can happen, for instance, when electrons propagate through a laser field with $\xi \gtrsim 1$.

Arguably, the most widely adopted tool to circumvent this issue in Strong-field physics is the "Furry Picture" [Furry, 1951]. It is based on the observation that an intense electromagnetic field such as, for instance, a laser beam or an atomic nucleus, can be regarded as a classical source. Then, the electromagnetic field can be split into two parts: the intense field, which is considered as an external classical field, unaffected by the dynamics of the rest of the system, and a quantized part. For the four-potential, this implies

$$A^\mu(x) = A^\mu_{\mathrm{Ext}}(x) + A^\mu_{\mathrm{Q}}(x), \tag{2.27}$$

where $A^\mu_{\mathrm{Ext}}(x)$ is the four-potential of the external field (and is a classical function) and $A^\mu_{\mathrm{Q}}(x)$ is a quantum field (operator-valued distribution). After splitting $A^\mu(x)$ in this way, the covariant derivative appearing in $\mathcal{L}_{QED}$ can be written as

$$D^\mu(x) = \tilde{D}^\mu(x) + ieA^\mu_{\mathrm{Q}}(x), \tag{2.28}$$

where

$$\tilde{D}^\mu(x) = \partial^\mu + ieA^\mu_{\mathrm{Ext}}(x). \tag{2.29}$$

The terms of $\mathcal{L}_{QED}$ which contain the fermion field can then be split as

$$\bar{\psi}\left(i\not{\tilde{D}} - m\right)\psi - e\bar{\psi}A^\mu_{\mathrm{Ext}}\psi = \mathcal{L}_0 + \mathcal{L}_{int}. \tag{2.30}$$

If one is able to solve the field equations induced by $\mathcal{L}_0$, one can perform a unitary transformation on the states and operators of the theory analogous to what is done in the interaction picture, and treat as a small interaction not the whole interaction $-e\bar{\psi}A^\mu\psi$, but only $-e\bar{\psi}A^\mu_{\text{Ext}}\psi$. For a strong laser field, these two terms are radically different, because whereas the first one scales as $\sim e\xi$, the second one does not depend explicitly on ξ.

There is a technical difference with respect to the interaction picture because the Hamiltonian that gives the free evolution of states is time-dependent (see [Fradkin et al., 1991] for more details).

The equation that governs the modes of the fermion field in the Furry picture is nothing but the Dirac equation in the presence of an external electromagnetic field. This equation can be solved analytically if the profile of the field is simple enough to allow it. In other cases, it could still be possible to solve the Dirac equation via approximate methods [Di Piazza, 2014; Heinzl and Ilderton, 2017*a*].

In case the external field can be considered as a plane-wave, it is indeed possible to solve the Dirac equation with such a background; the solutions of this equation are the Volkov states [Volkov, 1935]:

$$\Psi_{p,\sigma}(x) = \left[1 + \frac{e}{2(kp)}\not{k}\not{\mathcal{A}}_L(\eta)\right] u_{p,\sigma}\, e^{-ipx - i\int_{-\infty}^{\eta}\left[\frac{e}{(kp)}(p\mathcal{A}_L(\eta')) - \frac{e^2}{2(kp)}\mathcal{A}_L^2(\eta')\right]\mathrm{d}\eta'}, \tag{2.31}$$

where $u_{p,\sigma}$ is a positive-energy spinor solution of the free Dirac equation, i. e.,

$$(\not{p} - m)\, u_{p,\sigma} = 0, \tag{2.32}$$

while $\overline{u}_{p,\sigma}u_{p,\sigma} = 2m$, and $\overline{u}_{p,\sigma} = u^\dagger_{p,\sigma}\gamma^0$. The Volkov state $\Psi_{p,\sigma}(x)$ is characterized by the four-momentum $p^\mu = (\varepsilon, \boldsymbol{p})$ and by the spin quantum number σ at $t \to -\infty$. Technically, the states in Eq. (2.31) are just the so-called Volkov in-states, although Volkov out-state only differ from the in-ones by a phase independent of the coordinates. The Volkov states are normalized as

$$\int \mathrm{d}^3x\, \Psi^\dagger_{p',\sigma'}(x)\Psi_{p,\sigma}(x) = (2\pi)^3\,(2\varepsilon)\,\delta(\boldsymbol{p} - \boldsymbol{p}')\,\delta_{\sigma,\sigma'}. \tag{2.33}$$

It is convenient to write Volkov states in terms of a complete set of matrices (the so-called Ritus matrices [Ritus, 1985]), defined as

$$E_p(x) = \left[1 + \frac{e}{2(kp)}\not{k}\not{\mathcal{A}}_L(\eta)\right] e^{-ipx - i\int_{-\infty}^{\eta}\left[\frac{e}{(kp)}(p\mathcal{A}_L(\eta')) - \frac{e^2}{2(kp)}\mathcal{A}_L^2(\eta')\right]\mathrm{d}\eta'}, \tag{2.34}$$

in this way, we can write Volkov states simply as

$$\Psi_{p,\sigma}(x) = E_p(x)u_{p,\sigma}. \tag{2.35}$$

In Chapter 4 and Chapter 5, we will show how perturbative calculations with Volkov states are typically done, in the context of Nonlinear Single Compton Scattering.

Chapter 3

Numerical Methods

As we have mentioned in Chapter 1, the recent increase in the peak intensities of laser fields is essentially due to CPA [Strickland and Mourou, 1985] and OPCPA [Piskarskas et al., 1986]. Because both these techniques can produce only ultrashort laser pulses, the calculations of Strong-Field QED processes with such pulses as a background have to take into account the pulses' finite temporal duration. This poses some challenges because, as we will see in Chapter 4 and Chapter 5, in order to calculate Nonlinear Single Compton Scattering rates it is necessary to evaluate some integrals that contain the shape function of the laser. The situation is analogous for other processes, such as Nonlinear Breit-Wheeler Pair production. For specific shape functions it is possible to evaluate these integrals analytically, whereas in general this is not possible and it is necessary to perform the integration numerically. This can be a nontrivial task, because the above-mentioned integrals are typically strongly oscillating, and widely adopted quadrature methods (e. g. Simpson's rule) become less and less accurate as the frequency of oscillation of the integrand increases. In Section 3.1, we will review Filon's method [Filon, 1930], a quadrature scheme that instead is increasingly accurate with increasing frequency of the oscillation of the integrand.

Another tool that will be useful in the following chapters is Monte Carlo integration. This is because we will study the total energy (differential only in frequency) radiated by one electron in a wave packet state (Chapter 4) or by a two-electron wave packet (Chapter 5); in order to do so, we have to integrate the emission probability not only with respect to the direction of the emitted photon (which amounts to an integration over two polar angles), but also with respect to the initial momentum (or momenta) of the electron (or electrons). For such high-dimensional integrals, grid-based methods become increasingly less efficient, and Monte Carlo techniques are a natural choice. In Section 3.2 we will give an elementary explanation of how to perform an integral via Monte Carlo Integration, and also discuss a technique, Importance Sampling, that we used to speed up the

convergence of the integral.

3.1 Evaluation of Univariate Highly Oscillating Integrals

For nonoscillating integrands $f(x)$, a typical way to obtain quadrature formulae is given by the Newton-Cotes rules [Press et al., 2007], which can be derived by requiring that an integral should be approximated by the following weighted sum

$$I' = \int_{a'}^{b'} \mathrm{d}x' f(x') \approx \sum_{i=0}^{N} w'_i f(x'_i), \tag{3.1}$$

where the x'_is are $N+1$ equispaced points in $[a', b'] \subset \mathbb{R}$, with $x'_0 = a'$ and $x'_N = b'$. The weights w'_i appearing in Eq. (3.1) are then found by imposing that Eq. (3.1) is exact for polynomials of degree N; this condition implies a system of N equations that can be solved for w'_i. From this procedure, if we choose $N = 1$ we obtain the trapezoidal rule, while for $N = 2$ we can find another widely adopted method for numerical integration: Simpson's rule [Press et al., 2007]. All the rules that can be found with the method we illustrated are equivalent to approximating $f(x')$ with the only polynomial $p(x')$ of degree N which has the same value of $f(x')$ on the points x'_i (i. e., $f(x'_i) = p(x'_i)$ for every $i = 0, \ldots, N$), and using as an approximation to I' the integral of $p(x')$ on $[a', b']$ (which can be computed analytically). In many circumstances, applying directly Newton-Cotes rules with a high N, which is equivalent to approximating the whole function on $[a', b']$ with a high-order polynomial, yields unsatisfactory results; this is because of Runge's phenomenon [Runge, 1901]. In order to avoid the problems associated with high-order polynomial interpolations at equispaced points it is possible to divide $[a', b']$ in many subintervals and use in each of them a simpler Newton-Cotes scheme, e. g., the trapezoidal rule or Simpson's rule. Alternatively, one can relax the assumption that the x'_is are equispaced, and expand f on a basis of Chebyshev polynomials [Press et al., 2007].

For oscillating integrals of the kind we will need to compute in Chapter 4 and Chapter 5, i. e.,

$$\int_{\tilde{a}}^{\tilde{b}} \mathrm{d}x\, \tilde{f}(x) e^{i\tilde{\omega}\tilde{g}(x)}, \tag{3.2}$$

even if $|\tilde{g}(x)| < 1$, the error associated with Newton-Cotes schemes increases with $\tilde{\omega}$. In order to have sufficient accuracy one needs to divide $[a', b']$ into an unacceptably large number of subintervals. However, we will see that, since in our calculations $\tilde{g}(x)$ will always be strictly monotone, it is possible via a change of variables to transform the integral in Eq. (3.2) into

$$I = \int_{a}^{b} \mathrm{d}x\, f(x) e^{i\omega x}, \tag{3.3}$$

where $f(x)$ is smooth and not highly oscillating. Then a simple way to calculate I numerically is the so-called Filon's method [Filon, 1930]. It is equivalent to partitioning the interval $[a, b]$ in many subintervals where $f(x)$ (and not the whole integrand, $f(x)e^{i\omega x}$, as in the Newton-Cotes' formulae) can be approximated well by a second-order polynomial, and then one is left with the integral of a second-order polynomial multiplied by $e^{i\omega x}$, which can be performed analytically. For definiteness, let us partition $[a, b]$ in $2M + 3$ equispaced points x_k, where $x_0 = a$, and $x_{2M+2} = b$. Then, we can write

$$I = \sum_{i=0}^{M} \int_{x_{2i}}^{x_{2i+2}} \mathrm{d}x\, f(x) e^{i\omega x}. \tag{3.4}$$

Let us focus our attention now to each of the $M + 1$ integrals of Eq. (3.4); as we mentioned above, it would often be a bad choice just to use Eq. (3.1), because this would be equivalent to approximating, in this case, the oscillating function $f(x)e^{i\omega x}$ with a polynomial. A better choice is given by

$$\int_{x_{2i}}^{x_{2i+2}} \mathrm{d}x\, f(x) e^{i\omega x} \approx w_{2i} f(x_{2i}) + w_{2i+1} f(x_{2i+1}) + w_{2i+2} f(x_{2i+2}), \tag{3.5}$$

and also here, as one does for Newton-Cotes formulae, in order to find the weights w appearing in Eq. (3.5) we require that Eq. (3.5) is exact for functions $f(x)$ which are polynomials of second degree. This means that in each subinterval $[x_{2i}, x_{2i+2}]$ we could integrate the monomials 1, x, and x^2, and Eq. (3.5) needs to be exact. Thus, if we introduce the moments

$$J_{i,j} = \int_{x_{2i}}^{x_{2i+2}} \mathrm{d}x\, x^j e^{i\omega x}, \tag{3.6}$$

the following set of equations has to hold:

$$J_{i,0} = w_{2i} + w_{2i+1} + w_{2i+2}, \tag{3.7}$$

$$J_{i,1} = w_{2i} x_{2i} + w_{2i+1} x_{2i+1} + w_{2i+2} x_{2i+2}, \tag{3.8}$$

$$J_{i,2} = w_{2i} x_{2i}^2 + w_{2i+1} x_{2i+1}^2 + w_{2i+2} x_{2i+2}^2. \tag{3.9}$$

By introducing h as the spacing between successive points x_k and x_{k+1} (i. e., $h = (x_{2i+1} - x_{2i}) = (x_{2i+2} - x_{2i})/2$ for every $i = 0, \ldots, M$) we find that the weights are given by

$$w_{2i} = \frac{1}{2h^2} \left[J_{i,2} + J_{i,0} x_{2i+1} x_{2i+2} - (x_{2i+1} + x_{2i+2}) J_{i,1} \right], \tag{3.10}$$

$$w_{2i+1} = -\frac{1}{2h^2} \left(2J_{i,2} + 2J_{i,0} x_{2i} x_{2i+2} - 4x_{2i+1} J_{i,1} \right), \tag{3.11}$$

$$w_{2i+2} = \frac{1}{2h^2} \left[J_{i,2} + J_{i,0} x_{2i} x_{2i+1} - (x_{2i} + x_{2i+1}) J_{i,1} \right]. \tag{3.12}$$

$$\tag{3.13}$$

One can then evaluate analytically the moments defined in Eq. (3.6) and obtain

$$J_{i,0} = \int_{x_{2i}}^{x_{2i+2}} \mathrm{d}x e^{i\omega x} = \frac{e^{i\omega x_{2i+2}} - e^{i\omega x_{2i}}}{i\omega} \tag{3.14}$$

$$J_{i,1} = \int_{x_{2i}}^{x_{2i+2}} \mathrm{d}x x e^{i\omega x} = \frac{e^{i\omega x_{2i+2}} - e^{i\omega x_{2i}}}{\omega^2} + \frac{e^{i\omega x_{2i+2}} x_{2i+2} - e^{i\omega x_{2i}} x_{2i}}{i\omega} \tag{3.15}$$

$$J_{i,2} = \int_{x_{2i}}^{x_{2i+2}} \mathrm{d}x x^2 e^{i\omega x} = -2\frac{e^{i\omega x_{2i+2}} - e^{i\omega x_{2i}}}{i\omega^3} + 2\frac{e^{i\omega x_{2i+2}} x_{2i+2} - e^{i\omega x_{2i}} x_{2i}}{\omega^2} + 2\frac{e^{i\omega x_{2i+2}} x_{2i+2}^2 - e^{i\omega x_{2i}} x_{2i}^2}{i\omega}; \tag{3.16}$$

these expressions allow us to calculate explicitly the values of the weights. After the long but straightforward procedure of substituting everything back into Eq. (3.5), we find

$$\int_{x_{2i}}^{x_{2i+2}} \mathrm{d}x\, f(x) e^{i\omega x} \approx h\Big[i\alpha_{\mathrm{Filon}}(\Theta)\left(f_{2i} e^{i\omega x_{2i}} - f_{2i+2} e^{i\omega x_{2i+2}}\right) + \frac{\beta_{\mathrm{Filon}}(\Theta)}{2}\left(f_{2i} e^{i\omega x_{2i}} + f_{2i+2} e^{i\omega x_{2i+2}}\right) + \gamma_{\mathrm{Filon}}(\Theta) f_{2i+1} e^{i\omega x_{2i+1}}\Big], \tag{3.17}$$

where, for the sake of a simpler notation, we indicated with f_k the value of f at the point x_k (i. e., $f_k = f(x_k)$) and we introduced the parameters

$$\Theta = h\omega, \tag{3.18}$$

$$\alpha_{\mathrm{Filon}}(\Theta) = \frac{1}{\Theta} + \frac{\sin 2\Theta}{2\Theta^2} - \frac{2\sin^2\Theta}{\Theta^3} \tag{3.19}$$

$$\beta_{\mathrm{Filon}}(\Theta) = 2\left(\frac{1+\cos^2\Theta}{\Theta^2} - \frac{\sin 2\Theta}{\Theta^3}\right), \tag{3.20}$$

$$\gamma_{\mathrm{Filon}}(\Theta) = 4\left(-\frac{\cos\Theta}{\Theta^2} + \frac{\sin\Theta}{\Theta^3}\right). \tag{3.21}$$

If we now insert Eq. (3.17) into Eq. (3.4) and perform the sum over i, we obtain Filon's formula for the quadrature of univariate highly oscillating integrals:

$$\int_a^b \mathrm{d}x\, f(x) e^{i\omega x} \approx h\Bigg\{ i\alpha_{\mathrm{Filon}}(\Theta)\left(f_0 e^{i\omega x_0} - f_{2M+2} e^{i\omega x_{2M+2}}\right) + \beta_{\mathrm{Filon}}(\Theta)\left[\sum_{i=0}^{M+1}\left(f_{2i} e^{i\omega x_{2i}}\right) - \frac{1}{2}\left(f_0 e^{i\omega x_0} + f_{2M+2} e^{i\omega x_{2M+2}}\right)\right] + \gamma_{\mathrm{Filon}}(\Theta)\sum_{i=0}^{M} f_{2i+1} e^{i\omega x_{2i+1}}\Bigg\}. \tag{3.22}$$

The error associated with this procedure is of the order of h^4. It is possible to show that in the limit of $\Theta \to 0$ Eq. (3.22) reduces to Simpson's rule applied to the integrand $f(x)e^{i\omega x}$. However, notice that, because of how α_{Filon}, β_{Filon}, and γ_{Filon} are defined, for $\Theta \ll 1$ there can be significant numerical errors due to cancellation. This means that, depending on the value of ω, one has to use either Filon's method or Simpson's rule.

3.2 Monte Carlo Integration

In deterministic numerical quadrature techniques, the integration domain is divided in many elementary subdomains where the integrand is sufficiently regular (i. e., it can be approximated well by a low-order polynomial). Then, the value of the integrand is readily calculated by summing over all the contributions coming from the different subdomains.

In practice, deterministic methods are not always viable; this is because of the so-called "Curse of dimensionality" [Bellman, 1961]. In fact, methods that work on an equispaced grid with N points in one dimension can be extended in d dimensions by forming a d-dimensional grid, consisting of N^d points. Notice that the exponential scaling of the number of points with d already hints at some practical problem in doing computations with a potentially very large grid. Moreover, for the sake of definiteness, let us consider the one-dimensional trapezoidal rule and its extension to d-dimensions. With the trapezoidal rule in one dimension, we can integrate numerically twice-differentiable functions with an error that scales as $1/N^2$. If we extend it to a d-dimensional grid, it can be shown that the error scales as $1/N^{2/d}$; for large d this is a very slow scaling, and it can render calculations impossible even with modern computers.

With Monte Carlo methods [Metropolis et al., 1953; Caflisch, 1998], it is possible to do much better. The main idea behind Monte Carlo techniques of integration is to sample the integrand at N random points of the domain, instead of sampling it on some grid chosen deterministically, and estimate the value of the integral via these random samples of the integrand. The Law of Large Numbers [Taylor, 1998] guarantees that the deviation of this estimate with respect to the true value of the integral will decrease as $1/\sqrt{N}$, regardless of the dimensionality of the integration domain. Although this asymptotic behavior of the integral is not optimal for integrals in few dimensions, it is much better than deterministic methods in high dimensions (with the notable exception of methods based on sparse grids [Smolyak, 1963; Bungartz and Griebel, 2004]).

3.2.1 Uniform Sampling

Let us evaluate a one-dimensional integral via arguably the simplest Monte Carlo technique: uniform sampling. Consider the integral

$$I = \int_a^b f(x)\,\mathrm{d}x, \tag{3.23}$$

where $[a, b] \subset \mathbb{R}$ and f is a continuous function. By multiplying and dividing by the size of the interval, $(b - a)$, we obtain

$$I = (b-a)\frac{\int_a^b f(x)\,\mathrm{d}x}{(b-a)} = (b-a)\langle f\rangle, \tag{3.24}$$

where $\langle f\rangle$ is the mean value of f over the interval $[a, b]$. It is possible to calculate $\langle f\rangle$ with the aid of the Law of Large Numbers [Taylor, 1998]; this theorem in the present context implies that if $x_1, \ldots, x_N$ are random variables uniformly distributed on $[a, b]$, then the average value $\langle f\rangle$ on $[a, b]$ can also be calculated as

$$\langle f\rangle = \lim_{N\to\infty} \frac{1}{N}\sum_{i=1}^{N} f(x_i). \tag{3.25}$$

In practice, one cannot evaluate the infinite sum in Eq. (3.25), and so it has to be truncated at some finite N, i. e., what one can actually calculate in a finite time is

$$\langle f_N\rangle = \frac{1}{N}\sum_{i=1}^{N} f(x_i). \tag{3.26}$$

An estimator for the error associated with this procedure is the so-called "standard deviation of the mean"; that is, if the variance of f on the interval $[a, b]$ is $\sigma_f^2 = \langle f^2\rangle - \langle f\rangle^2$, where

$$\langle f^2\rangle = \frac{\int_a^b f(x)^2\mathrm{d}x}{(b-a)}, \tag{3.27}$$

then the standard deviation associated to $\langle f\rangle$ is

$$\sigma_{\langle f\rangle} = \frac{\sigma_f}{\sqrt{N}}. \tag{3.28}$$

The quantity σ_f depends on the shape of the function f on the interval $[a, b]$; however, by increasing N, we can reduce the standard deviation of the mean, thus rendering arbitrarily unlikely that the truncated average $\langle f_N\rangle$ deviates much from the true value of $\langle f\rangle$.

In conclusion, with the Monte Carlo technique, the integral I can be calculated as

$$I \approx \frac{(b-a)}{N} \sum_{i=1}^{N} f(x_i), \tag{3.29}$$

with an associated statistical error $(b-a)\sigma_f/\sqrt{N}$. Notice that this procedure can be extended trivially to multi-dimensional integration domains. In particular, whereas when extending to multiple dimensions integration rules derived in one dimension the error decreases much more slowly with N with respect to the one-dimensional case, with Monte Carlo integration the statistical error is always asymptotically decreasing as $1/\sqrt{N}$ for any dimension. This is, as mentioned at the beginning of this section, quite a bad scaling in one dimension (even the trapezoid rule can do much better), but one of the best and simplest methods to use in many dimensions.

3.2.2 Importance Sampling

In order to reduce the error associated with the Monte Carlo integration, there are several strategies; one of them is the so-called "Importance Sampling" [Caflisch, 1998]. The idea behind it is that in order to reduce the variance of the mean $\sigma_{\langle f \rangle}$, aside from increasing N, one can also try to reduce σ_f. For instance, in Section 3.2.1 we sampled uniformly the domain of f; thus, regions where f varies only a little are sampled as densely as regions where f varies significantly; it is intuitively clear that this is not an optimal strategy, and, by improving the sampling procedure, it could be possible to reduce σ_f.

Let us consider a probability density $g(x)$ on $[a, b]$; trivially, by multiplying and dividing the integrand by the probability density function $g(x)$ (normalized to one), we can write the integral in Eq. (3.25)) as

$$I = \int_a^b \frac{f(x)}{g(x)}\, g(x)\mathrm{d}x. \tag{3.30}$$

The integral I, as written in Eq. (3.30), can be interpreted as the expectation value of $f(x)/g(x)$ over the probability density function $g(x)$, i. e., $\langle f/g \rangle_g$. This quantity can be calculated as

$$\langle f/g \rangle_g = \lim_{N\to\infty} \frac{1}{N} \sum_{i=1}^{N} f(x_i)/g(x_i), \tag{3.31}$$

where the random variables $x_1, \ldots, x_N$ are distributed according to $g(x)$. Also in this case, one can truncate the sum in Eq. (3.31) at a finite N; the estimator for the deviation of the result of this procedure from the true value of $\langle f/g \rangle$ is given by

$$\sigma_{\langle f/g \rangle} = \frac{\sigma_{f/g}}{\sqrt{N}}, \tag{3.32}$$

where $\sigma^2_{f/g}$ is the variance of the random variable $f(x_i)/g(x_i)$ (the same for every i). If $\sigma^2_{f/g} < \sigma^2_f$, it is clear that, even for the same number of samples N, the value of the integral calculated with importance sampling will (on average) deviate less from the true value of the integral with respect to the same calculation done with uniform sampling.

If one chooses a uniform probability density function on $[a, b]$ as $g(x)$, it is trivial to show that one obtains again the results of Section 3.2.1, as it is also trivial to show that if $g(x) = f(x)$ this variance is zero. This last point should not be surprising, because if $f(x) = g(x)$ it means that f is a probability density function on $[a, b]$, thus its integral on the interval $[a, b]$ is normalized to one, and one does not need numerical integration schemes at all to know this. An appropriate choice of $g(x)$ can improve the accuracy of the result calculated via Monte Carlo Integration without introducing a significant overhead on computation time [Caflisch, 1998], provided that generating random numbers with a probability density function given by $g(x)$ is not much more expensive than to generate them uniformly distributed. The choice of a good $g(x)$ for importance sampling can be guided by the shape of the integrand; in Chapter 4 and Chapter 5 we will need to calculate expectation values over Gaussian wave packets, thus the choice of the Gaussian function that appears in the integrand as a prefactor in that case will be the most natural choice.

Chapter 4

Nonlinear Compton Scattering of an Electron Wave Packet

In this chapter we will show explicitly how to calculate the emission rates of Nonlinear Single Compton Scattering for an electron initially in a wave packet state; by doing this, we will also obtain the emission rates for electrons initially in a Volkov state as a particular case. We will then study how the emission rates depend on the shape of the wave packet and, by performing analytic calculations on the simpler case when the laser field is assumed monochromatic, derive some characteristic parameters that determine how the emitted radiation depends on the momentum of the electron. Moreover, we will plot some radiation spectra (either fully differential with respect to the emitted photon's energy and direction, or with one of these two quantities integrated out).

These results have already been published, and this chapter is adapted from [Angioi et al., 2016].

4.1 Theory

As we mentioned in Chapter 1, Nonlinear Single Compton Scattering is a process in which an electron scatters with an intense electromagnetic field and, while exchanging multiple photons with the laser, it emits a nonlaser photon. In the computation of Nonlinear Ningle Compton Scattering rates, perturbative approaches with respect to the laser field can quickly become impractical, when a sufficiently strong incoming electromagnetic field is considered Di Piazza et al. [2012]. This happens when the incoming laser field is such that $\xi \gtrsim 1$. The laser fields which reach these intensities consist of an enormous number of coherent photons; this makes it possible [Berestetskii et al., 1982] to neglect the quantum nature of the laser field and to treat it as a classical background electromagnetic field. Thus, we can perform our calculations in the Furry picture (see Chapter 2) and split the

electromagnetic field four-vector potential into two parts: a classical part, that accounts for the intense laser field, and a quantized part, that accounts for all the other excitations of the electromagnetic field (i. e., the radiation emitted by the electron). After that, the electron-positron field is quantized by taking into account exactly the background laser field, and if we approximate the laser field as a plane wave, a convenient basis of states will be given by Volkov states [Volkov, 1935; Berestetskii et al., 1982].

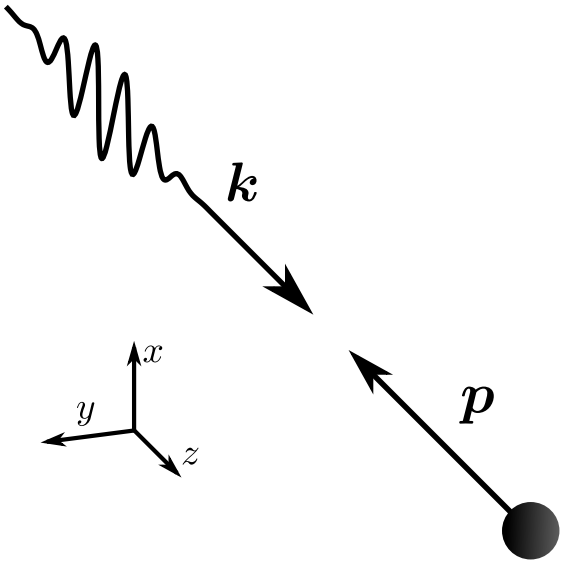

Figure 4.1 Representation of the reference frame we have chosen for the calculation of NSCS rates.

We assume that the incoming laser field is described by the linearly-polarized plane-wave four-vector potential

$$\mathcal{A}_L^\mu(\eta) = \mathcal{A}^\mu \, \psi_L(\eta). \tag{4.1}$$

Here, $\mathcal{A}^\mu = (0, \boldsymbol{\mathcal{A}})$ is a constant four-vector, the direction of $\boldsymbol{\mathcal{A}}$ defines the laser's polarization and its amplitude $\mathcal{A} = \mathcal{E}/\omega$ is related to the peak laser's intensity I as $I = \omega^2\mathcal{A}^2/4\pi = \mathcal{E}^2/4\pi$, and $\psi_L(\eta)$ is a function of the laser phase $\eta = (kx)$ describing the shape of the plane wave and such that $|\psi_L(\eta)| \sim |\mathrm{d}\psi_L(\eta)/\mathrm{d}\eta| \leq 1$. It is convenient to use a frame of reference in which one of the spatial axes is directed along $\boldsymbol{k}$, and another one is directed along the same direction as $\boldsymbol{\mathcal{A}}$. For a depiction of the frame of reference we have chosen in our calculations, see Fig. 4.1. Thereby, we have $\eta = \omega(t - z) = \omega\phi$, where $\phi = t - z$. It is also useful to introduce a coordinate $T = (t + z)/2$, linearly independent of ϕ, x and y, and the quantities ϕ, T, x and y provide the so-called light-cone coordinates of the space-time point x^μ. The factor of $1/2$ in the definition of T is arbitrary and we have included it in order

for the Jacobian of the transformation from Cartesian coordinates to light-cone ones to be unity. In the following, we will define the $-$ (minus) contravariant component of any four-vector a^μ to be $a^- = a^0 - a^3$.

In the expression of $A^\mu(\eta)$ we have introduced the shape function $\psi_L(\eta)$ in order to model short laser pulses; a typically chosen [Mackenroth and Di Piazza, 2011] shape function $\psi_L(\eta)$ for this purpose is (see Fig. 4.2)

$$\psi_L(\eta) = \begin{cases} \sin^4\left(\frac{\eta}{2n_C}\right)\sin(\eta+\eta_0) & \text{if } \eta \in [0, 2\pi n_C], \\ 0 & \text{otherwise.} \end{cases} \tag{4.2}$$

In this parametrization of the laser field we have introduced the parameters n_C, the number of cycles contained in the laser pulse, and η_0, the carrier-envelope phase (CEP) of the laser pulse. In all numerical calculations in the following, we will

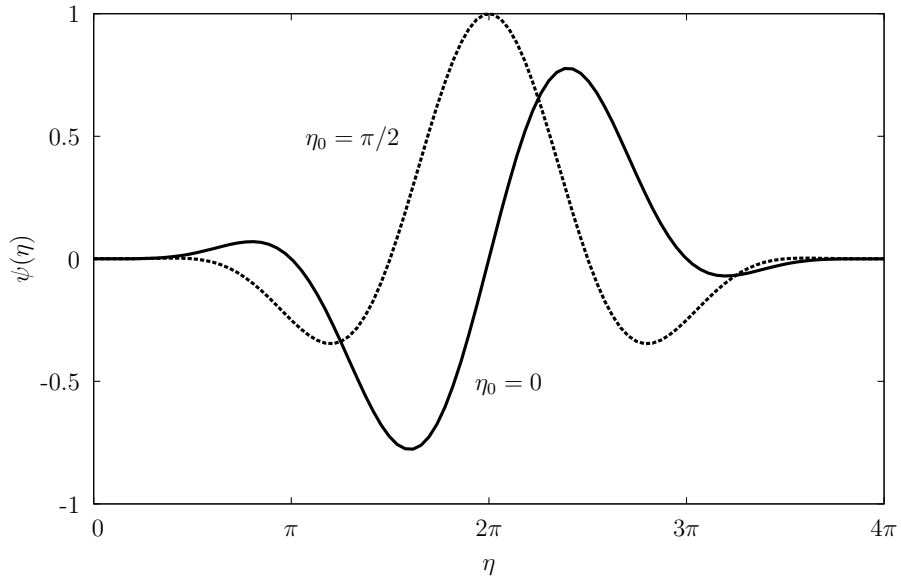

Figure 4.2 The function $\psi_L(\eta)$ for a two-cycle laser pulse ($n_C = 2$) and two choices of the carrier-envelope phase η_0. The solid curve corresponds to $\eta_0 = 0$, while the dotted one corresponds to $\eta_0 = \pi/2$.

chose $\eta_0 = 0$, $n_c = 2$, and $\omega = 1.55$ eV.

As previously mentioned, it is convenient to describe the initial and final quantum state of the electron in a basis of the solutions of the Dirac equation in the presence of the background field $\mathcal{A}^\mu_L(\eta)$, i. e., in a basis of Volkov states; in order to make this chapter self-contained, we report here their definition (see Section 2.2.1 for more details on Volkov states):

$$\Psi_{p,\sigma}(x) = \left[1 + \frac{e}{2(kp)}\not{k}\not{\mathcal{A}}_L(\eta)\right] u_{p,\sigma}\, e^{-ipx - i\int_{-\infty}^{\eta}\left[\frac{e}{(kp)}(p\mathcal{A}_L(\eta')) - \frac{e^2}{2(kp)}\mathcal{A}_L^2(\eta')\right]\mathrm{d}\eta'}, \tag{4.3}$$

As we have mentioned above, in our calculations for the NSCS rates we assume that the initial state of the electron is a wave packet made of a superposition of Volkov states with different momenta and a given spin number σ:

$$\Phi_\sigma(x) = \int \frac{\mathrm{d}^3p}{(2\pi)^3(2\varepsilon)}\, \rho(\boldsymbol{p})\, \Psi_{p,\sigma}(x). \tag{4.4}$$

Here, $\rho(\boldsymbol{p})$ is a complex-valued scalar weighting function; in order for the state $\Phi_\sigma(x)$ to be normalized to unity, $\rho(\boldsymbol{p})$ needs to be normalized in a covariant way as

$$\int \frac{\mathrm{d}^3p}{(2\pi)^3(2\varepsilon)}\, |\rho(\boldsymbol{p})|^2 = 1. \tag{4.5}$$

The leading order S-matrix element relative to the process of the emission of a photon, with wave four-vector $k'^\mu = (\omega', \boldsymbol{k}')$ and polarization four-vector $\epsilon_l'^\mu$, by an electron in the initial state $\Phi_\sigma(x)$ is given by

$$S_{fi} = -ie\sqrt{4\pi} \int \mathrm{d}^4x\, \frac{\mathrm{d}^3p}{(2\pi)^3(2\varepsilon)}\, \rho(\boldsymbol{p})\, \overline{\Psi}_{p',\sigma'}(x)\, \not{\epsilon}_l'^{*} e^{ik'x}\, \Psi_{p,\sigma}(x). \tag{4.6}$$

We notice that among the space-time coordinates the integrand in Eq. (4.6) depends non-trivially only on ϕ, while on the other three space-time coordinates we have integrals that evaluate to three delta functions. It is thus possible [Mackenroth and Di Piazza, 2011] to write S_{fi} in the form

$$S_{fi} = -ie\sqrt{4\pi}\,(2\pi)^3 \int \frac{\mathrm{d}^3p}{(2\pi)^3(2\varepsilon)}\, \rho(\boldsymbol{p})\, (\overline{u}_{p',\sigma'} M_{fi} u_{p,\sigma})\, \delta^{(-,x,y)}(p - k' - p')\,; \tag{4.7}$$

here, $\delta^{(-,x,y)}(p - k' - p')$ is a three dimensional Dirac delta that ensures the conservation of the three contravariant components $-$, x and y of the total four-momentum and

$$M_{fi} = \not{\epsilon}_l'^{*} f_0 + e\left(\frac{\not{\mathcal{A}}\not{k}\not{\epsilon}_l'^{*}}{2(kp')} + \frac{\not{\epsilon}_l'^{*}\not{k}\not{\mathcal{A}}}{2(kp)}\right) f_1 - \frac{e^2\mathcal{A}^2(k\epsilon_l'^{*})\not{k}}{2(kp)(kp')}\, f_2, \tag{4.8}$$

$$f_j = \int_{-\infty}^{+\infty} \mathrm{d}\eta\, \psi^j(\eta) e^{i\int_{-\infty}^{\eta}\mathrm{d}\eta'\left[\alpha\psi_L(\eta') + \beta\psi_L^2(\eta') + \gamma\right]}. \tag{4.9}$$

In Eq. (4.9) we have introduced the three parameters [Mackenroth and Di Piazza, 2011; Mackenroth, 2014]

$$\alpha = e\left[\frac{(p'\mathcal{A})}{(kp')} - \frac{(p\mathcal{A})}{(kp)}\right], \tag{4.10}$$

$$\beta = -\frac{e^2\mathcal{A}^2}{2}\, \frac{(k'k)}{(kp)(kp')}, \tag{4.11}$$

$$\gamma = \frac{(pk')}{(p'k)}. \tag{4.12}$$

The integrals f_j cannot in general be calculated analytically. Moreover, for $\xi \gg 1$, the integrands of the f_js become increasingly oscillating (notice how they depend on $\mathcal{A}^\mu$). However, it can be shown [Mackenroth, 2014] that for every η' it is

$$\alpha\psi_L(\eta') + \beta\psi_L^2(\eta') + \gamma > 0; \tag{4.13}$$

this implies that the definite integral over η' appearing in Eq. (4.9) is monotonically increasing with η. Thus, with a change of variables we can transform the exponent of e in Eq. (4.9) into a linear function, and the integral will have the same form as the one in Eq. (3.3), and this means it can be integrated numerically with Filon's method (see Section 3.1). Notice also that, even if the integral f_0 does not appear immediately convergent, it can be related to f_1 and f_2; in fact, via integration by parts, it can be proven that

$$\gamma f_0 = -\left(\alpha f_1 + \beta f_2\right). \tag{4.14}$$

It is worth mentioning that Eq. (4.14) can be interpreted as a manifestation of gauge invariance [Ilderton, 2011]. Thus, it is needed only to calculate numerically only the two oscillating integrals f_1 and f_2; f_0 can be calculated via Eq. (4.14).

In order to compute emission rates, it is necessary to calculate the square modulus of S_{fi}:

$$|S_{fi}|^2 = 4\pi e^2 \int \frac{\mathrm{d}^3p}{(2\varepsilon)}\,\frac{\mathrm{d}^3\tilde{p}}{(2\tilde{\varepsilon})}\;\rho^*(\tilde{\boldsymbol{p}})\,\rho(\boldsymbol{p})\,\left(\overline{u}_{p',\sigma'}M_{fi}u_{\tilde{p},\sigma}\right)^*\left(\overline{u}_{p',\sigma'}M_{fi}u_{p,\sigma}\right) \times \delta^{(-,x,y)}\left(p-k'-p'\right)\,\delta^{(-,x,y)}\left(\tilde{p}-k'-p'\right). \tag{4.15}$$

The integrations in Eq. (4.15) are along the components of $\boldsymbol{p}$ and $\tilde{\boldsymbol{p}}$ in Cartesian coordinates, while one of the delta functions in Eq. (4.15) is expressed in terms of light-cone coordinates. An easy way to perform these integrations is to change the measure for each momentum integration from $\mathrm{d}p_x\mathrm{d}p_y\mathrm{d}p_z = \mathrm{d}^2p_\perp\mathrm{d}p_z$ to $\mathrm{d}^2p_\perp\mathrm{d}p^-$; the Jacobian of this transformation is ε/p^-. Thus one can start from Eq. (4.15), change the integration measure to $\mathrm{d}^2p_\perp\mathrm{d}p^-\mathrm{d}^2\tilde{p}_\perp\mathrm{d}\tilde{p}^-$, perform the integrations in $\tilde{p}$ (that are just integrations of delta functions), and change back the measure to d^3p; this gives

$$|S_{fi}|^2 = 4\pi e^2 \int \frac{\mathrm{d}^3p}{(2\varepsilon)(2p^-)}\,|\rho(\boldsymbol{p})|^2\;\left|\overline{u}_{p',\sigma'}M_{fi}u_{p,\sigma}\right|^2\,\delta^{(-,x,y)}\left(p-k'-p'\right). \tag{4.16}$$

The unpolarized emission rate is obtained by integrating $|S_{fi}|^2$ over the electron's final momentum and on the wave-vector of the emitted photon, and by summing over the final electron spin and photon polarization, and averaging on the initial

electron spin [Peskin and Schroeder, 1995; Berestetskii et al., 1982]:

$$\mathrm{d}W = \frac{\mathrm{d}^3k}{(2\pi)^3(2\omega')} \int \frac{\mathrm{d}^3p'}{(2\pi)^3(2\varepsilon')} \frac{\mathrm{d}^3p}{(2\varepsilon)(2p^-)} \\ 4\pi e^2 \left|\rho(\boldsymbol{p})\right|^2 \delta^{(-,x,y)}\left(p - k' - p'\right) \frac{1}{2} \sum_{\sigma,\sigma',l} |\overline{u}_{p',\sigma'} M_{fi} u_{p,\sigma}|^2. \quad (4.17)$$

The integral on d^3p' can be readily evaluated with the same change of integration measure previously mentioned. By transforming the integral over $\boldsymbol{k}'$ in spherical coordinates ($\mathrm{d}^3k' = \omega'^2 \mathrm{d}\omega' \mathrm{d}\Omega'$) and remembering that the emission rate and the energy emission rate are related by $\mathrm{d}E = \omega' \mathrm{d}W$, it is possible to write the angular differential emission rate as

$$\frac{\mathrm{d}E}{\mathrm{d}\omega' \mathrm{d}\Omega'} = \int \frac{\mathrm{d}^3p}{(2\pi)^3(2\varepsilon)} \left|\rho(\boldsymbol{p})\right|^2 \frac{e^2\omega'^2}{2(4\pi)^2 p^- q^-} \sum_{\sigma,\sigma',l} |\overline{u}_{q,\sigma'} M_{fi} u_{p,\sigma}|^2, \quad (4.18)$$

where q^μ is a four vector such that $q^- = p^- - k'^{,-}$, $q_{x,y} = p_{x,y} - k'_{x,y}$ and $q^+ = (q^0+q^3)/2 = (m^2+q_x^2+q_y^2)/2q^-$ ($q^2 = m^2$). The sum of the quantities $|\overline{u}_{q,\sigma'} M_{fi} u_{p,\sigma}|^2$ over the spins of the electron and polarization states of the photon can be evaluated explicitly with the aid of trace technology. We do not show that tedious calculation here, but in Appendix A we will derive a more general technique which will be useful for the calculation of NSCS rates when two electrons are interacting with the laser field; the rates for a single electron will then be presented as a special case. The remaining 3D integral over the momentum $\boldsymbol{p}$ can be evaluated numerically via the Monte Carlo Integration technique discussed in Section 3.2; in particular, we can see that the integrand contains a probability distribution function $|\rho(\boldsymbol{p})|^2$, which we can exploit, via importance sampling (see Section 3.2.2), in order to have faster convergence of the numerical calculation.

Equation (4.18) can be easily identified as the incoherent average, weighted by the modulus squared of $\rho(\boldsymbol{p})$, of the well-known expression for the differential spectrum of Nonlinear Single Compton Scattering for an electron with definite initial four-momentum p^μ and final four-momentum q^μ [Boca and Florescu, 2009; Mackenroth, 2014; Mackenroth and Di Piazza, 2011; Seipt and Kämpfer, 2011]

$$\frac{\mathrm{d}E_p}{\mathrm{d}\omega' \, \mathrm{d}\Omega'} = \frac{e^2\omega'^2}{2(4\pi)^2 \, p^- \, q^-} \sum_{\sigma,\sigma',l} \left|\overline{u}_{q,\sigma'} \, M_{fi} \, u_{p,\sigma}\right|^2 . \quad (4.19)$$

Thus, there are no quantum interference effects between initial states of the electron having different values of the momentum. The physical reason behind the absence of interference is that, in principle, by measuring the final state of the electron and of the emitted photon one can retrieve the initial momentum of the electron, and so the initial state of the electron amongst the ones contained in the initial superposition.

The results we presented so far allow us to state that, as far as one is interested in nonlinear single Compton scattering rates, the state of the initial electron can be described equivalently either with a superposition of states like the one in Eq. (4.4) or as a statistical mixture

$$\hat{\rho}_\sigma = \int \frac{\mathrm{d}^3 p}{(2\pi)^3 (2\varepsilon)} \, |\rho(\boldsymbol{p})|^2 \, |\Psi_{p,\sigma}\rangle\langle\Psi_{p,\sigma}| \tag{4.20}$$

where the weighting function $\rho(\boldsymbol{p})$ is the same of Eq. (4.4) and $\Psi_{p,\sigma}(x) = \langle x|\Psi_{p,\sigma}\rangle$.

4.2 Electron Wave Packets with Normally Distributed Longitudinal Momentum

After describing the theory for arbitrary superpositions of Volkov states (for a given spin quantum number), in this section and in Section 4.3 we will make an explicit choice of $\rho(\boldsymbol{p})$. Let the initial state of the electron be a superposition of states with momenta always directed almost in the opposite direction of the laser wave-vector $\boldsymbol{k}$; this means, for the choice of the frame of reference we adopted in Section 4.1, that the momenta $\boldsymbol{p}$ are all directed almost along the negative z direction. In particular, we assume that the distribution of the momenta is a triple Gaussian distribution, with average momentum $\overline{\boldsymbol{p}} = (0, 0, \overline{p}_z)$, with $\overline{p}_z < 0$, and with variance $\sigma^2_{p_T}$ along the x and y direction and $\sigma^2_{p_z}$ along the z-direction; thus the initial wave packet is given by

$$\Phi_\sigma(x) = \int \frac{\mathrm{d}^3 p}{(2\pi)^3} \frac{1}{\sigma_{p_T} \sqrt[4]{\sigma^2_{p_z} (2\pi)^3}} \, e^{-\frac{(p_z - \overline{p}_z)^2}{4\sigma^2_{p_z}}} \, e^{-\frac{p_x^2 + p_y^2}{4\sigma^2_{p_T}}} \, \Psi_{p,\sigma}(x). \tag{4.21}$$

In the present section the transverse variance $\sigma^2_{p_T}$ is assumed to be sufficiently small, so that all transverse momenta (p_x, p_y) in Eq. (4.18) can be set equal to zero. Thus, the electron effectively always collides head-on with the laser beam.

In order to understand the modifications brought about by the electron being described by the wave packet in Eq. (4.21), we show in Fig. 4.3 the emission spectrum in the forward (negative z) direction for an incoming electron with definite momentum with components $p_x = p_y = 0$, and $p_z = -4.2$ GeV (electron beams with this energy can be even be produced via all-optical setups, see [Malka et al., 2008; Leemans et al., 2014]) interacting with a laser of intensity $I \approx 4.3 \times 10^{20}$ W/cm^2. The above parameters correspond to $\xi = 10$ and $\chi \approx 0.50$. As one can see from Fig. 4.3, the spectra in the regime of $|p_z| \gg m$ and $\xi \gg 1$ exhibit a large number of narrow peaks, and this is typical for differential NSCS rates [Mackenroth and Di Piazza, 2011; Mackenroth, 2014]. The position of the peaks depends on the momentum of the electron; in particular, from Fig. 4.4 one can deduce that, as the electron's initial momentum increases in modulus, these peaks will be shifted

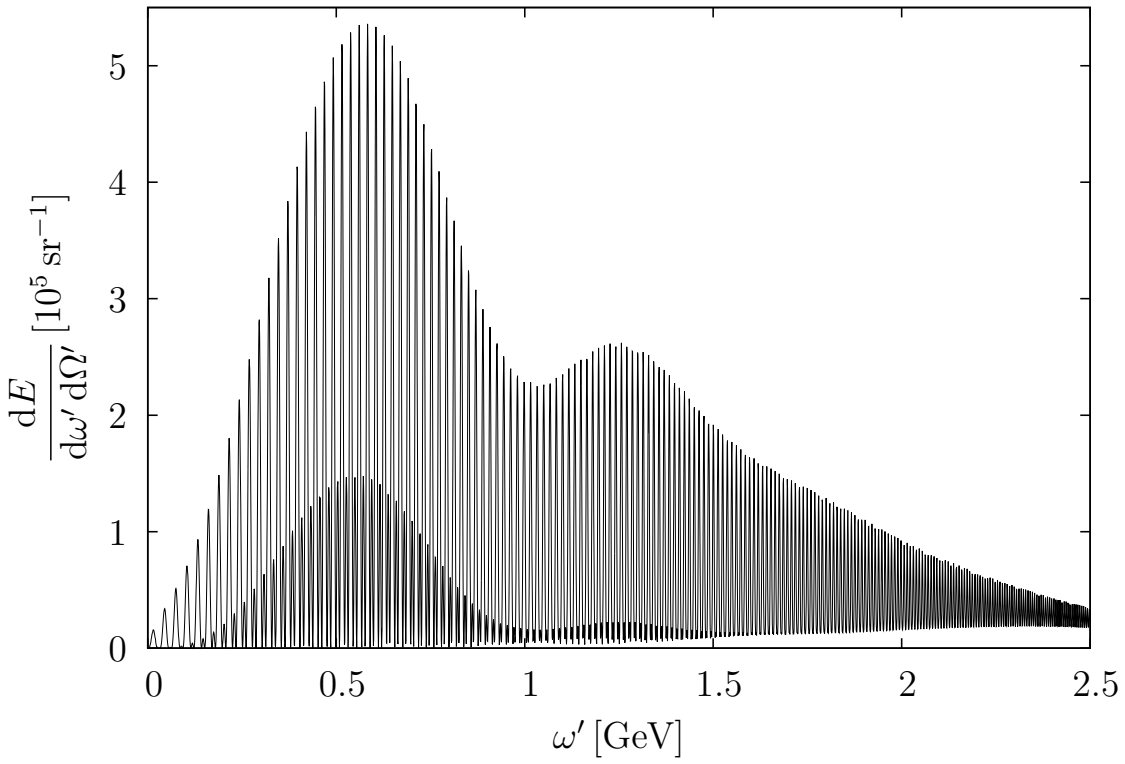

Figure 4.3 Energy emission spectrum along the negative z-direction for an incoming electron with definite initial momentum $\boldsymbol{p} = (0, 0, -4.2\ \mathrm{GeV})$ interacting with a laser of intensity $I \approx 4.3 \times 10^{20}\ \mathrm{W/cm^2}$.

towards higher frequencies. These shifts depend on the position of the peaks itself, i. e., different peaks are shifted by a different amount, when changing p_z. More specifically, by changing p_z of the same amount, the higher peak frequencies will be shifted more than the lower ones. The above results can be easily explained as a result of the Doppler effect. For the sake of simplicity, let us consider here the idealized case of a monochromatic laser field (with laser photon energy ω), and calculate in this simpler case how the emission frequencies are shifted as a function of p_z. In the monochromatic case, in fact, the frequency of the n^{th} harmonic emission along the negative z direction is given by [Ritus, 1985]

$$\omega'_n = \frac{n(pk)}{(pn') + \left(n + \frac{m^2\xi^2}{4(pk)}\right)(kn')} = \frac{n\omega\,(\varepsilon - p_z)^2}{m^2\left(1 + \frac{\xi^2}{2}\right) + 2n\omega(\varepsilon - p_z)} = \frac{\zeta_n}{1 + 2\zeta_n}(\varepsilon - p_z), \tag{4.22}$$

where $n'^{\mu} = (1, \boldsymbol{k}'/\omega')$ (in our frame of reference, $n'^{\mu} = (1, 0, 0, -1)$ and where we

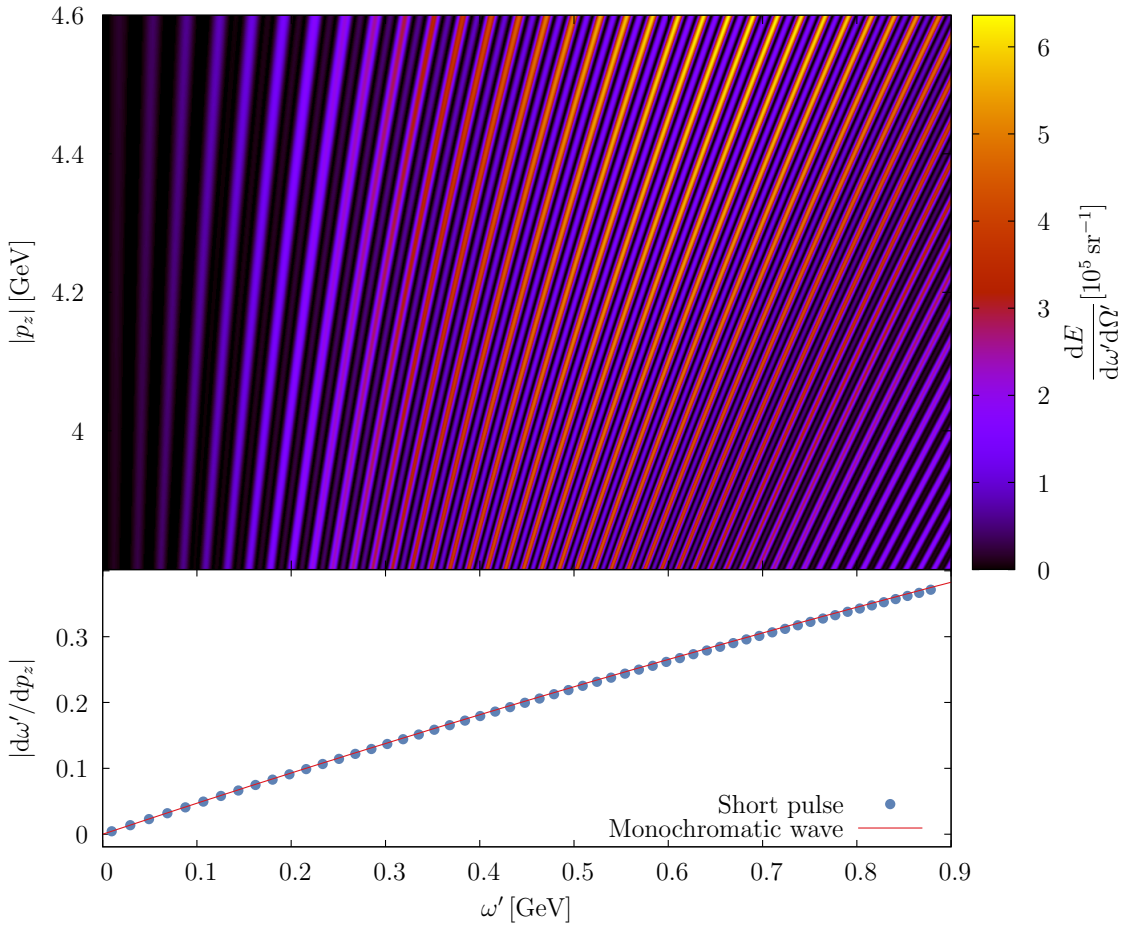

Figure 4.4 Change of the emission spectrum for an electron with definite initial momentum $(0, 0, p_z)$ as a function of $|p_z|$ (Fig. 4.3 corresponds to a section of the upper part of this figure for $p_z = -4.2$ GeV). In the range considered, the position of the peaks increases linearly with p_z, albeit with different slopes depending on the position of the peak. Some of these slopes were computed numerically and are shown in the bottom part of the plot (blue dots), together with the same quantity computed analytically for a monochromatic pulse (red continuous line).

have introduced the dimensionless parameter

$$\zeta_n = \frac{n\omega(\varepsilon - p_z)}{m^2\left(1+\frac{\xi^2}{2}\right)}. \tag{4.23}$$

By means of a first-order expansion with respect to a shift in momentum Δp_z, we can estimate the relative shift of the emission frequencies when slightly changing the value of p_z:

$$\frac{\Delta\omega_n'}{\omega_n'} = \frac{1}{\omega_n'}\frac{\partial\omega_n'}{\partial p_z}\Delta p_z = -2\,\frac{1+\zeta_n}{1+2\zeta_n}\,\frac{\Delta p_z}{\varepsilon}. \tag{4.24}$$

In the case of an ultrarelativistic electron, and in the relevant regime $\xi \gg 1$, it is $\varepsilon \approx |p_z|$ and $\zeta_n \approx 2n\chi/\xi^3$, such that we obtain

$$\frac{\Delta\omega_n'}{\Delta|p_z|} \approx 4\,\frac{\zeta_n(1+\zeta_n)}{(1+2\zeta_n)^2}. \tag{4.25}$$

As it can be easily shown, the quantity $\Delta\omega_n'/\Delta|p_z|$ increases monotonically with the harmonic number, in agreement with the findings in Fig. 4.4.

Notice that Eq. (4.25) is valid only for a monochromatic laser field, whereas we are interested here in the case of short pulses, i. e., pulses also characterized by a certain spread $\Delta\omega$ around a central angular frequency ω. It is thus interesting to compare the relative shift due to an uncertainty of p_z to the one due to an indeterminacy on the value of ω. In analogy to what we have discussed for Eq. (4.24), one can derive a similar relation, for a variation $\Delta\omega$ of the laser angular frequency. By adding the resulting expression to Eq. (4.24) and by assuming again that $|\bar{p}_z| \gg m$ and $\xi \gg 1$, it is possible to obtain the first-order relative variation of ω_n' with respect to the relative variations of ω and p_z as:

$$\frac{\Delta\omega_n'}{\omega_n'} \approx \frac{1}{1+2\zeta_n}\,\frac{\Delta\omega}{\omega} + 2\,\frac{1+\zeta_n}{1+2\zeta_n}\,\frac{\Delta|p_z|}{|p_z|}. \tag{4.26}$$

Since $\zeta_n > 0$ it is clear that for comparable relative variations in ω and p_z, the induced shift due to the spread in the incoming electron momentum is larger. From the aforementioned properties of the emitted photon's spectrum of a monochromatic initial electron we can infer the final spectrum when the state $\Phi_\sigma(x)$ of Eq. (4.4) is considered, since the emission spectrum resulting from that state, as it was shown above, is a weighted average of monochromatic emission spectra with different p_z. The sharp peaks present in the spectrum for a fixed value of p_z will be differently shifted and will tend to fill the valleys present in the spectrum relative to another value of p_z; when averaging many of these spectra, the net effect is a smoothing of the final spectrum.

Moreover, we have already mentioned the fact that the shift induced by the spread in the electron momentum is larger for higher emission frequencies. Thus,

the portion of the spectrum that will be smoothed earlier, i. e., even for relatively small values of σ_{p_z}, is that at high frequencies of the emitted photon. Indeed, this is the result we obtain in Fig. 4.5, where the final photon energy spectrum for different values of σ_{p_z} is plotted (the numerical parameters are the same as in Fig. 4.3 and the average value of the initial momentum of the electron is $\bar{\boldsymbol{p}} = (0, 0, -4.2\ \mathrm{GeV})$). We have chosen values of the standard deviation σ_{p_z} equal to 0.5%, 1% or 5% of the

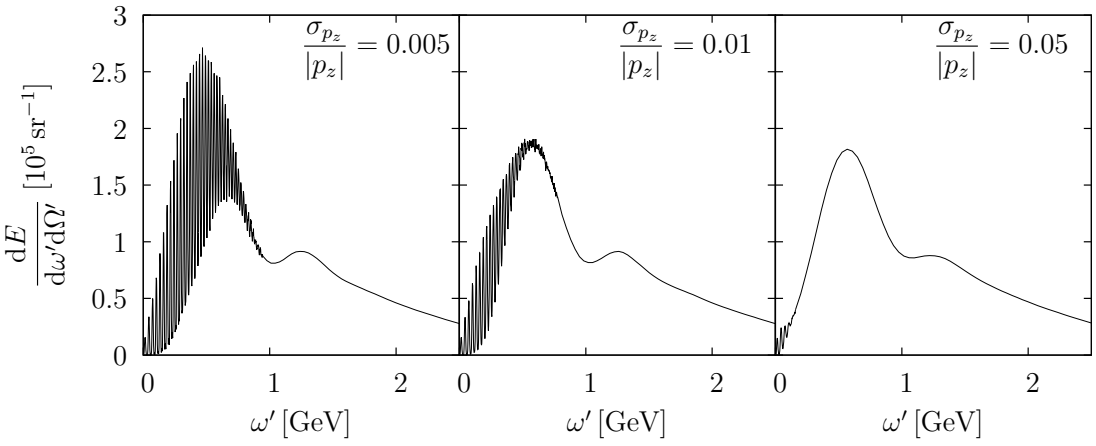

Figure 4.5 Emission spectra along the negative z-direction for an electron wave packet with $\bar{\boldsymbol{p}} = (0, 0, -4.2\ \mathrm{GeV})$ interacting with a laser pulse of peak intensity $I \approx 4.3 \times 10^{20}\ \mathrm{W/cm^2}$ for different values of the spread of the longitudinal momentum.

incoming momentum, corresponding to 21 MeV, 42 MeV or 210 MeV, respectively. Even when the relative indeterminacy on the momentum is only 0.5%, we can see that the height of the highest peaks is reduced by a factor of about two, and all the oscillatory features at $\omega' \gtrsim 1$ GeV are completely washed out (see Fig. 4.3 and Fig. 4.5). For larger values of σ_{p_z}, these effects are even more evident also for the lowest part of the spectrum. Concerning the choice of σ_{p_z} and in general of the properties of the wave packet $\Phi_\sigma(x)$ a comment is in order. In fact, in general, the state $\Phi_\sigma(x)$ describes a single electron. The properties of the corresponding wave packet depend on how the electron is produced and accelerated [Baum, 2013], and are in principle different from, for example, the corresponding properties of an electron bunch. However, in our case, as we have seen, the spectra for the state $\Phi_\sigma(x)$ coincide with those obtained by considering a corresponding electron bunch with an average electron number equal to unity. In this respect, the values of the momentum spreads are chosen according to the features of electron beams, which can be obtained presently experimentally [Leemans et al., 2014].

4.3 Multivariate Gaussian Wave Packets

We now turn our attention to the experimentally more realistic situation of an electron wave packet that can also have non-zero components of the transverse momentum. Our choice for the initial state is as in Eq. (4.21) but this time the variance $\sigma_{p_T}^2$ is assumed not to be small. Also in this case, as we did in Section 4.2, we will first consider how the spectrum of electrons initially in a Volkov state in a monochromatic field is modified as a function of the components of the initial momentum. Then, starting from those considerations, we will focus onto the case of an electron wave packet in a short laser pulse.

In order to understand how the emission spectrum is altered by the possibly non-zero value of the transverse components of the initial momentum, we show how the harmonic frequencies along the negative z-direction are shifted as the transverse momentum $p_T = \sqrt{p_x^2 + p_y^2}$ varies. We can thus proceed in analogy to the derivation of Eq. (4.25). The starting point is the initial form of ω_n' in Eq. (4.22), which can be rewritten in the more convenient form

$$\omega_n' = \frac{n\omega\,(\varepsilon - p_z)^2}{m^2\left(1 + \frac{\xi^2}{2}\right) + p_T^2 + 2n\omega(\varepsilon - p_z)}, \tag{4.27}$$

showing the explicit dependence also on p_T^2 (remember that now also the energy ε depends on p_T^2). By expanding ω_n' around $p_T = 0$ we obtain

$$\frac{\Delta\omega_n'}{\omega_n'} = \frac{1 - (\varepsilon/n\omega - 1)\zeta_n}{1 + 2\zeta_n}\frac{\Delta p_T^2}{\varepsilon(\varepsilon - p_z)}, \tag{4.28}$$

where all the energies are calculated at $p_T = 0$. This equation shows that again the relative shift depends on the harmonic number n. In a typical scenario where $\varepsilon \approx |p_z|$ and $\xi \gg 1$, the same approximations as in Section 4.2 can be applied. The result for $\Delta\omega_n'$ reads

$$\Delta\omega_n' = \zeta_n \frac{1 + \zeta_n - \varepsilon\chi/\xi^3\omega}{(1 + 2\zeta_n)^2}\frac{\Delta p_T^2}{\varepsilon}, \tag{4.29}$$

with ζ_n given in Eq. (4.23), which in the current approximations ($\varepsilon \approx |p_z|$, $\xi \gg 1$) is approximately equal to $n\chi/\xi^3$. Equation (4.29) shows that an important role is played by the parameter $\mu = \varepsilon\chi/\xi^3\omega$. If we want to consider the quantum regime where $\chi \sim 1$, which for $\xi \sim 10^2$ means that electron energies in the GeV-range are required, we can safely assume that $\mu \gg 1$. Moreover, for $\zeta_n \gg 1$ the emission spectrum is suppressed [Ritus, 1985] such that we can conveniently further approximate the expression for $\Delta\omega_n'$ as

$$\Delta\omega_n' = -\frac{\varepsilon\chi}{\xi^3\omega}\frac{\zeta_n}{(1 + 2\zeta_n)^2}\frac{\Delta p_T^2}{\varepsilon}. \tag{4.30}$$

From this expression we could expect as Δp_T^2 increases a negative shift of the harmonics, which becomes less pronounced at $\zeta_n \ll 1$ (low harmonics) and at $\zeta_n \gg 1$ (high harmonics). This is confirmed by Fig. 4.6, where we calculated for some values of n how the curves $\omega'_n = \omega'_n(p_T)$ depend on p_T , with the numerical parameters: $p_z = -4.2$ GeV and $I \approx 1.1 \times 10^{20}$ W/cm^2 ($\xi = 5$, $\chi \approx 0.25$, and $\mu \approx 5.4 \times 10^6$).

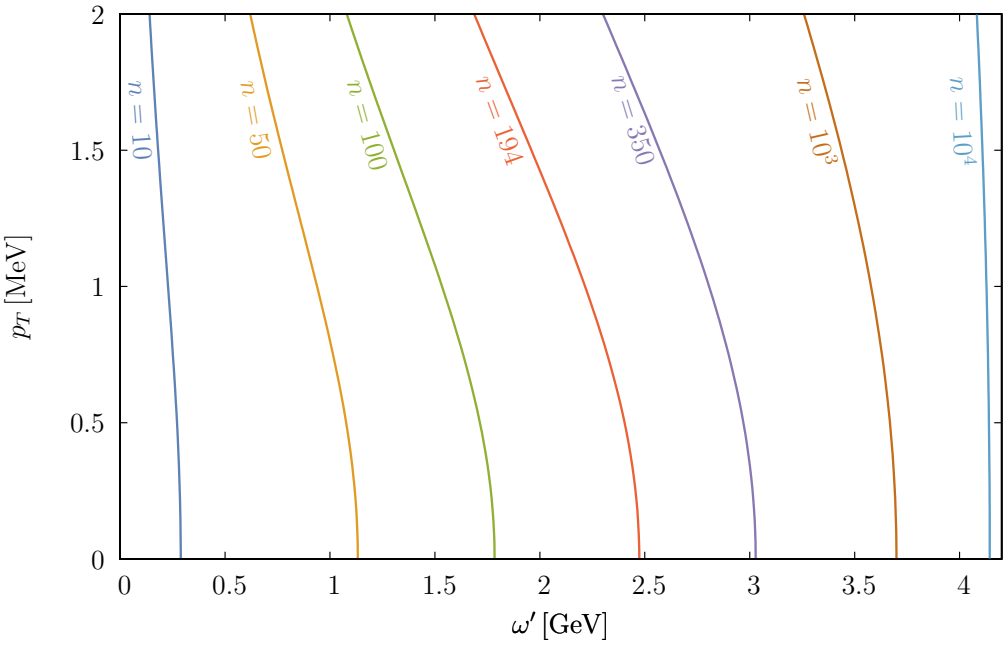

Figure 4.6 Shift of the emission frequencies ω'_n along the negative z-direction for different values of n as a function of p_T (vertical axis). The numerical parameters are $p_z = -4.2$ GeV and $I \approx 1.1 \times 10^{20}$ W/cm^2.

A typical collection of monochromatic emission spectra along the forward direction is shown in Fig. 4.7, where the electron has initially $p_z = -4.2$ GeV and either $p_y = 0$ or $p_x = 0$ (we recall that p_x (p_y) is the component of the momentum along the direction of the electric (magnetic) field of the laser), and is interacting with a short laser pulse with $I \approx 1.1 \times 10^{20}$ W/cm^2 ($\xi = 5$, $\chi \approx 0.25$). Apart from exhibiting the already mentioned shift of the peak frequencies as one of the transverse components varies, we also observe that by varying p_y by about 1-2 electron masses the spectrum is significantly suppressed. The reason is that the observation direction is the forward direction and that the angular emission range of the electron along the magnetic field of the laser is of about m/ε, whereas along the electric field of the laser, the electron emits up to angles of the order of $m\xi/\varepsilon$ [Mackenroth, 2014]. This is also the reason why the top panel of Fig. 4.7 shows that the values of p_x for which the emission is not negligible extends beyond

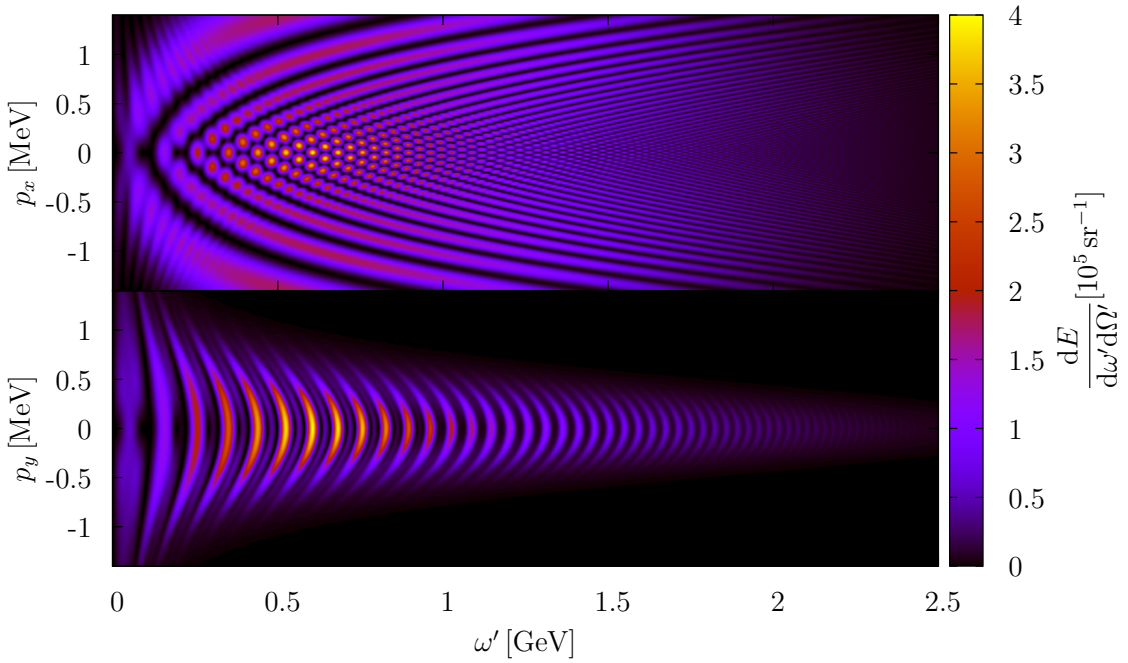

Figure 4.7 Emission spectra in the negative z-direction for electrons having initially $p_z = -4.2$ GeV and either $p_y = 0$ or $p_x = 0$, after the interaction with a short laser pulse with $I \approx 1.1 \times 10^{20}$ W/cm^2.

the plotted range. The large oscillations in the emitted intensity between successive peaks when varying p_x (top part of Fig. 4.7) are also worth noticing: we can expect these oscillations to have an important effect when averaging many spectra, even for $\sigma_{p_T} \ll m\xi$.

The above observations are confirmed by numerical calculations. In Fig. 4.8 (Fig. 4.9), we show the effects on the spectrum of the emitted photon along the negative z direction (or, in Fig. 4.9, along a direction that lies on the xz-plane, the laser polarization-propagation plane, and forms an angle $\theta = m\xi/2\bar{\varepsilon}$ with the negative z-axis, where $\bar{\varepsilon}$ is the average initial electron energy) of having either $\sigma_{p_T} \neq 0$ or $\sigma_{p_z} \neq 0$, or both σ_{p_T} and σ_{p_z} different from zero (in the first two cases σ_{p_z} and σ_{p_T}, respectively, are considered to be sufficiently small in order for their effects to be neglected, as explained below Eq. (4.21)).

In the numerical spectra in Fig. 4.8 and Fig. 4.9, the average initial momentum of the electron is $\bar{\boldsymbol{p}} = (0, 0, -4.2\ \mathrm{GeV})$, and the indeterminacy on the transverse components is $\sigma_{p_T} = 3 \times 10^{-4}\,|\bar{\boldsymbol{p}}|$, while the one on the z-component is $\sigma_{p_z} = 6 \times 10^{-2}\,|\bar{\boldsymbol{p}}|$ (these parameters for the electron beam are compatible with those in [Leemans et al., 2014]). The intensity of the laser field is $I \approx 1.1 \times 10^{20}$ W/cm^2 ($\xi = 5$, $\chi = \bar{\chi} \approx 0.25$ as calculated from the average electron momentum).

In Fig. 4.8 and Fig. 4.9 one can see that for the chosen values of the parameters

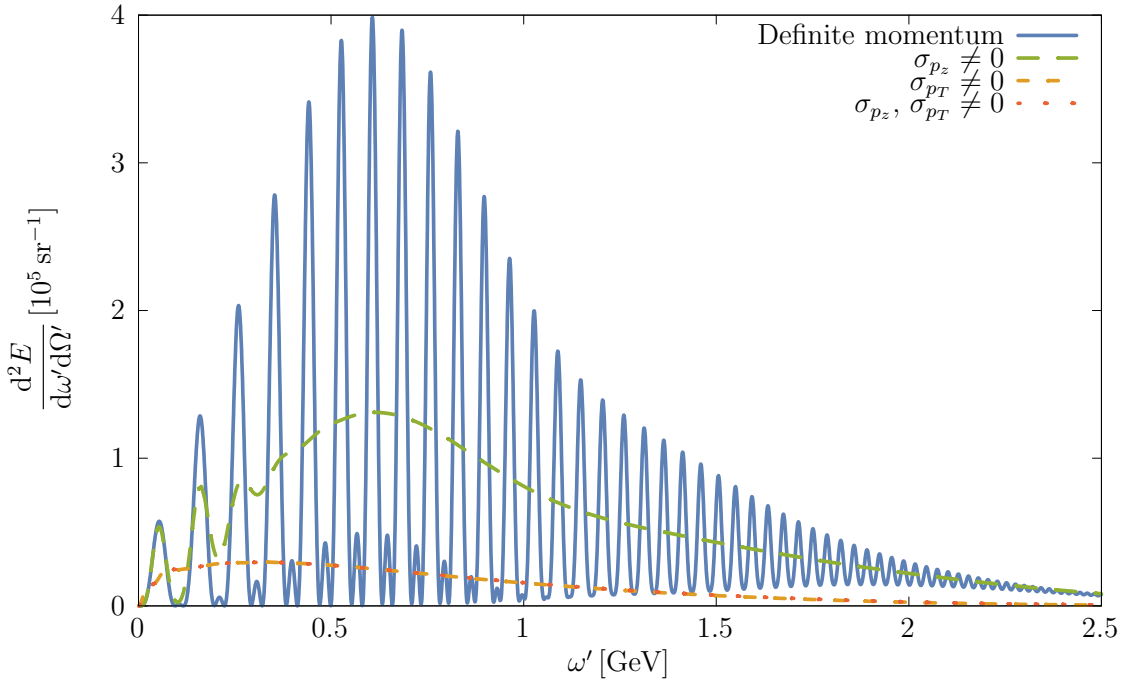

Figure 4.8 Energy emission spectrum in the negative z-direction, for some different initial electron states. Here, $\bar{\boldsymbol{p}} = (0, 0, -4.2 \text{ GeV})$, $\sigma_{p_T} = 3 \times 10^{-4} \, |\bar{\boldsymbol{p}}|$, and $\sigma_{p_z} = 6 \times 10^{-2} \, |\bar{\boldsymbol{p}}|$. The intensity of the laser field is $I \approx 1.1 \times 10^{20}$ W/cm^2.

σ_{p_T} and σ_{p_z}, the most dramatic alteration of the spectrum is due to the transverse momentum spread of the electron beam, even though its value is orders of magnitude smaller than the spread on p_z. In fact, the effect due to $\sigma_{p_T} \neq 0$ is so dominant that switching on also the longitudinal spread σ_{p_z} has no observable effect on the emitted spectrum (the dotted red curve is on top of the short-dashed orange one in both Fig. 4.8 and Fig. 4.9). As a result, the finer structures in the spectra are washed out and, in this respect, in order to at least partially observe them one should experimentally render the incoming electron beam as collimated as possible.

We also show in Fig. 4.10 the energy emission along a direction that lies on the laser polarization plane and forms an angle $m\xi/2\bar{\varepsilon}$ with the negative z-axis for $\chi = \bar{\chi} \approx 0.85$ (the parameters used for Fig. 4.10 are the same of Fig. 4.9, except that $I \approx 1.2 \times 10^{21}$ W/cm^2 corresponding to $\xi = 17$); the qualitative behavior for nonzero values of σ_{p_z} and σ_{p_T} is the the same as the one previously discussed. We should emphasize that, as we have already mentioned in the discussion below Eq. (4.30), the larger effect due to the transverse momentum uncertainty is also related to the fact that the considered spectra refer to some specific observation directions. In fact, if we integrate with respect to the emission angles the spectrum corresponding to the numerical parameters in Fig. 4.10, we obtain the results in

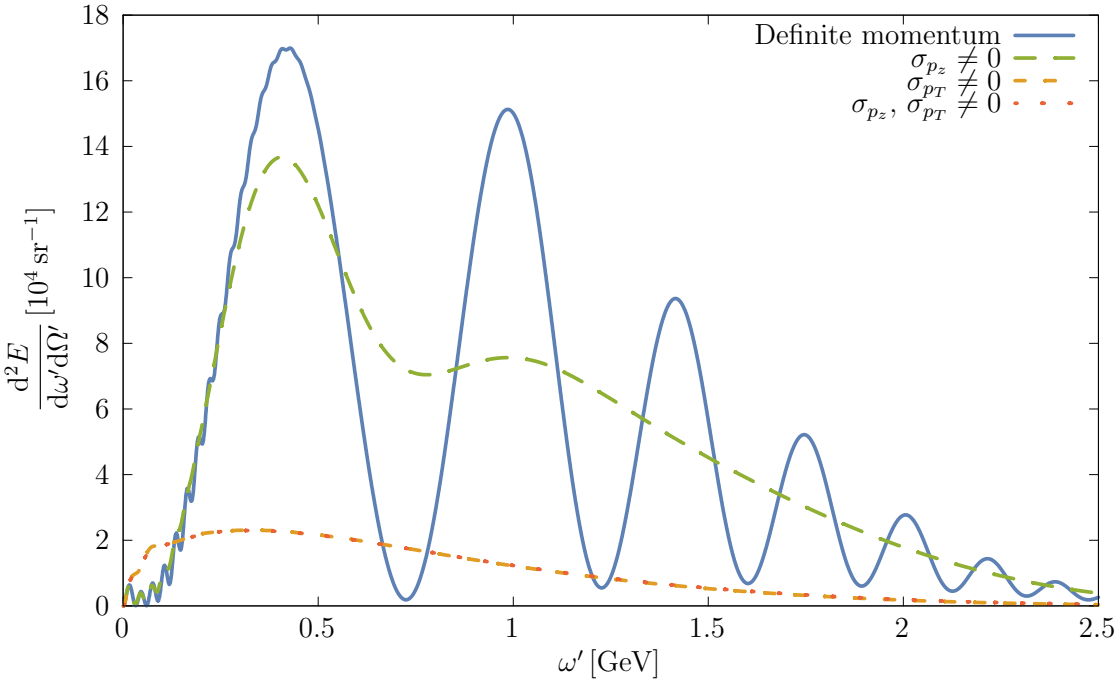

Figure 4.9 Energy emission spectrum on a direction in the xz-plane forming an angle $\theta = m\xi/2\bar{\varepsilon}$ with the negative z-axis, for some different initial electron states. The numerical parameters are the same as in Fig. 4.8.

Fig. 4.11; they show that the total emitted energy as a function of ω' changes only at frequencies $\omega' \approx \bar{\varepsilon} = 4.2$ GeV and that it is almost not affected by the momentum spreading of the incoming wave packet. The higher rates observed at these frequencies in the case of a wave packet with $\sigma_{p_z} \neq 0$ (see inset of Fig. 4.11) can be explained by the fact that, although the various components of the initial wave packet have energies almost centered symmetrically around $\bar{\varepsilon}$, the nonlinearity of the emission with respect to the energy of the incoming electron makes it possible for the higher energy components to slightly skew the average emitted energy towards a higher value.

In order to analyze the properties of the emitted radiation in the spatial domain, one can integrate $\mathrm{d}E/\mathrm{d}\omega'\,\mathrm{d}\Omega'$ with respect to ω' and obtain the total energy emitted along each direction. A typical result of this procedure is shown in Fig. 4.12. On the right panel is plotted the energy emitted per steradian by an electron in a Gaussian wave packet (the numerical parameters are the same as in Fig. 4.10). The left panel shows the same quantity, but calculated for an electron in a Volkov state with a definite momentum given by the $\bar{\boldsymbol{p}}$ of the above-mentioned Gaussian wave packet. In Fig. 4.12 the polar angle θ and the azimuthal angle φ are indicated assuming the negative z-axis as polar axis. As mentioned above, when the electron is initially in a Volkov state, and the laser is linearly polarized, the angular aperture

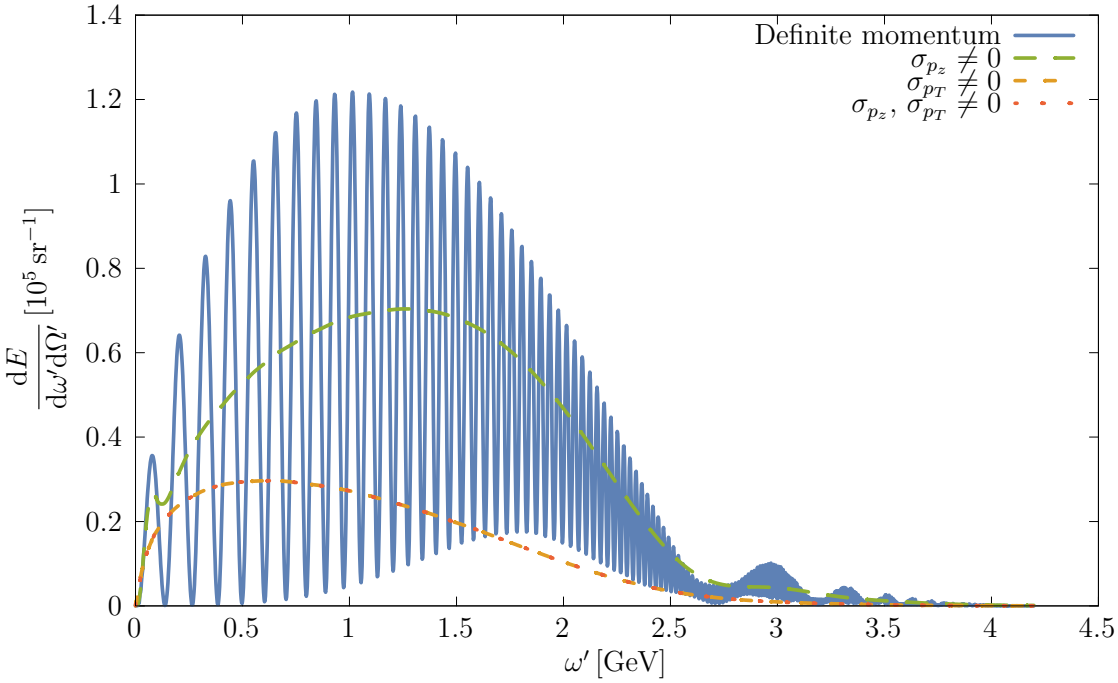

Figure 4.10 Energy emission spectrum for an electron wave packet in the quantum regime ($\chi \approx 0.85$), in the direction that lies on the laser polarization plane and forms an angle $m\xi/2\bar{\varepsilon}$ with the negative z-axis. The numerical parameters are the same as in Fig. 4.8, except that $I \approx 1.2 \times 10^{21}$ W/cm^2.

of the emitted radiation is $m\xi/\varepsilon$ (m/ε) along the polarization (magnetic-field) direction, which is confirmed by the the left panel in Fig. 4.12. The emission in the case of a multivariate Gaussian wave packet, in the right panel of Fig. 4.12, extends over a broader region and is thus less intense, in the regime where σ_{p_T} and σ_{p_z} are much smaller than $|\bar{p}_z| \gg m$. In fact, at $\xi \gg 1$, if $\sigma_{p_T} \ll |\bar{p}_z|$ and $\sigma_{p_z} \ll |\bar{p}_z|$, the total energy emitted when the electron is either in a Volkov state or in a Gaussian wave packet is almost the same (see Fig. 4.11). Then, as the region of emission becomes broader, the radiation intensity in the Gaussian wave packet case decreases. We briefly notice here that this effect might be also exploited in principle as a diagnostic tool of the momentum spreading of the electron beam, provided that the laser parameters like its intensity are known with sufficiently high accuracy.

4.4 Summary

In the present chapter we have studied Nonlinear Single Compton Scattering by an incoming electron described by a wave packet of Volkov states. We have obtained

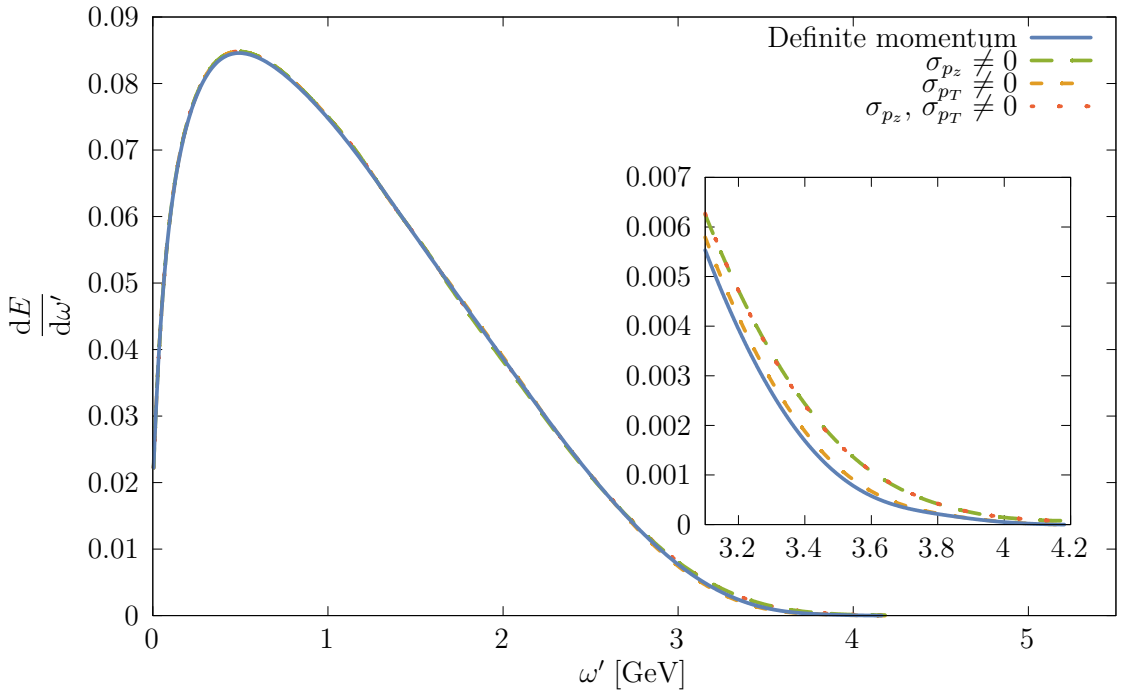

Figure 4.11 Distribution of the total emitted energy by an electron in a Volkov state or in a Gaussian wave packet as a function of the frequency of the emitted photon. All the numerical parameters for this figure are the same as in Fig. 4.10.

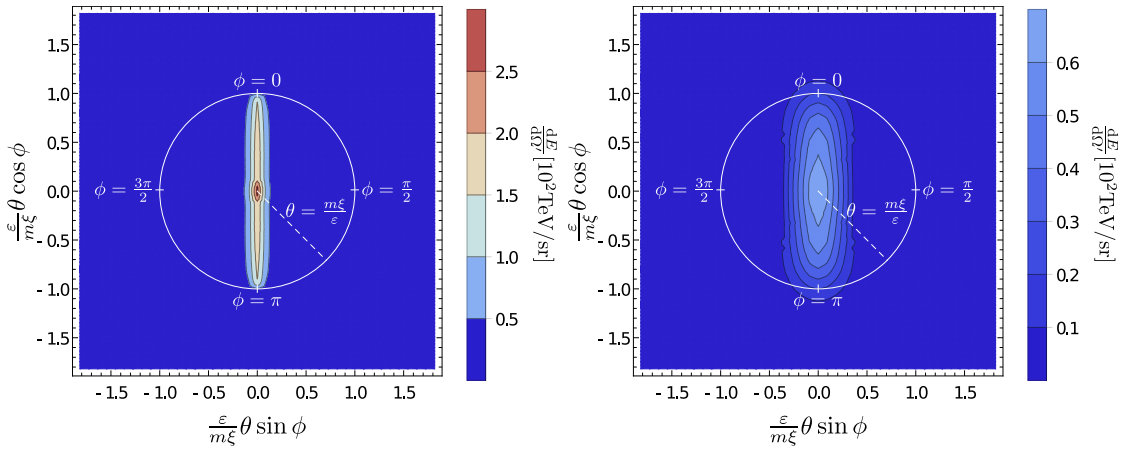

Figure 4.12 Angular distribution of the total energy emitted by an electron in a Volkov state (left) or in a Gaussian superposition of them (right) after interacting with a strong laser field. The numerical parameters used here are the same as in Fig. 4.10.

that the conservation of energy and momentum forbids interference effects among different momentum components of the wave packet, even if the electron is originally in a superposition of Volkov states. This means that an incoming electron wave packet can be equivalently described in this respect as a superposition of states or as a statistical mixture. The net effect of having a wave packet as initial electron state is a lowering and a smoothing of the angular resolved emission spectrum for an electron in a state with definite momentum; this effect tends to be more pronounced than the non-monochromaticity of the laser pulse (at comparable relative uncertainties in the electron and in the laser-photon energy). Furthermore, for realistic values of the parameters of the electron wave packet as compared with those available experimentally for electron beams, the transverse momentum spread, even if orders of magnitude smaller than the longitudinal one, dominates the alterations in the shape of the emission spectrum at a fixed observation direction. We have also observed that there is a broadening of the angular emission region in the case of an electron wave packet with respect to the case of a monoenergetic electron. The above mentioned effects vanish almost completely if we integrate the spectra over the observation directions.

Chapter 5

Nonlinear Compton Scattering of a Two-Electron Wave Packet

One of the main results presented in Chapter 4 is that when a single electron scatters with a laser field, even if it is in a wave packet state there cannot be effects due to quantum interference in the NSCS photon spectra. The main reason behind this is that the conservation laws enforced by the three delta functions of Eq. (4.7), together with the on-shell conditions, made it possible (in principle) measure the initial state of the electron by measuring its final state and the emitted photon; since there are not multiple pathways between the initial state and the final one, quantum interference cannot fundamentally take place. In this chapter we will show that in general it is not possible to apply the same argument when multiple electrons are interacting with the laser field. For the sake of definiteness, we will consider the paradigmatic case where only two electrons are present in the initial state; all the new phenomena we will show are captured in this setup, and can be easily generalized to the more general case of many incoming electrons.

This chapter is an extended version of [Angioi and Di Piazza, 2017], a manuscript that has been submitted to a peer-reviewed journal.

5.1 Quantum Spectrum of the Emitted Radiation

As in Section 4.1, we will assume that the laser field can be approximated by a linearly-polarized plane-wave; thus, it is described by the four-vector potential $\mathcal{A}_L^\mu(\phi) = (0, \boldsymbol{\mathcal{A}}_L^\mu(\phi)) = \mathcal{A}^\mu \psi_L(\phi)$, where $\psi_L(\phi)$ is a smooth function with compact support and $\phi = (nx)$, with $n^\mu = k^\mu/\omega$. We assume that the plane wave propagates along the positive z direction ($n^\mu = (1, 0, 0, 1)$) and that it is polarized along the x direction ($\mathcal{A}^\mu = (0, -\mathcal{E}/\omega, 0, 0)$). For the sake of definiteness, we set $\phi = 0$ as the initial light-cone "time" and thus assume that $\psi_L(\phi) = 0$ for $\phi \leq 0$. We also choose the initial two-electron state as being characterized by two definite spin quantum

numbers s_j ($j \in \{1,2\}$) and having the form

$$|\Psi\rangle = \frac{1}{\sqrt{\mathcal{N}}} \int \frac{\mathrm{d}^3p_1}{(2\pi)^3\sqrt{2\varepsilon_1}} \frac{\mathrm{d}^3p_2}{(2\pi)^3\sqrt{2\varepsilon_2}}\, \rho_1(\boldsymbol{p}_1)\, \rho_2(\boldsymbol{p}_2)\, a^\dagger_{s_2}(\boldsymbol{p}_2) a^\dagger_{s_1}(\boldsymbol{p}_1)|0\rangle; \tag{5.1}$$

Here, $\mathcal{N}$ is a normalization factor such that $\langle\Psi|\Psi\rangle = 1$, the operator $a^\dagger_{s_j}(\boldsymbol{p}_j)$ creates an electron with momentum $\boldsymbol{p}_j$ (energy $\varepsilon_j = \sqrt{m^2 + \boldsymbol{p}_j^2}$) and spin quantum number s_j, $\rho_j(\boldsymbol{p}_j)$ is an arbitrary square-integrable complex-valued function whose modulus square describes the initial momentum distribution of the corresponding electron wave packet, and $|0\rangle$ is the free vacuum state. From the anti-commutation relations $\{a_s(\boldsymbol{p}), a^\dagger_{s'}(\boldsymbol{p}')\} = (2\pi)^3\delta^{(3)}(\boldsymbol{p}-\boldsymbol{p}')\,\delta_{ss'}$ [Peskin and Schroeder, 1995], the normalization factor $\mathcal{N}$ turns out to have the form $\mathcal{N} = \mathcal{N}_d - \delta_{s_1 s_2}\mathcal{N}_e$, with

$$\mathcal{N}_d = \int \frac{\mathrm{d}^3p_1}{(2\pi)^3 2\varepsilon_1} \frac{\mathrm{d}^3p_2}{(2\pi)^3 2\varepsilon_2} |\rho_1(\boldsymbol{p}_1)|^2 |\rho_2(\boldsymbol{p}_2)|^2, \tag{5.2}$$

$$\mathcal{N}_e = \int \frac{\mathrm{d}^3p_1}{(2\pi)^3 2\varepsilon_1} \frac{\mathrm{d}^3p_2}{(2\pi)^3 2\varepsilon_2} \rho_1^*(\boldsymbol{p}_1)\rho_2(\boldsymbol{p}_1)\rho_2^*(\boldsymbol{p}_2)\rho_1(\boldsymbol{p}_2). \tag{5.3}$$

Notice that $\mathcal{N}$ is always positive; this is trivial to show if $s_1 \neq s_2$, whereas if $s_1 = s_2$ one has that the difference of the integrands in Eq. (5.2) and Eq. (5.3) can be written as

$$\begin{aligned}\frac{1}{2}\Big(&|\rho_1(\boldsymbol{p}_1)|^2\, |\rho_2(\boldsymbol{p}_2)|^2 - \rho^{(1)*}(\boldsymbol{p}_1)\, \rho_2(\boldsymbol{p}_1)\, \rho^{(2)*}(\boldsymbol{p}_2)\, \rho_1(\boldsymbol{p}_2) \\ &- \rho^{(1)*}(\boldsymbol{p}_2)\, \rho_2(\boldsymbol{p}_2)\, \rho^{(2)*}(\boldsymbol{p}_1)\, \rho_1(\boldsymbol{p}_1) + |\rho_1(\boldsymbol{p}_2)|^2\, |\rho_2(\boldsymbol{p}_1)|^2 \Big) \\ &= \frac{1}{2}\,|\rho_1(\boldsymbol{p}_1)\rho_2(\boldsymbol{p}_2) - \rho_1(\boldsymbol{p}_2)\rho_2(\boldsymbol{p}_1)|^2 \geq 0, \end{aligned} \tag{5.4}$$

where in Eq. (5.4) we performed a "doubling" of each of the integrands in Eq. (5.2) and Eq. (5.3), and performed the substitution $\boldsymbol{p}_1 \leftrightarrow \boldsymbol{p}_2$.

If $c^\dagger_{l'}(\boldsymbol{k}')$ is the operator which creates a photon with momentum $\boldsymbol{k}'$ (energy $\omega' = \sqrt{\boldsymbol{k}'^2}$) and polarization $\epsilon^\mu_{l'}$, the final state in NSCS has the form

$$|\Psi'\rangle = \sqrt{8\omega'\varepsilon'_1\varepsilon'_2}\, c^\dagger_{l'}(\boldsymbol{k}') a^\dagger_{s'_2}(\boldsymbol{p}'_2) a^\dagger_{s'_1}(\boldsymbol{p}'_1)|0\rangle, \tag{5.5}$$

with $\varepsilon'_j = \sqrt{m^2 + \boldsymbol{p}'^2_j}$. In order to take into account exactly the effects of the plane wave on the electrons' dynamics, we work in the Furry picture [Furry, 1951; Berestetskii et al., 1982], where the Dirac field $\psi(x)$ is expanded with respect to fermion states "dressed" by the classical background plane wave, which are known as Volkov states [Furry, 1951; Berestetskii et al., 1982; Ritus, 1985]. The leading-order S-matrix element S of NSCS reads

$$S = -ie \int \mathrm{d}^4x \langle\Psi'|\bar\psi(x)\gamma^\mu\psi(x)A_\mu(x)|\Psi\rangle, \tag{5.6}$$

where $A^\mu(x)$ is the quantized part of the electromagnetic field. Here, we neglect the interaction between the electrons as their dynamics is predominantly determined by the intense plane wave.

The calculation of S is straightforward because the corresponding Feynman diagrams are composed of two disconnected pieces (see Fig. 5.1). At this order of perturbation theory, in fact, only one of the two electrons emits a photon; and by applying Wick's theorem [Peskin and Schroeder, 1995] to Eq. (5.6), we can see that the only terms different from 0 are those where $\psi(x)$ is contracted with a creation operator ($a_s^\dagger(\boldsymbol{p})$) to its right, whereas $\bar{\psi}(x)$ is contracted with an annihilation operator ($a_s^\dagger(\boldsymbol{p})$) to its left (and A_μ can only be contracted with the $c_{\lambda'}(\boldsymbol{k'})$ on its left). This gives rise to four terms; by expanding $\psi(x)$ in a basis of Volkov states $\Psi_{ps}(x) = E_p(x)u_{ps}$, where $E_p(x)$ is a Ritus matrix (see Section 2.2.1), we can write them (omitting the x dependencies of the Ψ functions) as

$$
\begin{aligned}
S = -ie\sqrt{2\pi}\,\frac{\sqrt{4\varepsilon_1'\varepsilon_2'}}{(2\pi)^3\sqrt{\mathcal{N}}}\int \frac{\mathrm{d}^3p_1}{\sqrt{2\varepsilon_1}}\,\frac{\mathrm{d}^3p_2}{\sqrt{2\varepsilon_2}}\,\mathrm{d}^4x\;\rho_1(\boldsymbol{p}_1)\,\rho_2(\boldsymbol{p}_2)\\
\left[\frac{\bar{\Psi}_{p_1's_1'}\not{\epsilon}^*_{\boldsymbol{k}'\lambda'}e^{ik'x}\Psi_{p_1s_1}}{\sqrt{4\varepsilon_1'\varepsilon_1}}\,\delta(\boldsymbol{p}_2'-\boldsymbol{p}_2)\delta_{s_2's_2}+\frac{\bar{\Psi}_{p_2's_2'}\not{\epsilon}^*_{\boldsymbol{k}'\lambda'}e^{ik'x}\Psi_{p_2s_2}}{\sqrt{4\varepsilon_2'\varepsilon_2}}\,\delta(\boldsymbol{p}_1'-\boldsymbol{p}_1)\delta_{s_1's_1}\right.\\
\left.-\frac{\bar{\Psi}_{p_1's_1'}\not{\epsilon}^*_{\boldsymbol{k}'\lambda'}e^{ik'x}\Psi_{p_2s_2}}{\sqrt{4\varepsilon_1'\varepsilon_2}}\,\delta(\boldsymbol{p}_2'-\boldsymbol{p}_1)\delta_{s_2's_1}-\frac{\bar{\Psi}_{p_2's_2'}\not{\epsilon}^*_{\boldsymbol{k}'\lambda'}e^{ik'x}\Psi_{p_1s_1}}{\sqrt{4\varepsilon_2'\varepsilon_1}}\,\delta(\boldsymbol{p}_1'-\boldsymbol{p}_2)\delta_{s_1's_2}\right].
\end{aligned}
\tag{5.7}
$$

Now, the orthogonality of Volkov states [Ritus, 1985; Boca and Florescu, 2011] yields a three-dimensional Dirac (Kronecker) delta-function between the initial and the final momentum (spin) of non-emitting electrons. Instead, since the plane wave depends on the spacetime coordinates only via $\phi = t - z$, the amplitudes involving the photon emission include a three-dimensional Dirac delta-function, which enforces the conservation of the transverse ($\perp$) components (x- and y-components) and of the minus ($-$) component (time- minus z-component) of the four-momenta of the involved particles (see Chapter 4). We exploit the altogether six Dirac delta-functions to carry out the six integrals in the initial wave-packet

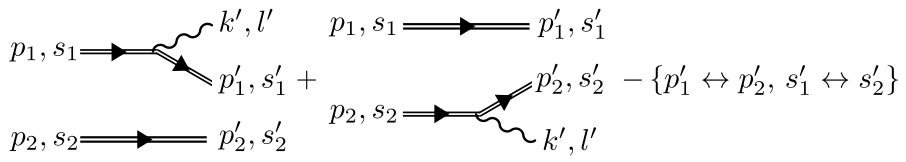

Figure 5.1 Leading-order Feynman diagrams of NSCS by two electrons. The double lines indicate Volkov states and the symbol $\{p_1' \leftrightarrow p_2', s_1' \leftrightarrow s_2'\}$ indicates the exchange diagrams.

$|\Psi\rangle$ (see Eq. (5.1)). More explicitly, we can write [Ritus, 1985; Mackenroth, 2014]

$$\int \mathrm{d}^4x\ \bar{\Psi}_{p's'} \not{\epsilon}^*_{\boldsymbol{k}'\lambda'} e^{ik'x} \Psi_{ps} = (2\pi)^3\, \delta^{(-,x,y)}(p - p' - k')\ (\bar{u}_{p's'} M_{p'p} u_{ps})\,, \tag{5.8}$$

where $M_{p'p}$ is

$$M_{p'p} = \not{\epsilon}'^*_{\lambda'} f_0(p', p) + e\left(\frac{\not{A}\not{k}\not{\epsilon}'^*_{\lambda'}}{2(kp')} + \frac{\not{\epsilon}'^*_{\lambda'}\not{k}\not{A}}{2(kp)}\right) f_1(p', p) - \frac{e^2\mathcal{A}^2(k\epsilon'^*_{\lambda'})\not{k}}{2(kp)(kp')}\, f_2(p', p). \tag{5.9}$$

Thus, it is convenient to introduce the two on-shell four-momenta q_j^μ ($q_j^2 = m^2$) such that $\boldsymbol{q}_{j,\perp} = \boldsymbol{p}'_{j,\perp} + \boldsymbol{k}'_\perp$ and $q_{j,-} = p'_{j,-} + k'_-$, i.e.,

$$q_j^\mu = p_j'^\mu + k'^\mu - \frac{(k'p'_j)}{p'_{j,-} + k'_-} n^\mu. \tag{5.10}$$

The amplitude S can then be written then as

$$\begin{aligned} S = -\frac{ie\sqrt{2\pi}}{\sqrt{\mathcal{N}}} \Big\{ & \frac{1}{2q_1^-}\, \rho_1(\boldsymbol{q}_1)\, \rho_2(\boldsymbol{p}'_2)\, \left(\bar{u}_{p'_1 s'_1} M_{p'_1 q_1} u_{q_1 s_1}\right) \delta_{s'_2 s_2} \\ & + \frac{1}{2q_2^-} \rho_1(\boldsymbol{p}'_1)\, \rho_2(\boldsymbol{q}_2)\, \left(\bar{u}_{p'_2 s'_2} M_{p'_2 q_2} u_{q_2 s_2}\right) \delta_{s'_1 s_1} \\ & - \frac{1}{2q_1^-} \rho_1(\boldsymbol{p}'_2)\, \rho_2(\boldsymbol{q}_1)\, \left(\bar{u}_{p'_1 s'_1} M_{p'_1 q_1} u_{q_1 s_2}\right) \delta_{s'_2 s_1} \\ & - \frac{1}{2q_2^-}\, \rho_1(\boldsymbol{q}_2)\, \rho_2(\boldsymbol{p}'_1)\, \left(\bar{u}_{p'_2 s'_2} M_{p'_2 q_2} u_{q_2 s_1}\right) \delta_{s'_1 s_2} \Big\}; \end{aligned} \tag{5.11}$$

it is possible to write the S-matrix more compactly in the form $S = S_{12} - S_{21}$, where

$$\begin{aligned} S_{12} = -ie\sqrt{\frac{4\pi}{\mathcal{N}}} \Big[& \rho_1(\boldsymbol{q}_1)\rho_2(\boldsymbol{p}'_2)\delta_{s'_2 s_2} \frac{M_{s'_1 l', s_1}(p'_1, k'; q_1)}{2q_{1,-}} \\ & + \rho_1(\boldsymbol{p}'_1)\rho_2(\boldsymbol{q}_2)\delta_{s'_1 s_1} \frac{M_{s'_2 l', s_2}(p'_2, k'; q_2)}{2q_{2,-}} \Big] \end{aligned} \tag{5.12}$$

and where S_{21} can be obtained from S_{12} by substituting $p'_1 \leftrightarrow p'_2$,$q_1 \leftrightarrow q_2$, and $s'_1 \leftrightarrow s'_2$. Notice that Eq. (5.12) allows us to interpret S_{12} as a weighted sum of the reduced amplitudes $M_{s'l',s}(p', k'; p)$ characteristic of NSCS by a single electron (with definite initial four-momentum p^μ and spin quantum number s, final four-momentum p'^μ and spin quantum number s'). Moreover, if we were considering the emission by two distinguishable particles, the only term that would be present in the S-matrix would be S_{12}

Let us calculate the emitted photon energy spectrum $dE_Q/d\omega'$ averaged (summed) with respect to all initial (final) discrete quantum numbers. Since we also integrate

over the final electrons momenta, in order to avoid double-counting, we divide the final result by two; thus we find

$$\frac{\mathrm{d}E_Q}{\mathrm{d}\omega'} = \frac{\omega'^2}{8} \sum_{s_j, s_j', l'} \int \frac{\mathrm{d}\Omega'}{(2\pi)^3 2} \frac{\mathrm{d}^3 p_1'}{(2\pi)^3 2\varepsilon_1'} \frac{\mathrm{d}^3 p_2'}{(2\pi)^3 2\varepsilon_2'} |S|^2, \tag{5.13}$$

where Ω' denotes the solid angle corresponding to $\boldsymbol{n}' = \boldsymbol{k}'/\omega'$. Note that if the electrons were distinguishable, the energy emission spectrum would have the same form as in Eq. (5.13), with the replacement $|S|^2 \to 2(\mathcal{N}/\mathcal{N}_d)|S_{12}|^2$.

There is a subtle difficulty in the explicit calculation of Eq. (5.13). Remember that in the calculation of the modulus squared of the NSCS S-matrix for one electron, as we have shown in Chapter 4, one needs only to calculate products of the reduced amplitudes of the form

$$(\bar{u}_{p's'} M_{p'p} u_{ps})^* \, (\bar{u}_{p's'} M_{p'p} u_{ps}), \tag{5.14}$$

and we can cast these products in the language of traces by exploiting the identity

$$\sum_s u_{ps} \bar{u}_{ps} = (\not{p} + m). \tag{5.15}$$

For two electrons, the above mentioned technique is not sufficient anymore, because in Eq. (5.13) there are terms of the form

$$(\bar{u}_{p_1' s_1'} M_{p_1' p_1} u_{p_1 s_1})^* \, (\bar{u}_{p_2' s_2'} M_{p_2' p_2} u_{p_2 s_2}), \tag{5.16}$$

with in general $\boldsymbol{p}_1' \neq \boldsymbol{p}_2'$ and $\boldsymbol{p}_1 \neq \boldsymbol{p}_2$. We will not show here the technique we derived in order to compute products like the one in Eq. (5.16), but it is reported in Appendix A.

In order to investigate the coherence properties of the emitted radiation, in the following we chose to consider the paradigmatic case in which the two electron wave packets in position space differ only by a translation by a vector $\boldsymbol{r}'$, i.e., $\rho_2(\boldsymbol{p}_2) = \rho_1(\boldsymbol{p}_2) \exp(-i\boldsymbol{p}_2 \cdot \boldsymbol{r}')$, such that $|\rho_1(\boldsymbol{p})|^2 = |\rho_2(\boldsymbol{p})|^2$. Also, without loss of generality we choose the function $\rho_1(\boldsymbol{p}_1)$ to be real and we denote it as $\rho(\boldsymbol{p}_1)$.

However, before we calculate the quantum spectrum $\mathrm{d}E_Q/\mathrm{d}\omega'$, it is interesting to calculate also the classical prediction for the emitted radiation. Naively, one would expect that when $\chi \ll 1$, these two predictions should coincide as it happens for the single-particle spectra; as we will see, this is not correct.

5.2 Classical Spectrum of the Emitted Radiation

Let us study the classically radiated energy (differential only with respect to the emitted frequency) $dE_C/d\omega'$ emitted by two electrons in a plane wave. Intuitively, it

is clear that in the total radiation emitted by two charges there will be interference effects: because of the superposition principle, the total electromagnetic field they emit is the sum of the field emitted by each particle. However, if they move along sufficiently close trajectories, they will emit radiation "in phase", thus interference will lead to an enhancement of the energy radiated. In this section, we will try to find a formula which will help us estimate when (i. e., at which frequencies) one has this coherent enhancement of the radiation. Since we will want to compare this prediction with the calculations of Section 5.1, in the derivation of this formula we will restrict ourselves to the case of interest where the two electrons have very similar (but not exactly equal) initial momenta (ultrarelativistic and mostly counterpropagating with respect to the laser field) and they start at some distance one with respect to the other.

From the Liénard–Wiechert potentials, one can prove [Jackson, 1999; Baier et al., 1998] that the classically radiated energy $dE_C/d\omega'$ for the above-mentioned system is given by the formula

$$\frac{\mathrm{d}E_C}{\mathrm{d}\omega'} = \frac{e^2\omega'^2}{4\pi^2}\int \mathrm{d}\Omega' \left| \sum_{j=1}^{2} \int \mathrm{d}\phi \frac{p_j'^{\mu}(\phi)}{p'_{j,-}} e^{i\omega'\Phi_j(\phi)} \right|^2 . \tag{5.17}$$

Here, for the sake of notational convenience in relation with the quantum case, we have indicated as $p_j'^{\mu}(\phi) = (\varepsilon'_j(\phi), \boldsymbol{p}'_j(\phi))$ (i. e., with primed quantities) the electrons' four-momenta in the plane wave. The analytic expression of $p_j'^{\mu}(\phi)$ is given by [Berestetskii et al., 1982]

$$p_j'^{\mu}(\phi) = p_j'^{\mu} - e\mathcal{A}_L^{\mu}(\phi) + e\frac{(p'_j\mathcal{A}_L(\phi))}{p'_{j,-}}n^{\mu} - \frac{e^2}{2}\frac{\mathcal{A}_L^2(\phi)}{p'_{j,-}}n^{\mu}, \tag{5.18}$$

with initial (at $t = 0$) four-momenta $p_j'^{\mu} = (\varepsilon'_j, \boldsymbol{p}'_j)$. Notice that when the laser field is not present, i. e., at times when $\mathcal{A}_L^{\mu}(\phi) = 0$, we have $p_j'^{\mu}(\phi) = p_j'^{\mu}$.

If we choose to label with $j = 1$ the electron which first enters the plane wave, and by setting the origin of the coordinate system at the corresponding entering point, the initial positions of the electrons are $\boldsymbol{r}'_1 = \boldsymbol{0}$ and $\boldsymbol{r}'_2 = \boldsymbol{r}'$, with $r'_z > 0$ (this is guaranteed by the fact that the electron "2" enters the laser after the first, and the laser propagates along the positive z axis). The quantity $\Phi_j(\phi)$ in Eq. (5.17) thus reads

$$\Phi_j(\phi) = \int_0^{\phi} \mathrm{d}\phi' \frac{(n'p'_j(\phi'))}{p'_{j,-}} + \left[\frac{(n'p'_j)}{p'_{j,-}}\boldsymbol{n} - \boldsymbol{n}'\right]\cdot\boldsymbol{r}'_j, \tag{5.19}$$

with $n'^{\mu} = k'^{\mu}/\omega' = (1, \boldsymbol{n}')$. The extra term

$$\left[\frac{(n'p'_2)}{p'_{2,-}}\boldsymbol{n} - \boldsymbol{n}'\right]\cdot\boldsymbol{r}' \tag{5.20}$$

in the phase associated with the second electron, not present in the phase of the first, is due to the fact that the second electron needs to propagate for a certain distance before it reaches the laser. Notice that we can write the two phases also as

$$\Phi_j(\phi) = \Phi_j(0) + n'_- \int_0^\phi \mathrm{d}\phi' [m^2 + \boldsymbol{P}'^2_{j,\perp}(\phi')]/2p'^2_{j,-}, \tag{5.21}$$

where $\boldsymbol{P}'_{j,\perp}(\phi) = \boldsymbol{P}'_{j,\perp} - e\boldsymbol{\mathcal{A}}_{L,\perp}(\phi)$, with $\boldsymbol{P}'_{j,\perp} = \boldsymbol{p}'_{j,\perp} - p'_{j,-}\boldsymbol{n}'_\perp/n'_-$. Now, by indicating as φ_T a measure of the total laser phase $\omega\phi_T$ where the electrons experience the strong field, an order-of-magnitude condition for the emitted radiation to be coherent is obtained by requiring that $\omega'\Delta\Phi(\phi_T) \lesssim \pi/5$ [1], with $\Delta\Phi(\phi_T) = |\Phi_2(\phi_T) - \Phi_1(\phi_T)|$ (the absolute value of the variation of an arbitrary quantity f is indicated here and below as Δf). Now, we assume that the electrons have initial momenta (energies) of the same order of magnitude $\boldsymbol{p}'$ (ε'), and that are ultrarelativistic and initially counterpropagating with respect to the laser field ($p'_-/2 \approx \varepsilon' \gg m$). By summing the moduli of all contributions to $\Delta\Phi(\phi_T)$, the above condition provides an upper limit ω'_C on the frequencies which are emitted coherently given by

$$\omega'_C = \frac{2\pi\omega}{5n'_-\varphi_T}\left[\frac{\Delta\overline{\boldsymbol{P}'^2_\perp}}{4\varepsilon'^2} + \frac{\Delta\varepsilon'}{\varepsilon'}\frac{m^2 + \overline{\boldsymbol{P}'^2_\perp}}{2\varepsilon'^2} + \frac{2\omega\Delta\Phi(0)}{n'_-\varphi_T}\right]^{-1}, \tag{5.22}$$

where $\overline{\boldsymbol{P}'^2_\perp}$ is the average value of $\boldsymbol{P}'^2_\perp(\phi)$ over ϕ_T. It is physically clear that the larger the interaction time is and the larger the differences in the electrons' initial positions/momenta/energies are, the lower will be the highest frequency that can be emitted coherently.

Having in mind the quantum case where the electrons' momenta distributions are given by $\rho^2(\boldsymbol{p}'_1)$ and $\rho^2(\boldsymbol{p}'_2)$, we consider now a classical ensemble of pairs of electrons, each pair being characterized by the electrons' initial positions $\boldsymbol{r}'_1 = \boldsymbol{0}$ and $\boldsymbol{r}'_2 = \boldsymbol{r}'$ and initial (and final) momenta $\boldsymbol{p}'_j$ distributed as $\rho^2(\boldsymbol{p}'_1)$ and $\rho^2(\boldsymbol{p}'_2)$. The corresponding average classical energy spectrum $\langle dE_C/d\omega'\rangle$ is given by

$$\left\langle \frac{\mathrm{d}E_C}{\mathrm{d}\omega'} \right\rangle = \int \frac{\mathrm{d}^3p'_1}{(2\pi)^3 2\varepsilon'_1}\frac{\mathrm{d}^3p'_2}{(2\pi)^3 2\varepsilon'_2}\frac{\rho^2(\boldsymbol{p}'_1)\rho^2(\boldsymbol{p}'_2)}{\mathcal{N}_d}\frac{\mathrm{d}E_C}{\mathrm{d}\omega'}. \tag{5.23}$$

It is important to observe that this expression can also be obtained from the quantum spectrum $dE_Q/d\omega'$ in Eq. (5.13) by neglecting the photon recoil in $\rho(\boldsymbol{q}_j)$, i.e., by approximating $\rho(\boldsymbol{q}_j) \approx \rho(\boldsymbol{p}'_j)$, but by keeping linear corrections due to the recoil in the phase of $\rho_2(\boldsymbol{q}_2)$. This, in fact, allows to reproduce the term $\Phi_2(0)$ from the difference $\boldsymbol{q}_2 - \boldsymbol{p}'_2$ according to Eq. (5.10) after neglecting higher-than-linear recoil terms in it. On the one hand, this observation indicates that when

[1] This condition is obtained starting from the prototype function $g(\theta) = |1 + \exp(i\theta)|^2$ and by stating that it shows a "coherent" behavior for $\theta < \theta^*$, where θ^* is such that $|g(\theta^*) - 4|/4 = 0.1$, i.e. $\theta^* \approx \pi/5$

the photon recoil is negligible, the classical constraint in Eq. (5.22) also applies quantum mechanically. On the other hand, however, we will show below that the differences in the coherence properties of classical and quantum radiation precisely arise from the fact that the classical theory ignores the recoil in $\rho(\boldsymbol{q}_j)$.

5.3 Quantum Restriction to Coherent Emission

In fact, turning now to the quantum case, it is intuitively clear, as we have also ascertained in the numerical example below, that the electrons' indistinguishability does not play a significant role here. Indeed, the exchange terms become important only when the two electrons have very similar final momenta (and the same final spin), which corresponds to a negligibly small region of the available final phase space. Thus, in order to study coherence effects, we focus on the interference term in $|S_{12}|^2$, which is proportional to the product $\rho(\boldsymbol{q}_1)\rho(\boldsymbol{p}'_1)\rho(\boldsymbol{p}'_2)\rho(\boldsymbol{q}_2)$ (see Eq. (5.12)). In analogy with the classical case, we indicate as $\boldsymbol{p}'$ the average momentum of both electron distributions, corresponding to the on-shell four-momentum $p'^{\mu} = (\varepsilon', \boldsymbol{p}') = (\sqrt{m^2 + \boldsymbol{p}'^2}, \boldsymbol{p}')$, and as $\boldsymbol{\sigma}_{\boldsymbol{p}'}$ the three-dimensional width. As it is clear from Eq. (5.10), the difference between the momenta $\boldsymbol{p}'_j$ and $\boldsymbol{q}_j$ is due to the photon recoil. Thus, if the latter is so large that $|p'_{j,i} - q_{j,i}| \gg \sigma_{p'_i}$ for any $i \in \{x, y, z\}$, the interference term will be suppressed because the functions $\rho(\boldsymbol{q}_j) = \rho(\boldsymbol{q}_j(\boldsymbol{p}'_j))$ (see Eq. (5.10)) and $\rho(\boldsymbol{p}'_j)$ cannot be both significantly different from zero for the same $\boldsymbol{p}'_j$.

An invariant parameter $\tilde{\chi}(k')$ characterizing the quantum coherence of the emitted radiation with four-momentum k'^{μ} can be defined by introducing the average $\langle\langle \cdot \rangle\rangle$ with respect to the distribution $\rho^2(\boldsymbol{p}')/\mathcal{N}_0$, with $\mathcal{N}_0 = \int d^3p'(2\pi)^{-3}\rho^2(\boldsymbol{p}')/2\varepsilon'$:

$$\tilde{\chi}(k') = \sqrt{k'^{\mu} T^{-1}_{\mu\nu} k'^{\nu}}, \tag{5.24}$$

where $(T^{-1})^{\mu\nu}$ is the inverse of the positive-definite, symmetric covariance tensor

$$T^{\mu\nu} = \langle\langle p'^{\mu} p'^{\nu} \rangle\rangle - \langle\langle p'^{\mu} \rangle\rangle \langle\langle p'^{\nu} \rangle\rangle. \tag{5.25}$$

The matrix $T^{\mu\nu}$ can be diagonalized by means of a Lorentz transformation $\Lambda^{\star}$ [Blättel et al., 1989]. If the resulting diagonal matrix $T^{\star} = \Lambda^{\star} T \Lambda^{\star t}$ reads $T^{\star\mu\nu} = \mathrm{diag}(\Sigma^2_{\varepsilon'}, \Sigma^2_{p'_x}, \Sigma^2_{p'_y}, \Sigma^2_{p_z})$, then $\Sigma^2_{\varepsilon'}$ and $\Sigma^2_{p'_i}$ are the variances of the energy and of the i-th component of the momentum distribution in that frame. Thus, it is

$$\tilde{\chi}(k') = \sqrt{\frac{\omega'^{\star 2}}{\Sigma^2_{\varepsilon'}} + \frac{k'^{\star 2}_x}{\Sigma^2_{p'_x}} + \frac{k'^{\star 2}_y}{\Sigma^2_{p'_y}} + \frac{k'^{\star 2}_z}{\Sigma^2_{p'_z}}}, \tag{5.26}$$

and if $\tilde{\chi}(k') < 1$ the coherence of the radiation with k'^{μ} is not deteriorated by quantum effects.

The additional quantum restriction to the coherent emission of radiation is qualitatively different from the classical one and it can be related to the particles' "kinematic" indistinguishability. In fact, depending on the width of the electron wave packets, even a perfect knowledge of the final momenta of the two electrons and of the emitted photon combined with the momentum conservation laws does not allow to know with certainty which electron has emitted the photon. In this respect, different momentum components of the two-electron wave packet $|\Psi\rangle$ constructively interfere enhancing the radiation probability. This is in striking contrast with the case of an incoming single electron, where, indeed, the conservation laws allow to determine the initial momentum of the electron once the final electron and photon momenta are known, implying that the emission spectrum is given by the incoherent sum of the emissions spectra corresponding to each momentum component of the wave packet [Corson et al., 2011; Angioi et al., 2016].

5.4 Numerical Examples

Below, we show by means of a numerical example that the quantum restriction to the coherence of the emission can be essentially more restrictive than the classical one even in the striking case where the average quantum parameter $\chi' = (kp')\mathcal{E}/m\omega\mathcal{E}_{cr}$ of the two wave packets is much smaller than unity. To do this we compare in Fig. 5.2 the full quantum spectrum $dE_Q/d\omega'$ from Eq. (5.13) (solid black line) with the classical spectrum $\langle dE_C/d\omega'\rangle$ from Eq. (5.23) (dash-dotted red line). In order to calculate these spectra, we used Filon's rule (see Section 3.1) for the highly oscillating part of the integrals and used Monte Carlo Integration with importance sampling (see Section 3.2) for the remaining integrals over the electrons' momenta and emitted photon's direction.

Since the distributions of the momenta of the two electrons are the same, the two single-particle spectra are identical and do not depend strongly on the shape of $\rho(\boldsymbol{p})$ (Section 4.3). Thus, as references to discuss coherence effects, we also show these single-electron spectra multiplied by two and by four. Concerning the electrons, we have set the function $\rho^2(\boldsymbol{p}'_j)/2\varepsilon'_j$ to be a normalized Gaussian function, with average momentum $\boldsymbol{p}' = (0, 0, -10\,\mathrm{MeV})$, transverse standard deviation $\sigma_{p'_\perp} = \sigma_{p'_x} = \sigma_{p'_y} = 31\,\mathrm{eV}$, (corresponding to a spatial delocalization of 20 nm) and longitudinal standard deviation $\sigma_{p'_\parallel} = \sigma_{p'_z} = 0.62\,\mathrm{eV}$ (spatial delocalization of 1 µm). The wave packets are translated with respect to one another by $\boldsymbol{r}' = (10^{-2}, 10^{-2}, 10^{-3})\,\mathrm{eV}^{-1} \approx (12, 12, 1)\,\mathrm{nm}$. Concerning the plane wave, we have set $\omega = 1.55\,\mathrm{eV}$, $\mathcal{I} = 1.01 \times 10^{20}\,\mathrm{W/cm^2}$, and $\psi_L(\phi) = \sin^4(\omega\phi/4)\sin(\omega\phi)$ for $0 \leq \omega\phi \leq 4\pi$ and zero elsewhere. With these parameters $\chi' \approx 0.002$, thus the classical and the quantum single-particle spectra differential only with respect to ω' do not depend strongly on $\boldsymbol{\sigma}_{\boldsymbol{p}'}$ [Angioi et al., 2016].

Fig. 5.2 shows that the classical spectrum (dash-dotted red line) is coherent

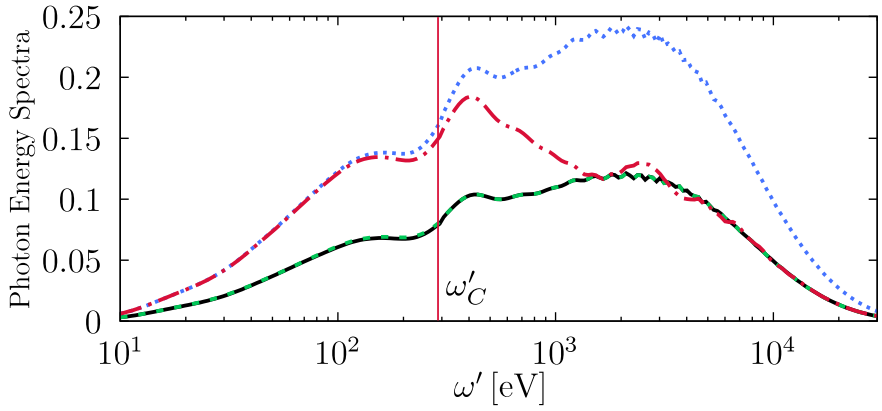

Figure 5.2 Emitted energy spectra for the numerical parameters given in the text. The solid black line shows the quantum spectrum $dE_Q/d\omega'$ and the dash-dotted red line shows the classical spectrum $\langle dE_C/d\omega' \rangle$. As reference, the corresponding single-electron spectrum multiplied by two (dashed green line) and by four (dotted blue line) are also shown.

up to a given frequency, that can be calculated with Eq. (5.22); for this estimate we choose $\boldsymbol{n}' \sim -(m\xi/2\varepsilon', 0, 1)$, with $\xi = |e|\mathcal{E}/m\omega = 5$, as a typical observation direction where the average radiated energy is large [Mackenroth and Di Piazza, 2011]. We estimate the variations $\Delta \boldsymbol{p}'_\perp$ and $\Delta\varepsilon' \approx \Delta p'_\parallel$ entering Eq. (5.22) as the standard deviations $\sigma_{p'_\perp}$ and $\sigma_{p'_\parallel}$, respectively, of the differences between the components of the two random variables $\boldsymbol{p}'_1$ and $\boldsymbol{p}'_2$. By also estimating $\varphi_T \sim 2\pi$ as the effective phase where the laser field is strong, we find from Eq. (5.22) that $\omega'_C \approx 278\,\mathrm{eV}$ (red vertical line), in good agreement with Fig. 5.2, accounting for the simplicity of the analytical model. The quantum spectrum (solid black line) is incoherent over the whole range shown in Fig. 5.2 because, by estimating $|\boldsymbol{k}'_\perp| \sim \omega' m\xi/\varepsilon'$, we obtain that $\omega'_Q \sim \min\{\sigma_{p'_\perp}\varepsilon'/m\xi, \sigma_{p'_\parallel}\}$, which corresponds to $\omega'_Q = \sigma_{p'_\parallel} = 0.62\,\mathrm{eV}$. Thus, even if classical arguments would predict coherent emission until ω'_C, the lower bound ω'_Q given by quantum mechanics, being orders of magnitude smaller, dominates.

In Fig. 5.3 we provide a compact visualization of the interplay between the classical and quantum limits on coherent emission. In order to show all the effects we mentioned in a single graph without changing multiple numerical parameters, we have fixed them at the same values of Fig. 5.2, except that $\boldsymbol{p}' = (0, 0, -100\,\mathrm{MeV})$, $\sigma_{p'_\perp} = 1\,\mathrm{keV}$, $\mathcal{I} = 1.2 \times 10^{21}\,\mathrm{W/cm^2}$ ($\chi' \approx 0.02$), $\boldsymbol{r}' = (0, 10^{-4}, 10^{-7})\,\mathrm{eV}^{-1}$, and $\sigma_{p'_\parallel}$ is varying in each panel. We have ensured that the spectra in Fig. 5.3, with the exception of the classical spectra, where oscillations due to classical interference may appear, do not change significantly with $\boldsymbol{r}'$ as long as $|\boldsymbol{r}' \cdot \boldsymbol{\sigma}_{\boldsymbol{p}'}| \ll 1$.

The values of ω'_Q, calculated in the same way as Fig. 5.2, and of ω'_C, estimated

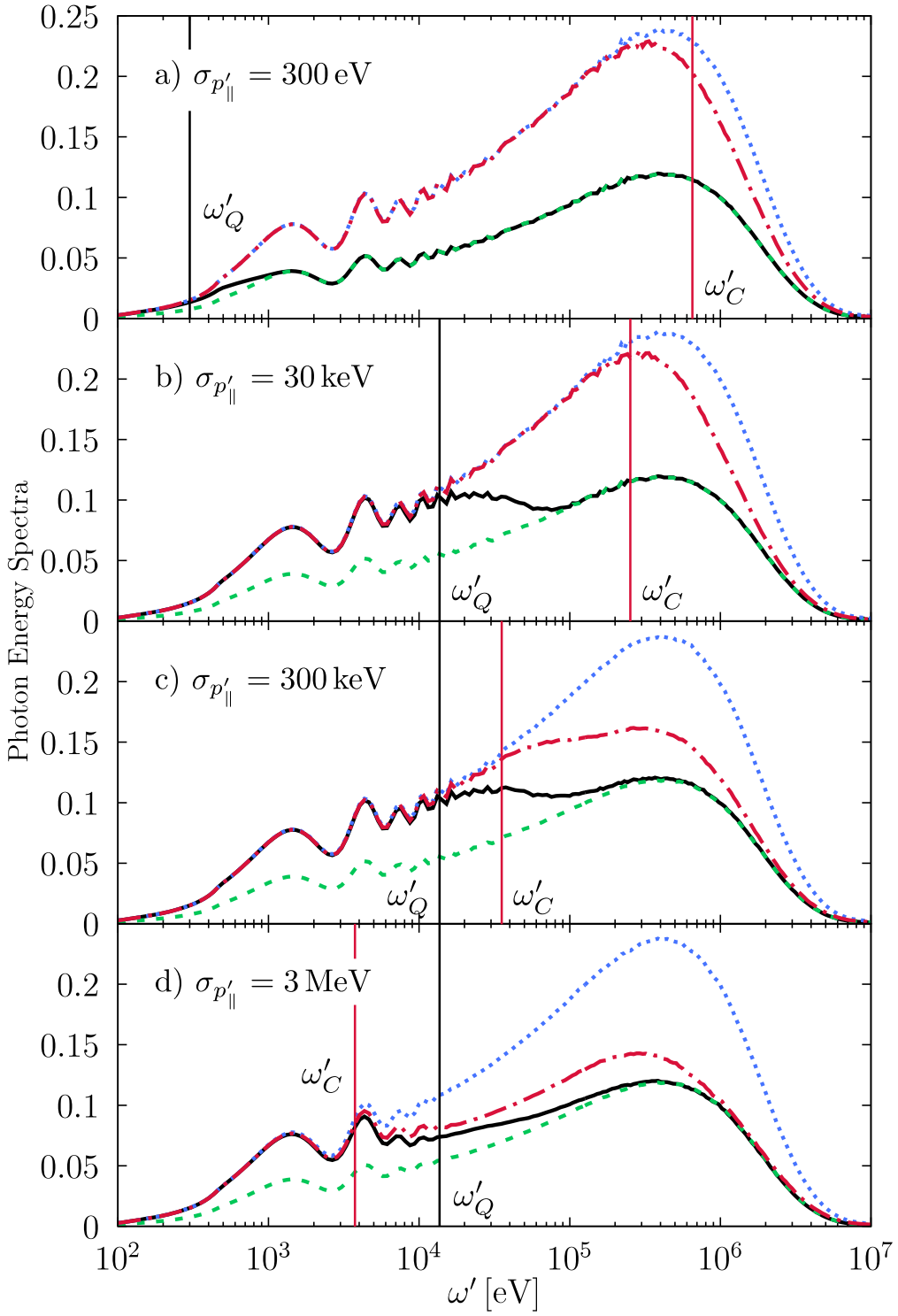

Figure 5.3 Emitted energy spectra for different values of $\sigma_{p'_\parallel}$; as this parameter varies, the interplay between ω'_Q and ω'_C determines the maximum frequency for coherent emission. The meaning of each line is the same as Fig. 5.2, and the vertical black line which shows ω'_Q

via Eq. 5.22, are in reasonable agreement with the numerical results. In particular, it is interesting to observe that the quantum limit dominates in panels a)-c), where $\omega'_C > \omega'_Q$, and the classical limit takes over in panel d) where $\omega'_C < \omega'_Q$, where it applies to both the classical and the quantum spectrum.

The properties of single-electron pulses with energies of the order of 100 keV and attosecond duration are already being exploited experimentally in order to perform high-precision microscopy (see [Baum, 2013; Kealhofer et al., 2016; Morimoto and Baum, 2018*b*,*a*]), and control schemes for electrons of MeV energy have been demonstrated recently [Curry et al., 2018]. Moreover, recent theoretical studies indicate the feasibility of generating arbitrarily-delayed single-electron wave packets with GeV energies [Krajewska et al., 2017]. The extension of these techniques to few-electron beams seems possible, for instance by combining two single-electron pulses with the methods of [Kealhofer et al., 2016; Morimoto and Baum, 2018*a*] or via an ultracold gas source [Claessens et al., 2005; van der Geer et al., 2009; Franssen et al., 2017], where the electrons are already highly correlated from the beginning. Our results suggest that the development of similar techniques at higher energies would have important applications also in fundamental strong-field physics. By reversing the argument, we can also say that the NSCS spectra as calculated here can be exploited, provided a detailed knowledge of the laser pulse, as a diagnostic tool for two- or few-electron high-energy pulses.

5.5 Effect of Coulomb Repulsion

In the calculations of this section, we neglected the effect of the Coulomb interaction between the two electrons. On the one hand, this is a very good approximation when the electrons are inside the laser field, due to the overwhelming force due to the latter. On the other hand, however, the close proximity of the two charges could in principle render the Coulomb interaction non-negligible when the charges have not entered the laser field yet.

In order to estimate the strength of Coulomb interaction, since in the considered setup the electrons move along the same direction with the same average energy, one can start by evaluating the expectation value of the Coulomb force in the frame of reference where the electrons are on average at rest. In this frame of reference, the longitudinal indeterminacy of the electrons in position space $\tilde{\sigma}_\parallel$ is dilated by the average Lorentz gamma factor γ with respect to the longitudinal indeterminacy in the lab frame $\sigma_\parallel = 1/2\sigma_{p'_\parallel}$, thus:

$$\tilde{\sigma}_\parallel = \frac{\gamma}{2\sigma_{p'_\parallel}}. \tag{5.27}$$

Moreover, also the longitudinal displacement between the two wave packets in the average rest frame $r'_\parallel$ is dilated: $\tilde{r}'_\parallel = \gamma r'_\parallel$. Instead, the transverse displacement

and indeterminacy are not affected by the Lorentz boost, thus $\tilde{\sigma}_\perp = 1/2\sigma_{p'_\perp}$ and $\tilde{\boldsymbol{r}}'_\perp = \boldsymbol{r}'_\perp$.

We assume the electrons' wave packets to be Gaussian as in the main text such that the average value of the Coulomb force between the two electrons is given by

$$\langle \tilde{\boldsymbol{F}}_C \rangle = \alpha \int \frac{\mathrm{d}^3 r_1 \mathrm{d}^3 r_2}{(2\pi)^3 \tilde{\sigma}_\parallel^2 \tilde{\sigma}_\perp^4} \frac{\boldsymbol{r}_1 - \boldsymbol{r}_2}{|\boldsymbol{r}_1 - \boldsymbol{r}_2|^3} e^{-\sum_{l=1}^{3} \frac{r_{1,l}^2 + (r_{2,l} - r'_l)^2}{2\tilde{\sigma}_l^2}}, \tag{5.28}$$

where $\alpha = e^2 \approx 1/137$ is the fine-structure constant. The integrals in Eq. 5.28 can be transformed into a simple one-dimensional integral (see Appendix B); for the parameters corresponding to Fig. 2, we obtain that $|\langle \tilde{\boldsymbol{F}}_C \rangle| \approx 3 \times 10^{-3}$ eV^2. The repulsive force is thus completely negligible with respect to the peak electric force that the laser field exerts on an electron in the same frame ($|e|\tilde{\mathcal{E}} \sim m\omega\gamma\xi = 1.6 \times 10^8$ eV^2). The same conclusion can be drawn for the numerical example corresponding to Fig. 5.3. Although this implies that the interaction between the electrons is negligible with respect to their interaction with the laser field, the interaction between the electrons before they enter the laser field could push them so far apart that there would be no interference in their radiation, neither classically nor quantum mechanically.

In order to determine the length scale at which this can occur, we can estimate after how much time $\tilde{t}$ in the average rest frame two electrons, initially at rest at a distance $\tilde{d}$ from each other, are at a distance, e.g., of $1.1\tilde{d}$, when being accelerated by a constant repulsive force $|\langle \tilde{\boldsymbol{F}}_C \rangle|$. Simple non-relativistic kinematics implies that $\tilde{t} \sim \sqrt{m\tilde{d}/10|\langle \tilde{\boldsymbol{F}}_C \rangle|}$. In the laboratory frame, $\tilde{t}$ is dilated by a factor γ and during this time the two electrons propagate along the longitudinal direction over a distance $l_\parallel \sim \gamma\tilde{t}$. By estimating $\tilde{d} \sim \tilde{r}'$, we obtain that for the parameters used for Fig. 2, $l_\parallel \sim 3\,$mm and the experimental results, e.g., in [Cole et al., 2018] show that distances between the electron source and a strong laser field much smaller than 300 μm are achieved. However, in the case of the second numerical example reported in Fig. 3, a similar estimation provides $l_\parallel$ equal to 80 μm for the panel a) (which is still acceptable), equal to 8 μm for the panel b), equal to 3 μm for the panel c), and, finally, equal to 2 μm for the panel d). Notice that while with the parameters of Fig. 2 and Fig. 3 the longitudinal component of the force $\tilde{F}_{C,\parallel}$ is typically many orders of magnitude smaller than each of the transverse components, in the panels c) and d) it is actually of the same order of magnitude. This still implies that the parallel displacement between the electrons $\tilde{d}_\parallel \sim \tilde{r}'_\parallel$ increases by 10% after a propagation in the laboratory frame of 3 μm for panel c), but for panel d) this happens already after 0.6 μm.

Finally, we observe that it is possible, via Ehrenfest's theorem, to relate this classical estimate to the evolution of the wave packets; thus, even quantum mechanically, if the wave packets drift in the laboratory a distance shorter than l, Coulomb repulsion will not change significantly the distance between their centroids. In

order to be sure that Coulomb repulsion does not change significantly the quantum states we are considering, thus a more careful analysis dependent on the experiment is needed.

5.6 Summary

In conclusion, we have shown that in the process of emission of radiation by a system of two electrons, classical predictions can significantly differ from the quantum ones even when the typical quantum nonlinearity parameter of the system is much smaller than unity. In fact, a qualitative new limit arises quantum mechanically on the frequencies which can be emitted coherently as compared to classical electrodynamics. We have shown that this limit depends on the ratio between the photon recoil and the width of the electron wave packets in momentum space.

Chapter 6

Conclusions and Outlook

In summary, we found that if an electron is in a wave packet state, the spectrum of the radiation it emits while colliding with an electromagnetic plane wave is quite different with respect to the case where it is in a Volkov state (i. e., a state with definite initial momentum); this is not due to quantum interference [Corson and Peatross, 2011; Angioi et al., 2016]. In fact, as we have shown in Chapter 4, the emission of a single-electron wave packet is nothing but a weighted average of the emission spectra of each of its components. The effects due to the uncertainty of the electron's initial momentum dominate the ones due to the indetermination of the electromagnetic pulse's frequency (due to its finiteness in time), when the two relative uncertainties are comparable.

Whereas there can be significant differences in spectra which are completely differential with respect to the emitted photon's wave-vector, by integrating over the emitted photon's direction these differences disappear, provided that the indeterminacy on the initial momentum is small with respect to the average initial momentum.

For initial states consisting of multiple electrons, the situation is radically different [Angioi and Di Piazza, 2017]. In fact, if the initial state satisfies a set of conditions we found (see Chapter 5), the energy radiated at some frequencies does not scale linearly with the number of particles, but with its square. This scaling is expected also classically when some charged particles move along sufficiently close trajectories [Klepikov, 1985; Jackson, 1999]; quantum effects due to interference can, however, suppress the radiation at frequencies where classically one would expect coherent emission.

The description of multi-electron initial states of Nonlinear Single Compton Scattering as localized wave packets is essential if one wants to recover the coherent scaling of the radiation that accelerated particles emit classically [Klepikov, 1985; Jackson, 1999; Angioi and Di Piazza, 2017].

As stated above, our results rely on the assumption that the laser field is a plane

wave; in fact, even in the case of a single electron, whereas in a plane wave to each final state of NSCS corresponds uniquely one initial state, for more complicated spatio-temporal profiles of the laser pulse this is not true anymore and there can be quantum interference effects. The study of processes in focused fields is challenging since the Dirac equation cannot be solved in such backgrounds; however, thanks to recent developments in this area [Di Piazza, 2014; Heinzl and Ilderton, 2017*a*], the effect that a focused field has on NSCS by electron wave packets can be calculated. To this day, the question of how a focused field could alter emission spectra of wave packets remains still largely unexplored, and would constitute a natural continuation of the results we presented in this thesis.

Another topic that demands further inspection is the generation of electron pulses that would make it possible to measure experimentally the spectra we have shown in Chapter 5. The coherent electron pulses which are currently used in microscopy [Baum, 2013; Kealhofer et al., 2016; Morimoto and Baum, 2018*b*,*a*]) have nonrelativistic energies, but control schemes for electrons of MeV energy with Terahertz radiation have been realized experimentally [Curry et al., 2018] and they could be a significant tool for the measurement of NSCS at the level of quantum amplitudes.

Appendix A

Explicit Evaluation of NSCS Reduced Amplitudes

The reduced amplitudes of NSCS ($\bar{u}_{p's'} M_{p'p} u_{ps}$), appearing in Chapter 4 and Chapter 5, are seldom calculated directly; it is typically more convenient to compute their modulus square via trace technology. In this appendix we will show how to compute directly the amplitudes also via traces; in order to do so, one could write $u_{ps}\bar{u}_{p's'}$ as

$$u_{ps}\bar{u}_{p's'} = a_{psp's'}\mathbb{1} + b^{\mu}_{psp's'}\gamma_\mu + ic^{\mu}_{psp's'}\gamma_\mu\gamma^5 + d^{\mu\nu}_{psp's'}\sigma_{\mu\nu} + e_{psp's'}\gamma^5, \tag{A.1}$$

where $\sigma_{\mu\nu} = i[\gamma_\mu, \gamma_\nu]/2$, the coefficients $\{a, b^\mu, c^\mu, d^{\mu\nu}, e\}_{\mu=0\ldots4,\nu<\mu}$ are arbitrary (pseudo-)scalars, (pseudo-)vectors and $d^{\mu\nu}_{psp's'}$ can be chosen as a totally antisymmetric tensor. In Eq. (A.1) we wrote $u_{ps}\bar{u}_{p's'}$ in a complete basis

$$\{\mathcal{H}_i\}_{i=1\ldots16} = \{\mathbb{1}, \gamma^\mu, i\gamma^\mu\gamma^5, \sigma^{\mu\nu}, \gamma^5\}_{\mu=1\ldots4,\nu<\mu} \tag{A.2}$$

normalized in the following way:

$$\mathrm{Trace}[\mathcal{H}_i\mathcal{H}_j] = \pm 4\delta_{ij} \qquad \forall i,j \in \{1,\ldots,16\}, \tag{A.3}$$

where the plus sign holds $\forall i, j$ with the only exception of $\{\sigma^{01}, \sigma^{02}, \sigma^{03}\}$, for which

$$\mathrm{Trace}[\sigma^{\mu\nu}\sigma^{\rho\sigma}] = 4(g^{\mu\rho}g^{\nu\sigma} - g^{\mu\sigma}g^{\nu\rho}). \tag{A.4}$$

The coefficients for the expansion of a generic matrix Θ on the basis $\{\mathcal{H}_i\}_i$ are given by

$$\begin{aligned} a = \frac{1}{4}\mathrm{Trace}[\Theta\,\mathbb{1}], \quad b^\mu &= \frac{1}{4}\mathrm{Trace}[\Theta\,\gamma^\mu], \quad c^\mu = \frac{1}{4}\mathrm{Trace}[\Theta\, i\gamma^\mu\gamma^5], \\ d^{\mu\nu} = \frac{1}{8}\mathrm{Trace}[\Theta\sigma^{\mu\nu}], \quad e &= \frac{1}{4}\mathrm{Trace}[\Theta\,\gamma^5]. \end{aligned} \tag{A.5}$$

From Eq. (A.5), we find that $M_{p'p}$ can be written in this basis as

$$\begin{aligned} M_{p'p} = & \left\{ \epsilon'^{*}_{\lambda'\,\mu}\, f_0(p',p) + \frac{e(k(p+p'))}{2(kp)(kp')} \left[(k\epsilon'^{*}_{\lambda'}) A_\mu - (A\epsilon'^{*}_{\lambda'}) k_\mu \right] f_1(p',p) \right. \\ & \left. - \frac{e^2 A^2 (k\epsilon'^{*}_{\lambda'})}{2(kp)(kp')}\, k_\mu\, f_2(p',p) \right\} \gamma^\mu \\ & + \left\{ - \frac{e(kk')}{2(kp)(kp')} \iota^{\mu\nu\rho\sigma} A_\nu k_\rho (\epsilon'^{*}_{\lambda'})_\sigma\, f_1(p',p) \right\} i\gamma_\mu\gamma^5 \\ = & \Lambda^\mu_{pp'}\gamma_\mu + \Delta^\mu_{pp'} i\gamma_\mu\gamma^5, \end{aligned} \tag{A.6}$$

where $\iota^{\mu\nu\rho\sigma}$ is the Levi-Civita symbol ($\iota^{0123} = 1$). Since the basis of matrices we have chosen is orthogonal, in order to calculate bilinear products between M and two Dirac spinors (one at M's right, the other on its left) the only coefficients we need from the expansion of Eq. A.1 are $b^\mu_{psp's'}$ and $c^\mu_{psp's'}$. By writing the spinors in Dirac's representation, after a long but straightforward calculation, we can derive the following formulas:

$$b^0_{psp's'} = \frac{1}{4}\sqrt{(\varepsilon_{\boldsymbol{p}'}+m)(\varepsilon_{\boldsymbol{p}}+m)}\; \phi^{(s')\dagger} \left[1 + \frac{\boldsymbol{p}\boldsymbol{p}' + i\,\boldsymbol{\sigma}(\boldsymbol{p}'\times\boldsymbol{p})}{(\varepsilon_{\boldsymbol{p}'}+m)(\varepsilon_{\boldsymbol{p}}+m)} \right] \phi^{(s)} \tag{A.7}$$

$$\boldsymbol{b}_{psp's'} = \frac{1}{4}\sqrt{(\varepsilon_{\boldsymbol{p}'}+m)(\varepsilon_{\boldsymbol{p}}+m)}\; \phi^{(s')\dagger} \left[\frac{\boldsymbol{p} + i\,\boldsymbol{p}\times\boldsymbol{\sigma}}{(\varepsilon_{\boldsymbol{p}}+m)} + \frac{\boldsymbol{p}' - i\,\boldsymbol{p}'\times\boldsymbol{\sigma}}{(\varepsilon_{\boldsymbol{p}'}+m)} \right] \phi^{(s)} \tag{A.8}$$

$$c^0_{psp's'} = \frac{i}{4}\sqrt{(\varepsilon_{\boldsymbol{p}'}+m)(\varepsilon_{\boldsymbol{p}}+m)}\; \phi^{(s')\dagger} \left[\frac{\boldsymbol{\sigma}\boldsymbol{p}}{(\varepsilon_{\boldsymbol{p}}+m)} + \frac{\boldsymbol{\sigma}\boldsymbol{p}'}{(\varepsilon_{\boldsymbol{p}'}+m)} \right] \phi^{(s)} \tag{A.9}$$

$$\boldsymbol{c}_{psp's'} = \frac{i}{4}\sqrt{(\varepsilon_{\boldsymbol{p}'}+m)(\varepsilon_{\boldsymbol{p}}+m)}\; \phi^{(s')\dagger} \left[\boldsymbol{\sigma} + \frac{(\boldsymbol{\sigma}\boldsymbol{p})\boldsymbol{p}' + (\boldsymbol{\sigma}\boldsymbol{p}')\boldsymbol{p} + i(\boldsymbol{p}\times\boldsymbol{p}') - (\boldsymbol{p}'\boldsymbol{p})\boldsymbol{\sigma}}{(\varepsilon_{\boldsymbol{p}'}+m)(\varepsilon_{\boldsymbol{p}}+m)} \right] \phi^{(s)} \tag{A.10}$$

where $\boldsymbol{\sigma} = (\sigma^1, \sigma^2, \sigma^3)$ are the Pauli matrices and the i^{th} component of $\boldsymbol{p}\times\boldsymbol{\sigma}$ is $\iota^{ijk} p^j \sigma^k$. We were never able to find the expressions for $b^\mu_{psp's'}$ and $c^\mu_{psp's'}$ in the literature.

A.1 Polarization sums

We turn now to the problem of calculating bilinear products of the form

$$(\bar{u}_{p'_1 s'_1} M_{p'_1 q_1} u_{q_1 s_1})^* \, (\bar{u}_{p'_2 s'_2} M_{p'_2 q_2} u_{q_2 s_2}) \tag{A.11}$$

and, in particular, how to calculate sums over the polarization of the emitted photon. Starting from the relation $\sum_{\lambda'} \epsilon'^{*\mu}_{\lambda'} \epsilon'^{\nu}_{\lambda'} = -g^{\mu\nu}$, we will now calculate the tensor

products of the form $\Lambda^{\mu}\Lambda^{*\mu'}$, $\Lambda^{\mu}\Delta^{*\mu'}$, and $\Delta^{\mu}\Delta^{*\mu'}$ (we don't calculate explicitly $\Delta^{\mu}\Lambda^{*\mu'}$ since it is just the complex conjugate of $\Lambda^{\mu}\Delta^{*\mu'}$).

Let us begin with

$$\sum_{\lambda'} \Delta^{\mu}_{q_1 p_1'} \Delta^{*\mu'}_{q_2 p_2'} = \\ = -\frac{e(kk')}{2(kq_1)(kp_1')} \frac{e(kk')}{2(kq_2)(kp_2')} \iota^{\mu\nu\rho\sigma} \iota^{\mu'\nu'\rho'\sigma'} g_{\sigma\sigma'} A_{\nu} k_{\rho} A_{\nu'} k_{\rho'} \, f_1(p_1', q_1) f_1^*(p_2', q_2); \tag{A.12}$$

From the property of the Levi-Civita symbol under contractions with the metric

$$\iota^{\mu\nu\rho\sigma} \iota^{\mu'\nu'\rho'\sigma'} g_{\sigma\sigma'} = \\ = g^{\mu\rho'} g^{\mu'\rho} g^{\nu\nu'} - g^{\mu\mu'} g^{\nu\nu'} g^{\rho\rho'} - g^{\mu\nu'} g^{\mu'\rho} g^{\nu\rho'} - g^{\mu\rho'} g^{\mu'\nu} g^{\nu'\rho} + g^{\mu\mu'} g^{\nu\rho'} g^{\nu'\rho} + g^{\mu\nu'} g^{\mu'\nu} g^{\rho\rho'} \tag{A.13}$$

and from the fact that $(Ak) = 0$ and $k^2 = 0$ we find that in the previous equation only the first term is important, so that

$$\iota^{\mu\nu\rho\sigma} \iota^{\mu'\nu'\rho'\sigma} A_{\nu} k_{\rho} A_{\nu'} k_{\rho'} = k^{\mu} k^{\mu'} A^2, \tag{A.14}$$

thus finally

$$\sum_{\lambda'} \Delta^{\mu}_{q_1 p_1'} \Delta^{*\mu'}_{q_2 p_2'} = -\frac{e(kk')}{2(kq_1)(kp_1')} \frac{e(kk')}{2(kq_2)(kp_2')} k^{\mu} k^{\mu'} A^2 \, f_1(p_1', q_1) f_1^*(p_2', q_2). \tag{A.15}$$

From this relation we also see that, regardless of the initial and final momenta, $\Delta^{\mu}\Delta^{*}_{\mu} = 0$ (this comes from $k^2 = 0$).

Another quantity we need is

$$\sum_{\lambda'} \Lambda^{\mu}_{q_1 p_1'} \Delta^{*\mu'}_{q_2 p_2'} = \\ = -\frac{e(kk')}{2(kq_2)(kp_2')} f_1^*(p_2', q_2) \\ \Big\{ \iota^{\mu\,\mu'\nu'\rho'} A_{\nu'} k_{\rho'} \, f_0(p_1', q_1) + \frac{e(k(q_1 + p_1'))}{2(kq_1)(kp_1')} \iota^{\mu'\nu'\rho'\sigma'} A_{\nu'} k_{\rho'} (k_{\sigma'} A^{\mu} - A_{\sigma'} k^{\mu}) \, f_1(p_1', q_1) \\ - \frac{e^2 A^2}{2(kq_1)(kp_1')} \, \iota^{\mu'\nu'\rho'\sigma'} A_{\nu'} k_{\rho'} k_{\sigma'} k^{\mu} \, f_2(p_1', q_1) \Big\}, \tag{A.16}$$

and since for any four-vector w^{μ}

$$\iota^{\mu\nu\rho\sigma} w_{\mu} w_{\nu} = -\iota^{\nu\mu\rho\sigma} w_{\nu} w_{\mu} = -\iota^{\mu\nu\rho\sigma} w_{\mu} w_{\nu}, \quad \Rightarrow \quad \iota^{\mu\nu\rho\sigma} w_{\mu} w_{\nu} = 0 \tag{A.17}$$

we see that in Eq. A.16 only the first term in curly brackets gives a nonzero contribution, and so

$$\sum_{\lambda'} \Lambda^{\mu}_{q_1 p_1'} \Delta^{*\mu'}_{q_2 p_2'} = -\frac{e(kk')}{2(kq_2)(kp_2')} \iota^{\mu\,\mu'\nu'\rho'} A_{\nu'} k_{\rho'}\, f_0(p_1', q_1) f_1^*(p_2', q_2), \tag{A.18}$$

and of course, regardless of the momenta,

$$\sum_{\lambda'} \Lambda^{\mu} \Delta^{*}_{\mu} = 0. \tag{A.19}$$

For convenience, we also write

$$\sum_{\lambda'} \Delta^{\mu}_{q_1 p_1'} \Lambda^{*\mu'}_{q_2 p_2'} = \sum_{\lambda'} \left(\Lambda^{\mu'}_{q_2 p_2'} \Delta^{*\mu}_{q_1 p_1'} \right)^* = \frac{e(kk')}{2(kq_1)(kp_1')} \iota^{\mu\,\mu'\nu'\rho'} A_{\nu'} k_{\rho'}\, f_0^*(p_2', q_2) f_1(p_1', q_1). \tag{A.20}$$

Finally, we evaluate the last term:

$$\begin{aligned}
&\sum_{\lambda'} \Lambda^{\mu}_{q_1 p_1'} \Lambda^{*\mu'}_{q_2 p_2'} = \\
&\qquad = -\Bigg\{ f_0(p_1', q_1) \\
&\left[g^{\mu\mu'} f_0^*(p_2', q_2) + \frac{e(k(q_2 + p_2'))}{2(kq_2)(kp_2')}\, 2k^{[\mu} A^{\mu']}\, f_1^*(p_2', q_2) - \frac{e^2 A^2}{2(kq_2)(kp_2')}\, k^{\mu} k^{\mu'}\, f_2^*(p_2', q_2) \right] \\
&+ \frac{e(k(q_1 + p_1'))}{2(kq_1)(kp_1')} f_1(p_1', q_1) \left[-2k^{[\mu} A^{\mu']} f_0^*(p_2', q_2) + \frac{e(k(q_2 + p_2'))}{2(kq_2)(kp_2')}\, A^2\, k^{\mu} k^{\mu'} f_1^*(p_2', q_2) \right] \\
&\qquad\qquad - \frac{e^2 A^2}{2(kq_1)(kp_1')}\, k^{\mu} k^{\mu'}\, f_2(p_1', q_1) f_0^*(p_2', q_2) \Bigg\},
\end{aligned} \tag{A.21}$$

where we introduced the shorthand notation $k^{[\mu} A^{\mu']} = (k^{\mu} A^{\mu'} - k^{\mu'} A^{\mu})/2$. From the last expression, it is also clear that

$$\sum_{\lambda'} \Lambda^{\mu}_{q_1 p_1'} \Lambda^{*\mu'}_{q_2 p_2'}\, g_{\mu\mu'} = -4 f_0(p_1', q_1) f_0^*(p_2', q_2). \tag{A.22}$$

Notice that while the other sums we calculated had some definite symmetry under the exchange of the two free indexes μ and μ', the right-hand side of Eq. A.21 is neither symmetric nor antisymmetric. Let us write it again, but by explicitly

splitting the symmetric part and the antisymmetric part:

$$\sum_{\lambda'} \Lambda^{\mu}_{q_1 p'_1} \Lambda^{*\mu'}_{q_2 p'_2} = \left\{ \left[\frac{e^2 A^2}{2(kq_2)(kp'_2)} f_0(p'_1, q_1) f_2^*(p'_2, q_2) + \frac{e^2 A^2}{2(kq_1)(kp'_1)} f_2(p'_1, q_1) f_0^*(p'_2, q_2) \right.\right.$$
$$\left.\left. - \frac{e(k(q_1 + p'_1))}{2(kq_1)(kp'_1)} \frac{e(k(q_2 + p'_2))}{2(kq_2)(kp'_2)} A^2 \, f_1(p'_1, q_1) f_1^*(p'_2, q_2) \right] k^{\mu} k^{\mu'} - f_0(p'_1, q_1) f_0^*(p'_2, q_2) g^{\mu\mu'} \right\}$$
$$+ \left\{ \left[\frac{e(k(q_1 + p'_1))}{(kq_1)(kp'_1)} f_1(p'_1, q_1) f_0^*(p'_2, q_2) - \frac{e(k(q_2 + p'_2))}{(kq_2)(kp'_2)} f_0(p'_1, q_1) f_1^*(p'_2, q_2) \right] k^{[\mu} A^{\mu']} \right\}. \tag{A.23}$$

A.2 Single-Electron Reduced Probability

When $p'_1 = p'_2 \equiv p'$ and $q_1 = q_2 \equiv p$, the bilinear products we have been calculating are known in the literature, and can be derived via trace technology. They give the square modulus of the reduced transition amplitude for Nonlinear Single Compton Scattering, and they are equal to

$$\sum_{\lambda' s' s} |\bar{u}_{p' s'} M u_{p s}|^2 =$$
$$= -8 \left\{ \left[\frac{e^2 A^2}{2} \left(\frac{(pk)}{(p'k)} + \frac{(p'k)}{(pk)} \right) - \frac{e\alpha}{\gamma} (kk') \left(\frac{(Ap)}{kp} - \frac{(Ap')}{kp'} \right) - \frac{\alpha^2}{\gamma^2} \left((pp') - 2m^2 \right) \right] |f_1|^2 \right.$$
$$- \left[\frac{\alpha\beta}{\gamma^2} \left((pp') - 2m^2 \right) - \frac{\alpha}{\gamma} \frac{e^2 A^2}{2} - \frac{e\beta}{2\gamma} (kk') \left(\frac{(Ap)}{kp} - \frac{(Ap')}{kp'} \right) \right] (f_1^* f_2 + f_1 f_2^*)$$
$$\left. + \left[\frac{\beta}{\gamma} e^2 A^2 - \frac{\beta^2}{\gamma^2} \left((pp') - 2m^2 \right) \right] |f_2|^2 \right\}. \tag{A.24}$$

All the terms that one obtains with the previously described polarization sum procedure have to reduce to the ones in Eq. (A.24). In the basis we have chosen, $\sum_{\lambda' s' s} |\bar{u}_{p' s'} M u_{p s}|^2 = \sum_{\lambda' s' s} |4(b_{p s p' s'} \Lambda_{p p'}) + 4(c_{p s p' s'} \Delta_{p p'})|^2$, so proving that this relation gives the same result as Eq. A.24 is only a matter of contracting the tensors $\sum_{\lambda'} \Lambda^{\mu}_{p p'} \Lambda^{*\mu'}_{p p'}$, $\sum_{\lambda'} \Lambda^{\mu}_{p p'} \Delta^{*\mu'}_{p p'}$, $\sum_{\lambda'} \Delta^{\mu}_{p p'} \Lambda^{*\mu'}_{p p'}$, and $\sum_{\lambda'} \Delta^{\mu}_{p p'} \Delta^{*\mu'}_{p p'}$ with the appropriate (pseudo)four-vectors. Moreover, in Eq. A.24 f_0 is not present, and this is because it has been written in terms of f_1 and f_2, according to the formula $f_0 = -(\alpha f_1 + \beta f_2)/\gamma$. Let us start with $\sum_{\lambda' s' s} (b_{p s p' s'} \Lambda_{p p'})(\Lambda^*_{p p'} b^*_{p s p' s'})$; in order to calculate it we need the

following three quantities:

$$\sum_{s's}(b_{psp's'}k)(b^*_{psp's'}k)=\sum_{s's}\frac{1}{16}k_\mu k_\nu(\bar u_{p's'}\gamma^\mu u_{ps})(\bar u_{ps}\gamma^\nu u_{p's'})=\frac{(kp)(kp')}{2}, \tag{A.25}$$

$$\sum_{s's}(b_{psp's'}b^*_{psp's'})=\sum_{s's}\ \frac{1}{16}\ g_{\mu\nu}(\bar u_{p's'}\gamma^\mu u_{ps})(\bar u_{ps}\gamma^\nu u_{p's'})=-\frac{1}{2}\left[(p'p)-2m^2\right], \tag{A.26}$$

$$\sum_{s's}b^\mu_{psp's'}b^{\nu\,*}_{psp's'}k_{[\mu}A_{\nu]}=0. \tag{A.27}$$

And so we can obtain

$$\sum_{\lambda's's}(b_{psp's'}\Lambda_{pp'})(\Lambda^*_{pp'}b^*_{psp's'})=$$
$$\left\{\left[-\frac{e^2A^2}{4}\left(\frac{\alpha}{\gamma}(f_1f_2^*+f_1^*f_2)+2\frac{\beta}{\gamma}|f_2|^2\right)+\frac{e^2A^2}{8}\left(\frac{(pk)}{(p'k)}+\frac{(p'k)}{(pk)}+2\right)|f_1|^2\right]\right.$$
$$\left.+\frac{1}{2}\left[(p'p)-2m^2\right]\left(\frac{\alpha^2}{\gamma^2}|f_1|^2+\frac{\alpha\beta}{\gamma^2}(f_1f_2^*+f_1^*f_2)+\frac{\beta^2}{\gamma^2}|f_2|^2\right)\right\}. \tag{A.28}$$

For the term $\sum_{\lambda's's}(c_{psp's'}\Delta_{pp'})(\Delta^*_{pp'}c^*_{psp's'})$ we need to calculate only one contraction[1]

$$\sum_{s's}(c_{psp's'}k)(c^*_{psp's'}k)=\sum_{s's}\frac{1}{16}k_\mu k_\nu\left[\bar u_{p's'}(i\gamma^\mu\gamma^5)u_{ps}\right]\left[\bar u_{ps}(-i\gamma^\nu\gamma^5)u_{p's'}\right]$$
$$=\frac{(kp)(kp')}{2}, \tag{A.30}$$

(notice that it is the same as Eq. A.25), and so

$$\sum_{\lambda's's}(c_{psp's'}\Delta_{pp'})(\Delta^*_{pp'}c^*_{psp's'})=-\frac{e^2A^2}{8}\left(\frac{(pk)}{(p'k)}+\frac{(p'k)}{(pk)}-2\right)|f_1|^2. \tag{A.31}$$

Finally, for $\sum_{\lambda's's}(b_{psp's'}\Lambda_{pp'})(\Delta^*_{pp'}c^*_{psp's'})$, by noting that

$$\sum_{s's}b^\alpha_{psp's'}c^{\beta\,*}_{psp's'}=-p'_\gamma p_\delta\iota^{\gamma\alpha\delta\beta}/4 \tag{A.32}$$

[1]Notice that

$$4c^{\mu*}_{psp's'}=(\bar u_{p's'}(i\gamma^\mu\gamma^5)u_{ps})^*=u^\dagger_{ps}(-i\gamma^5(\gamma^\mu)^\dagger)\gamma^0u_{p's'}=\bar u_{ps}(-i\gamma^\mu\gamma^5)u_{p's'} \tag{A.29}$$

we can calculate

$$\sum_{s's} \iota^{\mu\mu'\nu'\rho'} g_{\mu\alpha} g_{\mu'\beta}\, b^{\alpha}_{psp's'} c^{\beta\,*}_{psp's'} = -\frac{\iota^{\mu\mu'\nu'\rho'}\iota^{\alpha\beta\delta\gamma}}{4} g_{\mu\alpha} g_{\mu'\beta} p'_{\gamma} p_{\delta} = \frac{p'_{\gamma} p_{\delta}}{2}(g^{\nu'\delta} g^{\rho'\gamma} - g^{\nu'\gamma} g^{\rho'\delta}), \tag{A.33}$$

where we used $\iota^{\mu\mu'\nu'\rho'}\iota^{\alpha\beta\delta\gamma} g_{\mu\alpha} g_{\mu'\beta} = -2(g^{\nu'\delta} g^{\rho'\gamma} - g^{\nu'\gamma} g^{\rho'\delta})$ (in order to check this relation, especially whether it has correct sign, one can start from Eq. A.13) and so we get

$$\sum_{\lambda' s' s} (b_{psp's'} \Lambda_{pp'})(\Delta^{*}_{pp'} c^{*}_{psp's'}) = \frac{e(kk')}{4} \left(\frac{(Ap)}{kp} - \frac{(Ap')}{kp'} \right) \left(\frac{\alpha}{\gamma} |f_1|^2 + \frac{\beta}{\gamma} f_1^{*} f_2 \right). \tag{A.34}$$

If we sum all the expressions we found, without forgetting that there is also another term that is the complex conjugate of Eq. A.34, we can recover the correct formula stated in Eq. A.24.

Appendix B

Coulomb Integral with Gaussian Wave Packets

In Section 5.5, in order to estimate the effect of Coulomb repulsion between two electrons, each in a Gaussian wave packet state, translated one with respect to the other by a constant vector $\boldsymbol{r}'$, we had to calculate the expectation value

$$\langle \tilde{\boldsymbol{F}}_C \rangle = \frac{e^2}{(2\pi)^3 \sigma_\parallel^2 \sigma_\perp^4} \int \mathrm{d}^3 r_1 \mathrm{d}^3 r_2 \, \frac{\boldsymbol{r}_1 - \boldsymbol{r}_2}{|\boldsymbol{r}_1 - \boldsymbol{r}_2|^3} \, e^{-\frac{\boldsymbol{r}_{1,\perp}^2 + (\boldsymbol{r}_{2,\perp} - \boldsymbol{r}'_\perp)^2}{2\sigma_\perp^2}} e^{-\frac{r_{1,\parallel}^2 + (r_{2,\parallel} - r'_\parallel)^2}{2\sigma_\parallel^2}} . \quad \text{(B.1)}$$

After a variable transformation (with Jacobian equal to unity)

$$\boldsymbol{u} = \frac{\boldsymbol{r}_1 + \boldsymbol{r}_2}{2}, \qquad \boldsymbol{v} = \boldsymbol{r}_1 - \boldsymbol{r}_2, \quad \text{(B.2)}$$

the numerators of the exponents of the Gaussians can be written as

$$r_{1,j}^2 + (r_{2,j} - r'_j)^2 = 2(u_j^2 - u_j r'_j) + \frac{v_j^2}{2} + v_j r'_j + r_j'^2. \quad \text{(B.3)}$$

Thus, the integral in Eq. (B.1) splits in two parts: a 3D integral over $\boldsymbol{u}$ and another 3D integral over $\boldsymbol{v}$; The first one can be evaluated analytically, as

$$\int \mathrm{d}^3 u \, e^{-\frac{\boldsymbol{u}_\perp^2 - \boldsymbol{u}_\perp \cdot \boldsymbol{r}'_\perp}{\sigma_\perp^2}} e^{-\frac{u_\parallel^2 - u_\parallel \cdot r'_\parallel}{\sigma_\parallel^2}} = \sqrt{\pi^3} \sigma_\perp^2 \sigma_\parallel e^{\frac{\boldsymbol{r}_\perp'^2}{4\sigma_\perp^2} + \frac{r_\parallel'^2}{4\sigma_\parallel^2}}. \quad \text{(B.4)}$$

The remaining integral is more involved; let us write it as

$$\boldsymbol{I} = e^{-\frac{\boldsymbol{r}_\perp'^2}{4\sigma_\perp^2} - \frac{r_\parallel'^2}{4\sigma_\parallel^2}} \int \mathrm{d}^3 v \, \frac{\boldsymbol{v}}{v^3} \, e^{-\frac{(\boldsymbol{v}_\perp + \boldsymbol{r}'_\perp)^2}{4\sigma_\perp^2} - \frac{(v_\parallel + r'_\parallel)^2}{4\sigma_\parallel^2}} \quad \text{(B.5)}$$

(here we used $\frac{v_j^2}{2} + v_j r'_j + r'^2_j = (v_j + r'_j)^2/2 + r'^2_j/2$). Notice that

$$\frac{\boldsymbol{v}}{v^3} = -\boldsymbol{\nabla}\frac{1}{v}, \tag{B.6}$$

and that the function $1/v$ has the following integral representation:

$$\frac{1}{v} = \frac{2}{\sqrt{\pi}} \int_0^\infty \mathrm{d}s\, e^{-v^2 s^2}. \tag{B.7}$$

The integral $\boldsymbol{I}$ now has the form

$$\int \mathrm{d}^3 v\, (\boldsymbol{\nabla} f) g = \int \mathrm{d}^3 v\, \boldsymbol{\nabla}(fg) - \int \mathrm{d}^3 v\, f(\boldsymbol{\nabla} g). \tag{B.8}$$

The integral $\int \mathrm{d}^3 v\, \boldsymbol{\nabla}(fg)$ can be transformed into a surface integral, and since fg becomes exponentially small as $v \to \infty$ (and, in particular, since it decays faster than $1/v^2$) the value of this integral is zero. This implies that we can write $\boldsymbol{I}$ as

$$\boldsymbol{I} = \frac{2e^{-\frac{\boldsymbol{r}'^2_\perp}{4\sigma_\perp^2} - \frac{r'^2_\parallel}{4\sigma_\parallel^2}}}{\sqrt{\pi}} \int_0^\infty \mathrm{d}s \int \mathrm{d}^3 v \left(-\frac{(\boldsymbol{v}_\perp + \boldsymbol{r}'_\perp)}{2\sigma_\perp^2}, -\frac{(v_\parallel + r'_\parallel)}{2\sigma_\parallel^2} \right) e^{-\frac{(\boldsymbol{v}_\perp + \boldsymbol{r}'_\perp)^2}{4\sigma_\perp^2} - s^2 \boldsymbol{v}_\perp^2} e^{-\frac{(v_\parallel + r'_\parallel)^2}{4\sigma_\parallel^2} - s^2 v_\parallel^2}. \tag{B.9}$$

By adding and subtracting to the integrand the quantity

$$\frac{2e^{-\frac{\boldsymbol{r}'^2_\perp}{4\sigma_\perp^2} - \frac{r'^2_\parallel}{4\sigma_\parallel^2}}}{\sqrt{\pi}} 2s^2 \left(\boldsymbol{v}_\perp, v_\parallel\right) e^{-\frac{(\boldsymbol{v}_\perp + \boldsymbol{r}'_\perp)^2}{4\sigma_\perp^2} - s^2 \boldsymbol{v}_\perp^2} e^{-\frac{(v_\parallel + r'_\parallel)^2}{4\sigma_\parallel^2} - s^2 v_\parallel^2} \tag{B.10}$$

one can see that one part of the integral is again a surface term. The other reads

$$\boldsymbol{I} = \frac{2e^{-\frac{\boldsymbol{r}'^2_\perp}{4\sigma_\perp^2} - \frac{r'^2_\parallel}{4\sigma_\parallel^2}}}{\sqrt{\pi}} \int_0^\infty \mathrm{d}s \int \mathrm{d}^3 v\, 2s^2 \left(\boldsymbol{v}_\perp, v_\parallel\right) e^{-\frac{(\boldsymbol{v}_\perp + \boldsymbol{r}'_\perp)^2}{4\sigma_\perp^2} - s^2 \boldsymbol{v}_\perp^2} e^{-\frac{(v_\parallel + r'_\parallel)^2}{4\sigma_\parallel^2} - s^2 v_\parallel^2}. \tag{B.11}$$

A few manipulations to the exponents of the Gaussians lead to

$$\frac{(v_j + r'_j)^2}{4\sigma_j^2} + s^2 v_j^2 = A_j \left(v_j + \frac{r'_j}{4\sigma_j^2 A_j} \right)^2 - \frac{r'^2_j}{(4\sigma_j^2 A_j)^2} + \frac{r'^2_j}{4\sigma_j^2}, \tag{B.12}$$

where we introduced

$$A_j = \frac{1}{4\sigma_j^2} + s^2 \tag{B.13}$$

(notice that $4\sigma_j^2 A_j = 1+4\sigma_j^2 s^2$). One then arrives to this simple form of the integral in $\boldsymbol{v}$:

$$\boldsymbol{I} = \frac{4e^{-\frac{\boldsymbol{r}'^2_\perp}{2\sigma^2_\perp}-\frac{r'^2_\parallel}{2\sigma^2_\parallel}}}{\sqrt{\pi}} \int_0^\infty \mathrm{d}s\, s^2 e^{\sum_{j=1}^3 \frac{r'^2_j}{(1+4\sigma_j^2 s^2)^2}} \int \mathrm{d}^3 v\ \left(\boldsymbol{v}_\perp, v_\parallel\right)\ e^{-\sum_{j=1}^3 A_j\left(v_j+\frac{r'_j}{4\sigma_j^2 A_j}\right)^2}. \quad \text{(B.14)}$$

By remembering the elementary Gaussian integrals

$$\int_{-\infty}^{+\infty} \mathrm{d}x\, e^{-a(x-\mu)^2} = \sqrt{\frac{\pi}{a}} \quad \text{(B.15)}$$

and

$$\int_{-\infty}^{+\infty} \mathrm{d}x\, x e^{-a(x-\mu)^2} = \sqrt{\frac{\pi}{a}}\mu \quad \text{(B.16)}$$

we can perform all the integrals over $\boldsymbol{v}$ and finally arrive at

$$\boldsymbol{I} = -4\pi e^{-\frac{\boldsymbol{r}'^2_\perp}{2\sigma^2_\perp}-\frac{r'^2_\parallel}{2\sigma^2_\parallel}} \int_0^\infty \mathrm{d}s\, \frac{s^2 e^{\sum_{j=1}^3 \frac{r'^2_j}{(1+4\sigma_j^2 s^2)^2}}}{A_\perp \sqrt{A_\parallel}} \left(\frac{\boldsymbol{r}'_\perp}{1+4\sigma^2_\perp s^2}, \frac{r'_\parallel}{1+4\sigma^2_\parallel s^2}\right); \quad \text{(B.17)}$$

this form of the integral is particularly easy to integrate numerically since the integrand is a smooth function free of singularities and decaying at infinity as s^3.

Bibliography

Adler, S. L., Bahcall, J. N., Callan, C. G. and Rosenbluth, M. N. [1970], 'Photon splitting in a strong magnetic field', *Phys. Rev. Lett.* **25**, 1061–1065.
URL: https://link.aps.org/doi/10.1103/PhysRevLett.25.1061

Angioi, A. and Di Piazza, A. [2017], 'Quantum limitation to the coherent emission of accelerated charges'. *Submitted.*
URL: https://arxiv.org/abs/1712.01123

Angioi, A., Mackenroth, F. and Di Piazza, A. [2016], 'Nonlinear single Compton scattering of an electron wave packet', *Phys. Rev. A* **93**, 052102.
URL: https://link.aps.org/doi/10.1103/PhysRevA.93.052102

APOLLON Laser [website].
URL: www.apollon-laser.fr

Astra-Gemini Laser [website].
URL: https://www.clf.stfc.ac.uk/Pages/The-Astra-Gemini-Facility.aspx

ATLAS Collaboration [2017], 'Evidence for light-by-light scattering in heavy-ion collisions with the ATLAS detector at the LHC', *Nat. Phys.* **13**(9), 852–858.
URL: http://dx.doi.org/10.1038/nphys4208

Bagrov, V. G., Belov, V. V. and Trifonov, A. Y. [1993], 'Theory of spontaneous radiation by electrons in a trajectory-coherent approximation', *J. Phys. A: Math. Gen.* **26**(22), 6431.
URL: http://stacks.iop.org/0305-4470/26/i=22/a=038

Baier, R. and Breitenlohner, P. [1967], 'Photon Propagation in External Fields', *Acta Phys. Austriaca* **25**, 212–223.

Baier, V. N., Katkov, V. M. and Strakhovenko, V. M. [1998], *Electromagnetic processes at high energies in oriented single crystals*, World Scientific, Singapore.

Baier, V. N., Milstein, A. I. and Shaisultanov, R. Z. [1987], 'Photon splitting in a strong electromagnetic field and the possibility of its observation in single crystals', *Phys. Lett. A* **120**(5), 255 – 258.
URL: http://www.sciencedirect.com/science/article/pii/0375960187902209

Baier, V. N., Milstein, A. I. and Shaisultanov, R. Z. [1996], 'Photon splitting in a very strong magnetic field', *Phys. Rev. Lett.* **77**, 1691–1694.
URL: https://link.aps.org/doi/10.1103/PhysRevLett.77.1691

Bamber, C., Boege, S. J., Koffas, T., Kotseroglou, T., Melissinos, A. C., Meyerhofer, D. D., Reis, D. A., Ragg, W., Bula, C., McDonald, K. T., Prebys, E. J., Burke, D. L., Field, R. C., Horton-Smith, G., Spencer, J. E., Walz, D., Berridge, S. C., Bugg, W. M., Shmakov, K. and Weidemann, A. W. [1999], 'Studies of nonlinear QED in collisions of 46.6 GeV electrons with intense laser pulses', *Phys. Rev. D* **60**, 092004.
URL: https://link.aps.org/doi/10.1103/PhysRevD.60.092004

Bashinov, A. V., Efimenko, E. S., Gonoskov, A. A., Korzhimanov, A. V., Muraviev, A. A., Kim, A. V. and Sergeev, A. M. [2017], 'Towards attosecond-scale highly directed GeV gamma-ray sources with multipetawatt-class lasers', *J. Opt.* **19**(11), 114012.
URL: http://stacks.iop.org/2040-8986/19/i=11/a=114012

Baum, P. [2013], 'On the physics of ultrashort single-electron pulses for time-resolved microscopy and diffraction', *Chem. Phys.* **423**(Supplement C), 55 – 61.
URL: http://www.sciencedirect.com/science/article/pii/S0301010413002681

Bellman, R. E. [1961], *Adaptive Control Processes: A Guided Tour*, Princeton University Press, Princeton.

Berestetskii, V. B., Lifshitz, E. M. and Pitaevskiĭ, L. P. [1982], *Quantum Electrodynamics*, Butterworth-Heinemann, Oxford.

Berkeley Lab Laser Accelerator (BELLA) [website].
URL: http://bella.lbl.gov/

Bialynicka-Birula, Z. and Bialynicki-Birula, I. [1970], 'Nonlinear effects in Quantum Electrodynamics. photon propagation and photon splitting in an external field', *Phys. Rev. D* **2**, 2341–2345.
URL: https://link.aps.org/doi/10.1103/PhysRevD.2.2341

Blättel, B., Koch, V., Lang, A., Weber, K., Cassing, W. and Mosel, U. [1989], *The Nuclear Equation of State: Part A: Discovery of Nuclear Shock Waves and the EOS*, Springer, Boston, pp. 321–330.

Boca, M., Dinu, V. and Florescu, V. [2012], 'Electron distributions in nonlinear Compton scattering', *Phys. Rev. A* **86**, 013414.
URL: https://link.aps.org/doi/10.1103/PhysRevA.86.013414

Boca, M. and Florescu, V. [2009], 'Nonlinear Compton scattering with a laser pulse', *Phys. Rev. A* **80**(5), 053403.
URL: http://link.aps.org/doi/10.1103/PhysRevA.80.053403

Boca, M. and Florescu, V. [2011], 'Thomson and Compton scattering with an intense laser pulse', *Eur. Phys. J. D* **61**(2), 449–462.
URL: https://doi.org/10.1140/epjd/e2010-10429-y

Bragin, S., Meuren, S., Keitel, C. H. and Di Piazza, A. [2017], 'High-energy vacuum birefringence and dichroism in an ultrastrong laser field', *Phys. Rev. Lett.* **119**, 250403.
URL: https://link.aps.org/doi/10.1103/PhysRevLett.119.250403

Brown, L. S. and Kibble, T. W. B. [1964], 'Interaction of intense laser beams with electrons', *Phys. Rev.* **133**, A705–A719.
URL: https://link.aps.org/doi/10.1103/PhysRev.133.A705

Bungartz, H.-J. and Griebel, M. [2004], 'Sparse grids', *Acta Numer.* **13**, 147–269.
URL: https://doi.org/10.1017/S0962492904000182

Caflisch, R. E. [1998], 'Monte carlo and quasi-monte carlo methods', *Acta Numer.* **7**, 1–49.
URL: https://doi.org/10.1017/S0962492900002804

Claessens, B. J., van der Geer, S. B., Taban, G., Vredenbregt, E. J. D. and Luiten, O. J. [2005], 'Ultracold electron source', *Phys. Rev. Lett.* **95**, 164801.
URL: https://link.aps.org/doi/10.1103/PhysRevLett.95.164801

Cole, J. M., Behm, K. T., Gerstmayr, E., Blackburn, T. G., Wood, J. C., Baird, C. D., Duff, M. J., Harvey, C., Ilderton, A., Joglekar, A. S., Krushelnick, K., Kuschel, S., Marklund, M., McKenna, P., Murphy, C. D., Poder, K., Ridgers, C. P., Samarin, G. M., Sarri, G., Symes, D. R., Thomas, A. G. R., Warwick, J., Zepf, M., Najmudin, Z. and Mangles, S. P. D. [2018], 'Experimental evidence of radiation reaction in the collision of a high-intensity laser pulse with a laser-wakefield accelerated electron beam', *Phys. Rev. X* **8**, 011020.
URL: https://link.aps.org/doi/10.1103/PhysRevX.8.011020

Corson, J. P. and Peatross, J. [2011], 'Quantum-electrodynamic treatment of photoemission by a single-electron wave packet', *Phys. Rev. A* **84**, 053832.
URL: https://link.aps.org/doi/10.1103/PhysRevA.84.053832

Corson, J. P., Peatross, J., Müller, C. and Hatsagortsyan, K. Z. [2011], 'Scattering of intense laser radiation by a single-electron wave packet', *Phys. Rev. A* **84**, 053831.
URL: https://link.aps.org/doi/10.1103/PhysRevA.84.053831

Curry, E., Fabbri, S., Maxson, J., Musumeci, P. and Gover, A. [2018], 'Meter-scale terahertz-driven acceleration of a relativistic beam', *Phys. Rev. Lett.* **120**, 094801.
URL: https://link.aps.org/doi/10.1103/PhysRevLett.120.094801

Della Valle, F., Ejlli, A., Gastaldi, U., Messineo, G., Milotti, E., Pengo, R., Ruoso, G. and Zavattini, G. [2016], 'The PVLAS experiment: measuring vacuum magnetic birefringence and dichroism with a birefringent Fabry–Perot cavity', *Eur. Phys. J. C* **76**(1), 24.
URL: https://doi.org/10.1140/epjc/s10052-015-3869-8

Di Piazza, A. [2008], 'Exact solution of the Landau-Lifshitz equation in a plane wave', *Lett. Math. Phys.* **83**(3), 305–313.
URL: https://doi.org/10.1007/s11005-008-0228-9

Di Piazza, A. [2014], 'Ultrarelativistic electron states in a general background electromagnetic field', *Phys. Rev. Lett.* **113**, 040402.
URL: http://link.aps.org/doi/10.1103/PhysRevLett.113.040402

Di Piazza, A. [2015], 'Analytical tools for investigating strong-field QED processes in tightly focused laser fields', *Phys. Rev. A* **91**, 042118.
URL: https://link.aps.org/doi/10.1103/PhysRevA.91.042118

Di Piazza, A. [2017], 'First-order strong-field QED processes in a tightly focused laser beam', *Phys. Rev. A* **95**, 032121.
URL: https://link.aps.org/doi/10.1103/PhysRevA.95.032121

Di Piazza, A., Hatsagortsyan, K. Z. and Keitel, C. H. [2008], 'Laser-photon merging in proton-laser collisions', *Phys. Rev. A* **78**, 062109.
URL: https://link.aps.org/doi/10.1103/PhysRevA.78.062109

Di Piazza, A., Milstein, A. I. and Keitel, C. H. [2007], 'Photon splitting in a laser field', *Phys. Rev. A* **76**, 032103.
URL: https://link.aps.org/doi/10.1103/PhysRevA.76.032103

Di Piazza, A., Müller, C., Hatsagortsyan, K. Z. and Keitel, C. H. [2012], 'Extremely high-intensity laser interactions with fundamental quantum systems', *Rev. Mod. Phys.* **84**, 1177.
URL: https://link.aps.org/doi/10.1103/RevModPhys.84.1177

Di Piazza, A., Tamburini, M., Meuren, S. and Keitel, C. H. [2017], 'Implementing nonlinear Compton scattering beyond the local constant field approximation'.
URL: https://arxiv.org/abs/arXiv:1708.08276

Dinu, V. [2013], 'Exact final-state integrals for strong-field QED', *Phys. Rev. A* **87**, 052101.
URL: https://link.aps.org/doi/10.1103/PhysRevA.87.052101

Dinu, V., Heinzl, T. and Ilderton, A. [2012], 'Infrared divergences in plane wave backgrounds', *Phys. Rev. D* **86**, 085037.
URL: https://link.aps.org/doi/10.1103/PhysRevD.86.085037

Dinu, V., Heinzl, T., Ilderton, A., Marklund, M. and Torgrimsson, G. [2014], 'Vacuum refractive indices and helicity flip in strong-field QED', *Phys. Rev. D* **89**, 125003.
URL: https://link.aps.org/doi/10.1103/PhysRevD.89.125003

Döbrich, B. and Gies, H. [2010], 'Axion-like-particle search with high-intensity lasers', *J. High Energy Phys.* **2010**(10), 22.
URL: https://doi.org/10.1007/JHEP10(2010)022

Dyson, F. J. [1949], 'The radiation theories of Tomonaga, Schwinger, and Feynman', *Phys. Rev.* **75**, 486–502.
URL: https://link.aps.org/doi/10.1103/PhysRev.75.486

Ehlotzky, F., Krajewska, K. and Kamiński, J. Z. [2009], 'Fundamental processes of quantum electrodynamics in laser fields of relativistic power', *Rep. Prog. Phys.* **72**(4), 046401.
URL: http://stacks.iop.org/0034-4885/72/i=4/a=046401

Einstein, A. [1905], 'Zur Elektrodynamik bewegter Körper', *Ann. Phys.* **322**(10), 891–921.
URL: https://onlinelibrary.wiley.com/doi/abs/10.1002/andp.19053221004

Exawatt Center for Extreme Light Studies (XCELS) [website].
URL: http://www.xcels.iapras.ru/

Extreme Light Infrastructure (ELI) [website].
URL: https://eli-laser.eu/

Fedotov, A. and Narozhny, N. [2007], 'Generation of harmonics by a focused laser beam in the vacuum', *Phys. Lett. A* **362**(1), 1 – 5.
URL: http://www.sciencedirect.com/science/article/pii/S0375960106015271

Feynman, R. P. [1948], 'Relativistic cut-off for Quantum Electrodynamics', *Phys. Rev.* **74**, 1430–1438.
URL: https://link.aps.org/doi/10.1103/PhysRev.74.1430

Feynman, R. P. [1949], 'Space-time approach to Quantum Electrodynamics', *Phys. Rev.* **76**, 769–789.
URL: https://link.aps.org/doi/10.1103/PhysRev.76.769

Filon, L. N. G. [1930], 'On a quadrature formula for trigonometric integrals', *Proc. Royal Soc. Edinb.* **49**, 38–47.

Fradkin, E. S., Gitman, D. M. and Shvartsman, S. M. [1991], *Quantum Electrodynamics with Unstable Vacuum*, Springer, Berlin.

Franssen, J. G. H., Frankort, T. L. I., Vredenbregt, E. J. D. and Luiten, O. J. [2017], 'Pulse length of ultracold electron bunches extracted from a laser cooled gas', *Struct. Dyn.* **4**(4), 044010.
URL: https://doi.org/10.1063/1.4978996

Fried, Z. and Eberly, J. H. [1964], 'Scattering of a high-intensity, low-frequency electromagnetic wave by an unbound electron', *Phys. Rev.* **136**, B871–B887.
URL: https://link.aps.org/doi/10.1103/PhysRev.136.B871

Furry, W. H. [1951], 'On bound states and scattering in positron theory', *Phys. Rev.* **81**, 115–124.
URL: https://link.aps.org/doi/10.1103/PhysRev.81.115

Gabrielse, G., Hanneke, D., Kinoshita, T., Nio, M. and Odom, B. [2006], 'New determination of the fine structure constant from the electron g value and QED', *Phys. Rev. Lett.* **97**, 030802.
URL: https://link.aps.org/doi/10.1103/PhysRevLett.97.030802

Gell-Mann, M. and Low, F. E. [1954], 'Quantum Electrodynamics at small distances', *Phys. Rev.* **95**, 1300–1312.
URL: https://link.aps.org/doi/10.1103/PhysRev.95.1300

Gies, H. [2009], 'Strong laser fields as a probe for fundamental physics', *Eur. Phys. J. D* **55**(2), 311–317.
URL: https://doi.org/10.1140/epjd/e2009-00006-0

Gies, H., Jaeckel, J. and Ringwald, A. [2006], 'Polarized light propagating in a magnetic field as a probe for millicharged fermions', *Phys. Rev. Lett.* **97**, 140402.
URL: https://link.aps.org/doi/10.1103/PhysRevLett.97.140402

Gies, H., Karbstein, F. and Kohlfürst, C. [2018], 'All-optical signatures of strong-field QED in the vacuum emission picture', *Phys. Rev. D* **97**, 036022.
URL: https://link.aps.org/doi/10.1103/PhysRevD.97.036022

Goldman, I. I. [1964], 'Intensity effects in Compton scattering', *Phys. Lett.* **8**, 103.

Gong, Z., Hu, R. H., Lu, H. Y., Yu, J. Q., Wang, D. H., Fu, E. G., Chen, C. E., He, X. T. and Yan, X. Q. [2018], 'Brilliant gev gamma-ray flash from inverse Compton scattering in the QED regime', *Plasma Phys. Controlled Fusion* **60**(4), 044004.
URL: http://stacks.iop.org/0741-3335/60/i=4/a=044004

Gong, Z., Hu, R. H., Shou, Y. R., Qiao, B., Chen, C. E., He, X. T., Bulanov, S. S., Esirkepov, T. Z., Bulanov, S. V. and Yan, X. Q. [2017], 'High-efficiency γ-ray flash generation via multiple-laser scattering in ponderomotive potential well', *Phys. Rev. E* **95**, 013210.
URL: https://link.aps.org/doi/10.1103/PhysRevE.95.013210

Gonoskov, A., Bashinov, A., Bastrakov, S., Efimenko, E., Ilderton, A., Kim, A., Marklund, M., Meyerov, I., Muraviev, A. and Sergeev, A. [2017], 'Ultrabright GeV photon source via controlled electromagnetic cascades in laser-dipole waves', *Phys. Rev. X* **7**, 041003.
URL: https://link.aps.org/doi/10.1103/PhysRevX.7.041003

Gonoskov, A., Bastrakov, S., Efimenko, E., Ilderton, A., Marklund, M., Meyerov, I., Muraviev, A., Sergeev, A., Surmin, I. and Wallin, E. [2015], 'Extended particle-in-cell schemes for physics in ultrastrong laser fields: Review and developments', *Phys. Rev. E* **92**, 023305.
URL: https://link.aps.org/doi/10.1103/PhysRevE.92.023305

Harvey, C., Heinzl, T. and Ilderton, A. [2009], 'Signatures of high-intensity Compton scattering', *Phys. Rev. A* **79**, 063407.
URL: https://link.aps.org/doi/10.1103/PhysRevA.79.063407

Heinzl, T. and Ilderton, A. [2017*a*], 'Exact classical and quantum dynamics in background electromagnetic fields', *Phys. Rev. Lett.* **118**, 113202.
URL: https://link.aps.org/doi/10.1103/PhysRevLett.118.113202

Heinzl, T. and Ilderton, A. [2017*b*], 'Superintegrable relativistic systems in spacetime-dependent background fields', *J. Phys. A* **50**(34), 345204.
URL: http://stacks.iop.org/1751-8121/50/i=34/a=345204

Heinzl, T., Ilderton, A. and Marklund, M. [2010], 'Laser intensity effects in non-commutative QED', *Phys. Rev. D* **81**, 051902.
URL: https://link.aps.org/doi/10.1103/PhysRevD.81.051902

Heinzl, T., Seipt, D. and Kämpfer, B. [2010], 'Beam-shape effects in nonlinear Compton and Thomson scattering', *Phys. Rev. A* **81**, 022125.
URL: https://link.aps.org/doi/10.1103/PhysRevA.81.022125

Heisenberg, W. and Euler, H. [1936], 'Folgerungen aus der Diracschen Theorie des Positrons', *Z. Phys.* **98**(11), 714–732.
URL: https://doi.org/10.1007/BF01343663

HERCULES Laser [website].
URL: https://cuos.engin.umich.edu/researchgroups/hfs/facilities/hercules-petawatt-laser/

High Power laser Energy Research facility (HiPER) [website].
URL: http://www.hiperlaser.org/

Ilderton, A. [2011], 'Trident pair production in strong laser pulses', *Phys. Rev. Lett.* **106**, 020404.
URL: https://link.aps.org/doi/10.1103/PhysRevLett.106.020404

Ivanov, D. Y., Kotkin, G. L. and Serbo, V. G. [2004], 'Complete description of polarization effects in emission of a photon by an electron in the field of a strong laser wave', *Eur. Phys. J. C* **36**(1), 127–145.
URL: https://doi.org/10.1140/epjc/s2004-01861-x

Jackson, J. D. [1999], *Classical electrodynamics*, Wiley, New York.

Karbstein, F. and Shaisultanov, R. Z. [2015], 'Photon propagation in slowly varying inhomogeneous electromagnetic fields', *Phys. Rev. D* **91**, 085027.
URL: https://link.aps.org/doi/10.1103/PhysRevD.91.085027

Karbstein, F. and Sundqvist, C. [2016], 'Probing vacuum birefringence using x-ray free electron and optical high-intensity lasers', *Phys. Rev. D* **94**, 013004.
URL: https://link.aps.org/doi/10.1103/PhysRevD.94.013004

Karshenboim, S. G. [2005], 'Precision physics of simple atoms: QED tests, nuclear structure and fundamental constants', *Phys. Rep.* **422**(1), 1 – 63.
URL: http://www.sciencedirect.com/science/article/pii/S0370157305003637

Kealhofer, C., Schneider, W., Ehberger, D., Ryabov, A., Krausz, F. and Baum, P. [2016], 'All-optical control and metrology of electron pulses', *Science* **352**(6284), 429–433.
URL: http://science.sciencemag.org/content/352/6284/429

King, B., Di Piazza, A. and Keitel, C. H. [2010], 'A matterless double slit', *Nat. Photonics* **4**, 92–94.
URL: http://dx.doi.org/10.1038/nphoton.2009.261

Klein, J. J. and Nigam, B. P. [1964], 'Birefringence of the vacuum', *Phys. Rev.* **135**, B1279–B1280.
URL: https://link.aps.org/doi/10.1103/PhysRev.135.B1279

Klepikov, N. P. [1985], 'Radiation damping forces and radiation from charged particles', *Phys. Usp.* **28**(6), 506–520.
URL: http://iopscience.iop.org/article/10.1070/PU1985v028n06ABEH005205/meta

Krajewska, K., Cajiao Vélez, F. and Kamiński, J. Z. [2017], 'Generation of attosecond electron pulses using petawatt lasers', *Proc. SPIE* **10241**, 102411J.
URL: http://dx.doi.org/10.1117/12.2271138

Krajewska, K., Twardy, M. and Kamiński, J. Z. [2014], 'Global phase and frequency comb structures in nonlinear Compton and Thomson scattering', *Phys. Rev. A* **89**, 052123.
URL: https://link.aps.org/doi/10.1103/PhysRevA.89.052123

Kurilin, A. V. [1999], 'Particle physics in intense electromagnetic fields', *Nuovo Cimento A* **112**(9), 977–1000.
URL: https://doi.org/10.1007/BF03035905

Landau, L. D. and Lifshitz, E. M. [1975], *The Classical Theory of Fields*, Course of theoretical physics, Butterworth-Heinemann, Oxford.

Leemans, W. P., Gonsalves, A. J., Mao, H.-S., Nakamura, K., Benedetti, C., Schroeder, C. B., Tóth, C., Daniels, J., Mittelberger, D. E., Bulanov, S. S., Vay, J.-L., Geddes, C. G. R. and Esarey, E. [2014], 'Multi-GeV electron beams from capillary-discharge-guided subpetawatt laser pulses in the self-trapping regime', *Phys. Rev. Lett.* **113**, 245002.
URL: https://link.aps.org/doi/10.1103/PhysRevLett.113.245002

Levine, I., Koltick, D., Howell, B., Shibata, E., Fujimoto, J., Tauchi, T., Abe, K., Abe, T., Adachi, I., Adachi, K., Aoki, M., Aoki, M., Emi, K., Enomoto, R., Fujii, H., Fujii, K., Fujii, T., Fujiwara, N., Hayashii, H., Hirano, H., Ikeda, H., Ikeda, H., Inoue, Y., Itami, S., Itoh, R., Iwasaki, H., Iwasaki, M., Kajikawa, R., Kaneyuki, K., Kato, S., Kawabata, S., Kichimi, H., Kobayashi, M., Mamada, H., Miyabayashi, K., Miyamoto, A., Nagai, K., Nakabayashi, K., Nakamura, M., Nakano, E., Nitoh, O., Noguchi, S., Ochi, A., Ochiai, F., Ohishi, N., Ohnishi, Y., Ohshima, Y., Okuno, H., Okusawa, T., Sugiyama, A., Suzuki, S., Takahashi, K., Takahashi, T., Tanimori, T., Teramoto, Y., Tomoto, M., Tsukamoto,

T., Tsumura, T., Uno, S., Watanabe, K., Watanabe, Y., Yamamoto, A. and Yamauchi, M. [1997], 'Measurement of the electromagnetic coupling at large momentum transfer', *Phys. Rev. Lett.* **78**, 424–427.
URL: https://link.aps.org/doi/10.1103/PhysRevLett.78.424

Liu, C., Shen, B., Zhang, X., Ji, L., Bu, Z., Wang, W., Yi, L., Zhang, L., Xu, J., Xu, T. and Pei, Z. [2018], 'Ultra-bright, well-collimated, GeV gamma-ray production in the QED regime', *Phys. Plasmas* **25**(2), 023107.
URL: https://doi.org/10.1063/1.5005077

Mackenroth, F. [2014], *Quantum Radiation in Ultra-Intense Laser Pulses*, Springer International Publishing, Heidelberg.
URL: http://dx.doi.org/10.1007/978-3-319-07740-6_2

Mackenroth, F. and Di Piazza, A. [2011], 'Nonlinear Compton scattering in ultra-short laser pulses', *Phys. Rev. A* **83**, 032106.
URL: https://link.aps.org/doi/10.1103/PhysRevA.83.032106

Malka, V., Faure, J., Gauduel, Y. A., Lefebvre, E., Rousse, A. and Phuoc, K. T. [2008], 'Principles and applications of compact laser-plasma accelerators', *Nat. Phys.* **4**, 447 – 453.
URL: http://dx.doi.org/10.1038/nphys966

Mendonça, J. T. [2007], 'Axion excitation by intense laser fields', *EPL (Europhysics Letters)* **79**(2), 21001.
URL: http://stacks.iop.org/0295-5075/79/i=2/a=21001

Metropolis, N., Rosenbluth, A. W., Rosenbluth, M. N., Teller, A. H. and Teller, E. [1953], 'Equation of state calculations by fast computing machines', *J. Chem. Phys.* **21**(6), 1087–1092.
URL: https://doi.org/10.1063/1.1699114

Miller, J. P., de Rafael, E. and Roberts, B. L. [2007], 'Muon (g - 2): experiment and theory', *Rep. Prog. Phys.* **70**(5), 795.
URL: http://stacks.iop.org/0034-4885/70/i=5/a=R03

Morimoto, Y. and Baum, P. [2018*a*], 'Attosecond control of electron beams at dielectric and absorbing membranes', *Phys. Rev. A* **97**, 033815.
URL: https://link.aps.org/doi/10.1103/PhysRevA.97.033815

Morimoto, Y. and Baum, P. [2018*b*], 'Diffraction and microscopy with attosecond electron pulse trains', *Nat. Phys.* **14**(3), 252–256.
URL: https://doi.org/10.1038/s41567-017-0007-6

Nikishov, A. I. and Ritus, V. I. [1964], 'Quantum processes in the field of a plane electromagnetic wave and in a constant field. I', *Sov. Phys. JETP* **19**(2), 529–541.
URL: http://www.jetp.ac.ru/cgi-bin/e/index/e/19/2/p529?a=list

Odom, B., Hanneke, D., D'Urso, B. and Gabrielse, G. [2006], 'New measurement of the electron magnetic moment using a one-electron quantum cyclotron', *Phys. Rev. Lett.* **97**, 030801.
URL: https://link.aps.org/doi/10.1103/PhysRevLett.97.030801

Patrignani, C. et al. (Particle Data Group) [2017], 'Review of particle physics', *Chin. Phys. C* **40**, 100001.
URL: http://iopscience.iop.org/article/10.1088/1674-1137/40/10/100001/

Peskin, M. E. and Schroeder, D. V. [1995], *An Introduction to Quantum Field Theory*, Addison-Wesley, Reading.

Piskarskas, A., Stabinis, A. and Yankauskas, A. [1986], 'Phase phenomena in parametric amplifiers and generators of ultrashort light pulses', *Phys. Usp.* **29**(9), 869–879.

Press, W. H., Teukolsky, S. A., Vetterling, W. T. and Flannery, B. P. [2007], *Numerical Recipes: The Art of Scientific Computing*, Cambridge University Press, New York.

Ridgers, C. P., Brady, C. S., Duclous, R., Kirk, J. G., Bennett, K., Arber, T. D. and Bell, A. R. [2013], 'Dense electron-positron plasmas and bursts of gamma-rays from laser-generated quantum electrodynamic plasmas', *Phys. Plasmas* **20**(5), 056701.
URL: https://doi.org/10.1063/1.4801513

Ritus, V. I. [1985], 'Quantum effects of the interaction of elementary particles with an intense electromagnetic field', *J. Sov. Laser Res.* **6**(5), 497–617.
URL: http://dx.doi.org/10.1007/BF01120220

Rozanov, N. N. [1998], 'Self-action of intense electromagnetic radiation in an electron-positron vacuum', *J. Exp. Theor. Phys.* **86**(2), 284–288.
URL: https://doi.org/10.1134/1.558454

Runge, C. [1901], 'Über empirische Funktionen und die Interpolation zwischen äquidistanten Ordinaten', *Z. Mat. Phys.* **46**, 224–243.
URL: https://archive.org/details/zeitschriftfrma12runggoog

Sarri, G., Corvan, D. J., Schumaker, W., Cole, J. M., Di Piazza, A., Ahmed, H., Harvey, C., Keitel, C. H., Krushelnick, K., Mangles, S. P. D., Najmudin,

Z., Symes, D., Thomas, A. G. R., Yeung, M., Zhao, Z. and Zepf, M. [2014], 'Ultrahigh brilliance multi-mev γ-ray beams from nonlinear relativistic thomson scattering', *Phys. Rev. Lett.* **113**, 224801.
URL: https://link.aps.org/doi/10.1103/PhysRevLett.113.224801

Sauter, F. [1931], 'Über das Verhalten eines Elektrons im homogenen elektrischen Feld nach der relativistischen Theorie Diracs', *Z. Phys.* **69**(11), 742–764.
URL: https://doi.org/10.1007/BF01339461

Schwinger, J. [1948], 'Quantum Electrodynamics. I. a covariant formulation', *Phys. Rev.* **74**, 1439–1461.
URL: https://link.aps.org/doi/10.1103/PhysRev.74.1439

Schwinger, J. [1949], 'Quantum Electrodynamics. II. vacuum polarization and self-energy', *Phys. Rev.* **75**, 651–679.
URL: https://link.aps.org/doi/10.1103/PhysRev.75.651

Schwinger, J. [1951], 'On gauge invariance and vacuum polarization', *Phys. Rev.* **82**, 664–679.
URL: https://link.aps.org/doi/10.1103/PhysRev.82.664

Seipt, D. and Kämpfer, B. [2011], 'Nonlinear Compton scattering of ultrashort intense laser pulses', *Phys. Rev. A* **83**, 022101.
URL: http://link.aps.org/doi/10.1103/PhysRevA.83.022101

Skoromnik, O. D. and Feranchuk, I. D. [2014], 'Justification of the single-mode approximation for a finite-duration laser pulse interacting with an electron', *J. Phys. B* **47**(11), 115601.
URL: http://stacks.iop.org/0953-4075/47/i=11/a=115601

Smolyak, S. A. [1963], 'Quadrature and interpolation formulas for tensor products of certain classes of functions', *Soviet Math. Dokl.* **4**, 240–243.
URL: http://www.ams.org/mathscinet-getitem?mr=0147825

Strickland, D. and Mourou, G. [1985], 'Compression of amplified chirped optical pulses', *Opt. Commun.* **56**(3), 219 – 221.

Sturm, S., Köhler, F., Zatorski, J., Wagner, A., Harman, Z., Werth, G., Quint, W., Keitel, C. H. and Blaum, K. [2014], 'High-precision measurement of the atomic mass of the electron', *Nature* **506**, 467–470.
URL: http://dx.doi.org/10.1038/nature13026

Taylor, J. C. [1998], *An Introduction to Measure and Probability*, Springer-Verlag, New York.

Titov, A. I., Kämpfer, B., Shibata, T., Hosaka, A. and Takabe, H. [2014], 'Laser pulse-shape dependence of Compton scattering', *Eur. Phys. J. D* **68**(10), 299.
URL: https://doi.org/10.1140/epjd/e2014-50324-y

Tomonaga, S.-I. and Oppenheimer, J. R. [1948], 'On infinite field reactions in Quantum Field Theory', *Phys. Rev.* **74**, 224–225.
URL: https://link.aps.org/doi/10.1103/PhysRev.74.224

van der Geer, S. B., de Loos, M. J., Vredenbregt, E. J. D. and Luiten, O. J. [2009], 'Ultracold electron source for single-shot, ultrafast electron diffraction', *Microsc. Microanal.* **15**(4), 282–289.

Villalba-Chávez, S., Meuren, S. and Müller, C. [2016], 'Minicharged particles search by strong laser pulse-induced vacuum polarization effects', *Phys. Lett. B* **763**, 445 – 453.
URL: http://www.sciencedirect.com/science/article/pii/S0370269316306463

Volkov, D. M. [1935], 'Über eine Klasse von Lösungen der Diracschen Gleichung', *Z. Phys.* **94**(3), 250–260.
URL: https://doi.org/10.1007/BF01331022

Vulcan Laser [website].
URL: https://www.clf.stfc.ac.uk/Pages/Vulcan.aspx

Weinberg, S. [1995], *The Quantum Theory of Fields*, Cambridge University Press, New York.

Wistisen, T. N. [2014], 'Interference effect in nonlinear Compton scattering', *Phys. Rev. D* **90**, 125008.
URL: https://link.aps.org/doi/10.1103/PhysRevD.90.125008

Yanovsky, V., Chvykov, V., Kalinchenko, G., Rousseau, P., Planchon, T., Matsuoka, T., Maksimchuk, A., Nees, J., Chériaux, G., Mourou, G. and Krushelnick, K. [2008], 'Ultra-high intensity- 300-TW laser at 0.1 Hz repetition rate.', *Opt. Express* **16**, 2109.

Yu, C., Qi, R., Wang, W., Liu, J., Li, W., Wang, C., Zhang, Z., Liu, J., Qin, Z., Fang, M., Feng, K., Wu, Y., Tian, Y., Xu, Y., Wu, F., Leng, Y., Weng, X., Wang, J., Wei, F., Yi, Y., Song, Z., Li, R. and Xu, Z. [2016], 'Ultrahigh brilliance quasi-monochromatic MeV γ-rays based on self-synchronized all-optical Compton scattering', *Sci. Rep.* **6**, 29518.
URL: http://dx.doi.org/10.1038/srep29518

Acknowledgements

> "And when he dreams he does not want to write, he does not have the power to dream he wants to write; and when he dreams he wants to write, he does not have the power to dream he does not want to write."
>
> Baruch Spinoza
> (as quoted by Paul Auster in *The New York Trilogy*)

In these last pages I would like to express my gratitude to a large number of people which, in one way or another, contributed directly or indirectly to my work, and helped me somewhat retain my sanity during the time I spent in Heidelberg.

First and foremost, I am grateful to PD Dr. Antonino Di Piazza, my supervisor. I would like to thank him especially for his patience and for all the time he spent working with me at this project: I cannot imagine finishing this without his intuitions and physical insight. I thank him for the countless discussions, and for always being a source of great motivation.

I am also greatly indebted to Prof. Dr. Joerg Jaeckel for his time and willingness to review this thesis.

With immense sorrow, I thank Giampiero, my father, who did not live long enough to see the end of this project. I could fill many pages listing all the things I could thank him for; here I will only thank him for all the sacrifices he made for my education.

I acknowledge Dr. Felix Mackenroth; especially at the beginning of my project, his thesis and his advice were extremely useful to set me on the right path.

I want to thank Prof. Dr. Christoph H. Keitel for accepting me in his division; it was an honor for me to work in such a prestigious institution and stimulating environment, surrounded by some of the most amazing people I have ever met in my life. I would like to thank, in particular, Sibel Babacan for her support

during all these years. I acknowledge useful discussions with Dr. Sebastian Meuren, Dr. Matteo Tamburini, Dr. Tobias Wistisen, Dr. Naveen Kumar, Dr. Alberto Benedetti, Dr. Natalia Oreshkina, Dr. Vincent Debierre, Dr. Qingzheng Lyu, Dr. Erez Raicher, Dr. Tahir Shaaran, PD Dr. Jörg Evers, Dr. habil. Karen Z. Hatsagortsyan, and Suo Tang. Many thanks also to PD Dr. Zoltán Harman, PD Dr. Adriana Pálffy-Buß, Dr. Kilian Heeg, Dr. Norman Neitz, Dr. Margarita Khokhlova, Dr. Ujjwal Sinha, Shikha Bhadoria, Bastian Sikora, Pavlo Bilous, Jiri Danek, Sergei Kobzak, Dominik Lentrodt, Chunhai Lyu, Niklas Michel, Brenden Nickerson, Archana Sampath, Maitreyi Sangal, and Nicholas Teeny.

I would also like to thank a person that I got to know a lot during these years and that became for me a very close friend: Dr. Stefano M. Cavaletto. Thank you for your help during all these years; it was a blessing for me to have my desk next to yours... I hope has not been too much of a curse for you!

Similarly, I want to express my gratitude to other friends: thank you, Dr. Oleg Skoromnik and Sergey Bragin, for our (sometimes heated, but always enlightening) discussions. And thank you, Salvatore Castrignano, for too many things to list here. I am especially grateful to Dr. Stefano Cavaletto, Dr. Oleg Skoromnik, Sergey Bragin, Halil Cakir, Salvatore Castrignano, Daniel Bakucz Canário, and Dominik Lentrodt for their feedback on some parts of my thesis.

I thank Christian, Johanna, Andreas, Christina (each and every one of them, but especially my great former flatmate, Christina König), Alexander, Katja, Phillip, Paul, Ciryl, Alberto, and the rest of the Am Sportplatz crew. The happiest times I had in Heidelberg were with you guys, and I am extremely grateful for that. I also want to thank my former neighbors Laura and Andreas and wish them a wonderful future.

Even if we are far away most of the time, there are some people that I always feel close to me, and helped me with this project in their own ways. I thank for their friendship my oldest friends Luca and Giuseppe, from Deximu. Also, coming back to Cagliari would not feel right without the chance to see Stefano (Cirina and Tavera), Alessandro, Simone (Pisano and Seu), Matteo (Saderi and Quarantiello), Cinzia and all the FeL gang. Moreover, I would like to thank Amanda, Laura, Matilde, Peppe, Letizia, Luca, Gianluca, and all my friends from the years in Trieste. I miss you guys, and hope to see you as soon as possible. I am also grateful to Stefan Burnett, Zach Hill, and Andy Morin for being a constant source of inspiration.

I am extremely grateful to my family: Maura, Lucia, Gina, Claudia, Rina, and Marcello. Words cannot convey how much I love you. Thank you for everything you did for me since when I was born.

Finally, I feel extremely lucky to have my beloved girlfriend Maria on my side. Her material and emotional support during these last months of writing has been fundamental for me. I cannot wait to see where life brings us, but I am sure everything will be great. Forza e coraggio!